PHOTOACOUSTIC DRUG DELIVERY USING CARBON NANOPARTICLES ACTIVATED BY FEMTOSECOND AND NANOSECOND LASER PULSES

A Thesis
Presented to
The Academic Faculty

By

Prerona Chakravarty

In Partial Fulfillment
Of the Requirements for the Degree
Doctor of Philosophy in Chemical & Biomolecular Engineering

Georgia Institute of Technology
May, 2009

PHOTOACOUSTIC DRUG DELIVERY USING CARBON NANOPARTICLES ACTIVATED BY FEMTOSECOND AND NANOSECOND LASER PULSES

Approved by:

Dr. Mark R. Prausnitz, Advisor
School of Chemical & Biomolecular Engineering
Georgia Institute of Technology

Dr. Sankar Nair
School of Chemical & Biomolecular Engineering
Georgia Institute of Technology

Dr. Mostafa A. El-Sayed
School of Chemistry & Biochemistry
Georgia Institute of Technology

Dr. Gerald S. Pullman
School of Biology
Georgia Institute of Technology

Dr. Hang Lu
School of Chemical & Biomolecular Engineering
Georgia Institute of Technology

Date Approved: December 12, 2008

ACKNOWLEDGEMENTS

As I hold the finished thesis in my hand, it gives me great pleasure to thank the many people who made this journey possible. My utmost gratitude goes to my advisor, Dr. Mark Prausnitz for believing in me and taking me under his wing. His enthusiasm for new ideas, encouragement and sound advice inspired me to think outside the box and made this Ph.D. an exciting intellectual adventure.

I am indebted to Dr. Mostafa El-Sayed and Dr. Thomas Orlando for generously providing some of the most essential resources to conduct this study. I would also like to thank Dr. El-Sayed, Dr. Jerry Pullman, Dr. Sankar Nair and Dr. Hang Lu for serving as members of my thesis committee and helping shape this thesis. I would like to thank the National Institutes of Health and the Georgia Tech Institute of Paper Science and Technology for their financial support. I am grateful to Dr. Christopher Lane and Dr. Wei Qian for their assistance during experiments and for the stimulating scientific discussions which added new insights to this study. A special thanks to Dr. Brani Vidakovic and Dr. Thomas Burkholder for their guidance during some crucial moments in this study.

I would also like to express my sincere thanks to my friends and colleagues for providing a fun environment in which to learn and grow: Samantha Andrews for being my road-trip buddy, those lively discussions on everything from Project Runway to Indian politics and of course all the music CDs (especially the Amy Winehouse ones), Robyn Schlicher for sharing my passion for psycho movies and “masala dosas”, Daniel Hallow for his calm disposition, and fellow lab mates Yeu Chun Kim, Jeong-Woo Lee, Ying Liu, Harvinder Gill, Vladimir Zarnitsyn, Sean Sullivan, James Norman, Samir

Patel, Jyoti Gupta, Leonard Chu, Seong-O Choi, Youngbin Choy and Josh Hutcheson for their camaraderie.

My sincere thanks to Donna Bondy for help with all the paperwork and meeting arrangements that I could never imagine doing on my own. Her reassuring smile and delightful anecdotes always brightened my day. I would also like to thank Steve Woodard, Johnafel Crowe, Sha'aqua Asberry, Laura O'Farrell and the PRL staff for their help with using the IBB core facilities.

Lastly, and most importantly, I would like to thank the people closest to me: my best friend Carthik Anand Sharma for his love, wisdom and support which saw me through some of my most difficult times; my brother Konark Chakravarty for being the greatest brother ever; and my wonderful parents, Kamakhya Kumar Chakravarty and Rinu Chakravarty, whose unconditional love and implicit trust gave me the courage and perseverance to follow my dream. To them I dedicate this thesis.

TABLE OF CONTENTS

LIST OF TABLES

LIST OF FIGURES

LIST OF SYMBOLS AND ABBREVIATIONS

AFM	Atomic force microscopy
ANOVA	Analysis of variance
A. tumefaciens	Agrobacterium tumefaciens
BSA	Bovine serum albumin
C	Carbon
CB	Carbon black
CNT	Carbon nanotube
CO	Carbon monoxide
CO_2	Carbon dioxide
CPP	Cell penetrating peptides
CW	Continuous wave
DI	Deionized
DNA	Deoxyribonucleic acid
EDTA	Ethylenediaminetetraacetic acid
FBS	Fetal bovine serum
FDA	Food and Drug Administration
FITC	Fluorescein isothiocyanate
GFP	Green fluorescent protein
GUS	Beta-glucuronidase)
ΔH	Enthalpy change
H & E	Hematoxylin and eosin

H_2	Hydrogen
H_2O	Water
IR	Infrared
K^+	Potassium ion
LSW	Laser-generated stress wave
MWNT	Multi-walled carbon nanotube
NBT	Nitro blue tetrazolium
Nd: YAG	Neodymium-doped yttrium aluminium garnet
NIR	Near infrared
OCT	Optimal cutting temperature
PBS	Phosphate buffered saline
PDT	Photodynamic therapy
PI	Propidium iodide
PVC	Poly vinyl chloride
QMS	Quadrupole mass spectrometer
R	Molar gas constant
RLU	Relative light unit
RNA	Ribonucleic acid
RPMI	Roswell Park Memorial Institute Medium
SAAT	Sonication-assisted Agrobacterium-mediated transformation
SCMT	Silicon carbide-mediated transformation
SiC	Silicon carbide
siRNA	Small interfering ribonucleic acid

SEM	Standard error of the mean
SWNT	Single-walled carbon nanotube
TA	Tibialis anterior
TEM	Transmission electron microscopy
Ti plasmid	Tumor-inducing plasmid
Ti: Sapphire	Titanium: Sapphire
US	Ultrasound
UV	Ultraviolet
VIS	Visible

SUMMARY

Cellular internalization of large therapeutic agents such as proteins or nucleic acids is a challenging task because of the presence of the plasma membrane. One strategy to facilitate intracellular drug uptake is to induce transient pores in the cell membrane through physical delivery strategies. Physical approaches are attractive as they offer more generic applicability compared with viral or biochemical counterparts. Pulsed laser light can induce the endothermic carbon-steam reaction in carbon-nanoparticle suspensions to produce explosive photoacoustic effects in the surrounding medium. In this study, for the first time, these photoacoustic forces were used to transiently permeabilize the cell membrane to deliver macromolecules into cells. Intracellular delivery using this method was demonstrated in multiple cell types for uptake of small molecules, proteins and DNA. At optimized conditions, uptake was seen in up to 50% of cells with nearly 100% viability and in 90% of cells with ≥90% viability, which compared favorably with other physical methods of drug delivery. Cellular bioeffects were shown to be a consequence of laser-carbon interaction and correlated with properties of the carbon and laser, such as carbon concentration and size, laser pulse duration, wavelength, intensity and exposure time. Similar results were observed using two different lasers, a femtosecond Ti: Sapphire laser and a nanosecond Nd: YAG laser. Uptake was also shown in murine skeletal muscles in vivo with up to 40% efficiency compared to non-irradiated controls. This synergistic use of nanotechnology with advanced laser technology could provide an alternative to viral and chemical-based drug and gene delivery.

CHAPTER 1
INTRODUCTION

Advances in genomics, biotechnology and chemistry have led to the design of a significant number of therapeutic and diagnostic agents that are directed against intracellular targets. The conversion of such novel therapeutics into medicines is frequently delayed by the lack of parallel investment in the field of drug delivery. Hence it is often more cost efficient and beneficial to design a delivery system for existing drugs instead of designing a new pharmaceutical. The most common barrier to intracellular drug delivery is transport across the plasma membrane. Cellular delivery involving the transfer of various drugs and bio-active molecules (peptides, proteins, DNA, etc.) through the cell membrane into cells has attracted increasing attention because of its importance in medicine and drug delivery. One of the challenges for modern medicine is to deliver therapeutics like proteins, peptides and DNA intracellularly in a targeted manner with minimal side effects. To realize this objective, many drug delivery systems are under investigation, but few of them have fulfilled the ideal goal of high intracellular uptake with minimal unwanted cell death. Drug delivery systems based on physical methods are attractive because of their broad applicability and non-dependency on nature of drug or cell. The working principle behind such methods is to create a local perturbation near the cell membrane to create transient membrane openings and facilitate entry of drugs. The cell subsequently tries to repair these breaks and depending on the magnitude of wounding, it either succeeds or is permanently damaged. The recurring challenge for physical methods is therefore to optimize the size and lifetime of these holes so that the efficient intracellular uptake is followed by efficient cell repair. However, the forces

responsible for causing membrane breaks are not easy to control and so in most physical methods high intracellular uptake is invariably accompanied by high cell death. One such method that had been studied extensively in this context was ultrasound-mediated delivery which used acoustic cavitation to cause transient openings in cell membrane. Since cavitation energy is difficult to control the advancement of ultrasound towards clinical drug delivery has been slow.

The goal of this study was to find a new physical method of intracellular drug delivery that could overcome the limitations of existing methods by providing better control and understanding of forces that cause membrane openings and thereby promote efficient intracellular uptake with minimal cell death. We found that a phenomenon called "giant-photoacoustic wave" was widely documented in the physical and chemical literature as a strong acoustic force generated when pulsed laser light interacted with suspensions of carbon nanoparticles. The reason was attributed to the explosive volume change accompanying such an interaction as a result of the laser-initiated endothermic carbon-water reaction $C(s) + H_2O(l) \rightarrow CO(g) + H_2(g)$. The analogy between these chemically generated pressure forces (photoacoustic) and ultrasonically generated pressure forces (cavitation), led us to hypothesize that like acoustic cavitation, these photoacoustic forces could also lead to transient membrane openings and facilitate drug entry. Our expectation was that since the forces for membrane poration resulted from laser-carbon interaction, both of whose properties could be manipulated, it would offer better control over cellular bioeffects, viz. uptake and death. So the goals of this study were (i) to evaluate if photoacoustic forces produced by laser-carbon interaction led to intracellular uptake, and if so, to understand the effect of different operating parameters

on cellular bioeffects and (ii) to evaluate the ability of this method to deliver molecules in the size range of proteins, peptides and DNA, as well as the ability to deliver in vivo. Two laser systems in conjunction with carbon nanoparticles and cells were studied independently, one generating femtosecond pulses and the other generating nanosecond pulses. The details of each independent study are discussed in Chapter 5 and Chapter 6.

For the first part of the study, the strategy was to reproduce conditions which had been already reported in literature to cause laser-carbon initiated photoacoustic effects. Intracellular uptake was then studied under these conditions to see if uptake could be caused by such physical forces. Another strategy was to eliminate conditions which were known to cause photoacoustic forces and study uptake under those conditions. This was to determine if uptake was being caused by alternate mechanisms. The second part of the study involved using the optimized conditions obtained from the first part to deliver molecules in the size range of therapeutic proteins and DNA. Finally, the laser-carbon system was used to deliver a model drug to murine TA muscles in vivo.

Another area which this thesis sought to advance was genetic transformation of conifers. Conifers are an economically important species for industrial timber but they are mostly obtained from natural forests which is highly unsustainable. Clonal forests are a sustainable solution but realizing that goal will require methods for genetic transformation that can are simple and inexpensive with high throughput. The goal of this study was to use ultrasound to deliver genes to tissue cultured loblolly pine embryos. Using a low cost ultrasound apparatus, expression of GFP was shown in pine embryos without removing the cell wall. This study is the focus of Chapter 7.

The basic format of the entire study was to formulate a series of hypotheses and then test each hypothesis through experiments. The chapters that follow discuss in detail the driving hypotheses, experimental design, and interpretation of data, as well as the conclusions drawn and recommendations for future advancement.

CHAPTER 2
BACKGROUND

The ultimate aim of pharmacy and much of medicine is the delivery of a drug at the right time in a safe and reproducible manner to a specific target at the required level[1, 2]. For many drugs however, these essential requirements are hindered due to the lack of a suitable delivery method[3-5]. For example, although the oral route is one of the preferred methods of drug delivery, owing to its non-invasive nature, adequate peptide or protein drug delivery has not yet been attained via this route[6]. This is, in part, a consequence of the acidic conditions of the stomach, the first-pass effect of the liver (i.e. the loss of drug owing to metabolic processes before entering the systemic circulation) and the resistance exerted by the intestine, which alters, destroys or reduces absorption of nearly all macromolecules, thereby reducing their bioavailability[7].

The lack of suitable drug delivery systems not only has implications for conventional drug administration routes and dosage forms, but is becoming a drawback for the advance of novel therapeutic strategies like cell-therapy[8], RNA interference[9-12] and gene therapy[13, 14]. Major challenges are the intracellular delivery of macromolecular drugs[7], the chronic administration of drugs into tumors and the targeted delivery of drugs[15]. All these drawbacks have stimulated many pharmaceutical companies and start-up biotech companies to develop drug delivery systems that can exert their function in an efficient and safe manner. Drug delivery today has become a highly interdisciplinary field of research.

2.1. Assessment of current delivery strategies in mammalian systems

A key barrier to achieving the desired intracellular localization of many of these therapeutic compounds is their inability to cross the cell plasma membrane[16]. The plasma membrane is primarily composed of a lipid bilayer and embedded proteins which provide a barrier that excludes large molecules from entering the cell.

Methods for improving intracellular delivery can be broadly classified as (a) biological, (b) chemical and (c) physical. Each method has its inherent shortcomings and so far no method has been proved fully satisfactory for drug or gene delivery.

2.1.1. Biological methods

Biological approaches often involve the use of viral vectors[17]. They are usually the easiest and most effective way to introduce sequences of interest into eukaryotic cells. Millions of years of evolution have specialized these particular organisms to actively enter the hosts and enslave the cell machinery to the production of viral proteins. Since the beginning of gene transfer, they have appeared as the direct route to cell transduction. But they also suffer from many undesired side effects, such as viral toxicity, host immune rejection, as well as being difficult to prepare[13].

2.1.2. Chemical methods

During the past few decades there has been an increasing interest in the development of microparticles and nanoparticles for effective drug, peptide, protein and DNA delivery[4, 18, 19]. In general, the therapeutic product is immobilized, adsorbed, attached, dissolved or encapsulated into the chemical formulation, allowing precise control over targeting and drug-release profiles. When the size of the particles used for

encapsulation is reduced to less than 100 nm in size, the result is nanotechnology[20]. Nanoparticles generally have higher intracellular uptake compared with microparticles, which makes nanoparticles candidates for targeted drug delivery to specific intracellular compartments. Depending on the materials employed and the method of preparation, different nanosized particles can be distinguished, including nanocapsules, nanospheres, liposomes[21], polymeric micelles[32], ceramic nanoparticles and dendrimers[32]. These systems have unusual properties that can be exploited to improve the delivery of drugs, proteins and genes. The inclusion of therapeutic active molecules in microparticulate delivery systems presents a way to protect and transport the medication to exactly the right place. Examples of these systems include polymer-based microparticules, micelles and liposomes. Liposomes are formed from concentric spherical phospholipid bilayers with an inner compartment that can be used for the encapsulation of different drugs. Nanocomposites like nanocapsules, micellar systems[22], conjugates and nanoparticles represent submicron systems that can provide a higher intracellular uptake than microsized particles. This has special implications for gene delivery, as DNA can be easily encapsulated, protected from lysosomal enzymes and transfected with high efficiency. Drawbacks associated with chemical delivery vectors are related to stability in the systemic circulation and lysosomal or endosomal degradation upon endocytosis by the cell[23]. Cell penetrating peptides (CPPs) are also being investigated as carriers for the delivery of therapeutic agents[24, 25]. Some CPPs are used for delivery of nucleic acids and promote their delivery through the endosomal pathway, while others are believed to cross membranes independent of the endosomal pathway. To address the problem of gene therapy delivery, cationic b-cyclodextrin-based polymers have been synthesized that

complex DNA and can safely transfect cells[26]. Another approach is based on a "terplex," a combination of stearyl-polylysine, low-density lipoprotein and DNA[27]. The potential advantage of the terplex is that one molecule, stearyl-polylysine, can be used to complex DNA while a second molecule, low-density lipoprotein, can be used to target the DNA to a desired location, such as the myocardium.

2.1.3. Physical methods

Physical methods take advantage of a completely different approach in that they force the cells or tissues to take up the drug in a restricted area that has been subjected to the physical perturbation[28]. This results in better targeting, direct non-endocytic delivery and broad applicability. A common feature of these techniques is that they increase cell permeability via the creation of transient holes in the plasma membrane[29]. Better macromolecular delivery is possible if the pores are large and open for a long time; on the other hand, the larger the hole and the longer it is open, the greater is the chance that the cell will die. The challenge lies in optimizing physical conditions to obtain maximum drug uptake with minimal collateral damage. Discussed below are some physical methods of drug delivery.

2.1.3.1. Microinjection

The most direct method to introduce DNA into cells is microinjection, either into the cytoplasm or into the nucleus. Conceptually, microinjection is a simple method, but it is technically fastidious. Cells are transfected one by one, and the injection procedure requires a skilled operator. Although expression occurs in a high proportion of cells that receive a gene, it is limited by the number of cells that can be directly treated[30].

2.1.3.2. Particle bombardment

The idea behind particle bombardment-mediated gene delivery is to move naked DNA plasmid into target cells on an accelerated particle carrier[31, 32]. The gene gun approach is relatively straightforward, and the delivery vehicle is quick and easy to prepare. In contrast, the device and reagents for particle bombardment are expensive. With respect to targeting, the gene gun is limited by the shallow penetration of particles into biological tissues. Thus, while gene transfer into the epidermal layer of the skin is feasible, for example, application of the technology to deeper tissues has met with much less success[33].

2.1.3.3. Magnetofection

Magnetofection is a relatively new technique wherein magnetic nanoparticles are associated with the therapeutic agent of interest. The magnetic particles are then concentrated preferentially into the target cells by the influence of an external magnetic field[34, 35]. The major potential advantage of magnetofection is remote targeting in vivo. This will demand a magnetic field of sufficient strength to preferentially localize the magnetized vectors to their target zone. Whether this can be achieved without invasive intervention requires further study.

2.1.3.4. Electroporation

Electroporation involves subjecting the cell membrane to high-intensity electrical pulses that can cause localized destabilization creating transient pores in the membrane. This facilitates entry of exogenous molecules into the cell[36, 37]. The pore size depends on the electric field strength and pulse length. Gene transfer by electroporation has been

shown to be efficient both in vitro and in vivo, in several cell types and tissues[38, 39]. It has also being widely investigated for transdermal drug delivery. However, the approach becomes progressively more invasive as accessibility to the target tissue decreases. Since electroporation employs high electric fields exposure of the patient must be carefully monitored. The distribution of the electric field within the tissue affects the efficacy of electroporation and fine tuning of the electroporation device is required for each treatment, even for similar tissues. This sensitivity represents a hurdle of some importance for commercialization of the approach as a routine procedure. Electrochemotherapy is an approved medical procedure in Europe[40].

2.1.3.5. Ultrasound

Ultrasound-mediated delivery occurs due to the transient mechanical disruption of the cell membranes by acoustically-induced bubble activity or acoustic cavitation[41-43].
It has been shown to be a fast and non-invasive tool for drug and gene delivery. Although a relatively new technology, it has already been examined, in some detail, both in vitro and in vivo. It is also being used in conjunction with therapeutic microbubbles to obtain targeted delivery and transfection[44]. However the effects of ultrasound are heterogeneous and its intensity weakens as it penetrates deeper in the body[45, 46].

Recent studies have tried to explain the underlying mechanism behind ultrasound-induced uptake and death so as to have better control over this tool[47, 48]. The beneficial aspect of ultrasound exposure, i.e., increased permeability of the plasma membrane, must be balanced against a possibly undesired effect, i.e., the loss of cellular viability. Cavitation bubble dynamics cause mechanical damage to the cell membrane. Most ultrasound-mediated death initiates from plasma membrane wounding effects, either by

lytic necrosis or by secondary effects from intracellular mechanisms leading to programmed cell death modes. Two main factors are important in the recovery of cells after ultrasound exposure: the intensity of ultrasound seen by the cell and time for wound repair. As intensity increases, more cells are observed to be mechanically fragmented since cell repair is an energy intensive process[48, 49].

2.1.4. Advantages of physical methods of drug delivery

Physical approaches are attractive as they offer more generic applicability compared with viral or biochemical counterparts[29, 50]. In addition uptake occurs via purely physical mechanisms viz. transient breaks in the membrane, thereby avoiding the problem of endosomal degradation of the bioactive compounds. Localized, needle-free drug delivery is emerging as an effective technique to transfer adequate concentrations of pharmacologic agents directly to delicate and nonapproachable treatment sites in the body with minimum side effects. Moreover, the direct use of drugs in particulate form can be very useful in the treatment of certain cancer cells, thrombosis, and in gene therapy. Enhancing the performance of physical methods for drug/gene delivery translates into the need to transfer the right amount of drug into the desired tissue or number of cells while minimizing undesirable cell death or tissue damage. Crucially, the physical parameters of each approach require systematic investigation to ensure maximal delivery with minimal cell toxicity[51]. For the moment, each method demonstrates a reasonable correlation between intracellular uptake and cell killing; that is, the better the delivery achieved, the greater is the risk that a cell will be compromised. It represents a reality that demands optimization of the methodology to achieve an acceptable balance between cellular uptake and viability.

2.2. Lasers in medicine

Laser is a device that emits electromagnetic radiation through a process called stimulated emission[52]. A laser consists of a gain medium inside a highly reflective optical cavity, as well as a means to supply energy to the gain medium. Light of a specific wavelength that passes through the gain medium is amplified. In its simplest form, the optical cavity consists of two mirrors arranged such that light bounces back and forth, and getting amplified with each passage through the gain medium. Typically one of the two mirrors, the output coupler, is partially transparent and the amplified laser beam is emitted through this mirror. The process of supplying the energy required for amplification is called pumping and it is typically supplied as an electrical current or as light at a different wavelength. Based on the type of gain medium used, lasers can be of different types. The output of a laser may be a continuous constant-amplitude output (CW); or pulsed, by using Q-switching, modelocking, or gain-switching. In pulsed operation, the output of a laser varies with respect to time, typically taking the form of alternating 'on' and 'off' periods. In many applications one aims to deposit as much energy as possible at a given place in as short time as possible. In laser ablation for example, a small volume of material at the surface of a work piece might evaporate if it gets the energy required to heat it up far enough in very short time. If, however, the same energy is spread over a longer time, the heat may have time to disperse into the bulk of the piece, and less material evaporates.

The mode locked laser (eg. Ti:Sapphire) is a most versatile tool for researching processes happening at extremely fast time scales also known as femtosecond physics.

These pulses are typically separated by the time that a pulse takes to complete one round trip in the resonator cavity[53, 54].

In a Q-switched laser (eg. Nd:YAG), the population inversion (usually produced in the same way as CW operation) is allowed to build up by making the cavity conditions (the 'Q') unfavorable for lasing. Then, when the pump energy stored in the laser medium is at the desired level, the 'Q' is adjusted (electro- or acousto-optically) to favorable conditions, releasing the pulse. This results in high peak powers as the average power of the laser (were it running in CW mode) is packed into a shorter time frame[55].

The first use of lasers in medical history was in 1962 when a dermatologist named Leon Goldman used it to remove a tattoo. Since Dr. Goldman first used a laser to remove a tattoo, lasers have become an integral part of modern medicine[56]. Most common use of lasers is in bloodless surgery[54, 55], ophthalmology[57] and dermatology[58]. They are increasingly being used for other forms of surgery including cancer and kidney stone treatment[59]. Photodynamic therapy (PDT)[60-62] is now an approved therapy in several areas of medicine. In a sense, however, the problem of lasers in medicine lies not in discovering a magical wavelength, but in learning how to best deliver the right wavelength, the right pulse width, the right pulse shape, the right beam profile and the proper amount of energy to create the best medical outcome possible. That is a matter of choice for the medical device industry, which, nonetheless, must produce a safe, effective and competitive laser system. A new wave of laser and fiber optic devices is beginning to make its way from the research labs. One of these is the femtosecond laser which falls in the category of ultrafast laser. These lasers with Ti:Sapphire doped lasing medium enable exceedingly high power lasers and low energy pulsed systems that allow precise focusing

with minimal heating to surrounding tissue. The main advantage of ultrashort laser pulses is the extremely short interaction time which suppresses any unwanted side effects of the laser irradiation of the tissue[53]. Secondly the broad spectra of the femtosecond laser pulses give the advantage to use the same laser pulses for diagnostic applications like imaging. For instance visible light could be used for surface applications like transdermal delivery or tattoo removal, while near-infrared (NIR) light could be used for non-invasive focusing when targeted towards deeper tissue applications[63]. This is because hemoglobin and water, the major absorbers of VIS and IR light, respectively, have their lowest absorption coefficient in the NIR region around 650–900nm.

Optoinjection[64] and optoporation[65] are laser-based methods capable of loading exogenous molecules into selected cells. In optoinjection, a single cell is directly irradiated by the focused laser beam and this cell alone is loaded with exogenous molecules[66, 67]. In optoporation, the laser beam does not usually interact with the cell but rather interacts with an absorptive medium, frequently polyimide[68-70]. A mechanical transient or stress wave is then produced as a result of optical breakdown, ablation, or rapid heating of the absorbing medium. This pressure wave interacts with nearby cells, causing temporary increase in the plasma membrane permeability and facilitates drug uptake. The exact nature by which shock waves transiently permeabilize membranes remains unknown but is an active area of investigation. Most recently, in vivo gene transfer using a femtosecond IR laser has been reported[71]. Photochemical therapy is another method where light energy is used to activate therapeutic compounds[72]. The laser-induced change in cell membrane permeability is transient and very fast, and does not appear, therefore, to damage cells extensively.

LSWs are generated by one of the following mechanisms: optical breakdown, ablation, or rapid heating of an absorbing medium (thermoelastic generation)[73]. Laser-induced mechanical effects in tissue have been the subject of extensive research, especially as these effects pertain to ophthalmology as in photodisruption[74, 75]. Doukas et. al. designed a system to study the biological effect of LSWs[70]. These studies showed that cell cultures exposed to stress waves experience a transient increase of the plasma permeability[74, 76, 70]. In addition, if the stress gradient is below the damage threshold, the cells remain viable. This was, perhaps, the most notable observation of cellular response to stress waves with potential applications to medicine. The change of the membrane permeability was said to resemble to some extent, that induced by electroporation[77] but the exact mechanisms by which the cell membrane opened and closed were not known. The capability of stress waves to kill cells depending on the state of cell activity has motivated the use of stress waves for the treatment of tumors. Cell cultures exposed to stress waves showed decreased viability only when the cell cultures were preincubated with the chemotherapeutic drug and the drug was present in the medium during the application of the stress waves. The proposed mechanism was that stress waves induced a transient increase of the membrane permeability which results in the diffusion of molecules, present in the medium, into the cells[78]

2.3. Nanomedicine

The development of a wide spectrum of nanoscale technologies is beginning to change the foundations of disease diagnosis, treatment, and prevention[4, 20]. Nanomedicine is a large subject area and includes nanoparticles, nanofibers or polymeric constructs that act as biological mimetics; nanoscale microfabrication-based devices, sensors and

laboratory diagnostics; and nanoscale particulate technologies capable of targeting different cells and extracellular elements in the body to deliver drugs, genetic materials, and diagnostic agents specifically to these locations[20].

Therapeutic and diagnostic agents can be encapsulated, covalently attached, or adsorbed on to nanocarriers[79, 80]. By virtue of their small size and by functionalizing their surface with synthetic polymers and appropriate ligands, nanoparticulate carriers can be targeted to specific cells and locations within the body after intravenous or subcutaneous routes of injection[27, 28, 18, 81-83]. Specific targets being investigated include macrophage, endothelium and solid tumors. The development of "stealth" technologies has provided opportunities for passive accumulation of intravenously injected nanoparticles (20–150 nm) in pathological sites expressing "leaky" vasculature by extravasation[79, 84]. Although, attempts have included delivery of drugs and imaging agents with different nanoscale technologies to the underlying parenchyma of injured arteries and rheumatoid arthritis, the majority of efforts are concentrated on solid tumors[80, 85].

2.3.1. Carbon–based nanostructures used in drug delivery

Carbon nanotubes (CNTs) are being widely investigated for targeted drug delivery[86, 87]. Functionalized CNTs with molecules and proteins attached to them were shown to translocate across cell membranes suggesting promising applications in drug delivery. It has also been shown that for nucleus-targeted molecules transported inside living cells by single-walled carbon nanotubes (SWNTs) can translocate into cell nucleus upon endosomal rupture triggered by NIR laser pulses[88]. Direct non-endocytic delivery of plasmid DNA was also achieved using a technique called "nanotube spearing"[89].

2.3.1.1. Carbon black nanoparticles:

Carbon black (CB) is a particulate form of industrial carbon produced by thermal cracking or decomposition of a hydrocarbon raw material, similar to graphite in its microstructure[90]. Ninety-five percent of all CB is made using the furnace process. The feedstock (oil) is injected into a high temperature reactor where the hydrocarbon is cracked and dehydrogenated to form carbon with a quasi-graphitic microstructure. CB is composed of very small primary particles, which fuse to form branched aggregates. Aggregates are the smallest functional unit of CB. They are formed through the fusion of smaller units, called primary particles, into a three dimensional branched chain structure. This fusion can be controlled in the reactor to give varying degrees of clustering. Grades of CB in which the particles are allowed to cluster into relatively large, complex aggregates are known as high structure grades. Grades where the extent of aggregation is minimized are known as low structure grades. The size of primary particles can be controlled during production. Sizes can range from 8 nm for high surface area grades of CB up to 75 nm for a CB with low surface area.

2.3.1.2. Biocompatibility of carbon black

Finely divided amorphous carbon particles generally are well tolerated by the body. The essentially passive nature of carbon in human flesh has been known since ancient times, and India ink, charcoal and lampblack (roughly spherical 10-20 nm particles) have been used for ornamental and official tattoos[91]. Colloidal carbon is usually assumed to be nontoxic. Large amounts of carbon particulate debris loose in the body, even around the spinal dura and nerves, evidently are tolerable. CB, the most common

amorphous carbon particles that have been subjected to extensive biological experimentation, is regarded as largely inert. CB is distinctly different from, and more benign than, carbon soot. India ink, traditionally used for drawing, is a dispersion of CB in water. India ink is often used as a phagocytosis labeling agent or a cell differentiation tracer because CB is easily administered, is relatively nontoxic, and is easily observed in cells that have taken it up[92, 93]. CB is also employed in tattoos, both cosmetic and medical. For example, India ink is used for endoscopic colonic tattooing[91] and lymphatic mapping[94]. It produces a long-lasting stain with relatively low risk of adverse reaction and toxicity. Macrophages and platelets are known to clear colloidal carbon particles from the blood[95, 96]. However the ultimate fate of these particles in the body is still an area of active research. According to some studies, the macrophages ultimate circulate them to the lymphatic system through which they end up in lymph nodes[97, 98].

2.4. Laser–CB interaction for intracellular drug delivery

Since the 1990s, there has been a large volume of literature establishing the phenomenon of photoacoustic shock generation in CB suspensions irradiated with short laser pulse. In 1995, Chen et al. showed that this anomalous photoacoustic effect was due to high-temperature chemical reactions between surface carbon and surrounding water, or the endothermic carbon-steam reaction, $C(s) + H_2O(l) \rightarrow CO(g) + H_2(g)$[99]. Irradiation of carbon nanoparticle suspensions with high power pulsed laser radiation have been reported to produce shock waves[100, 101], various chemical species[102, 103], sonoluminescence[104] and an anomalously large sound wave called the "Giant Photoacoustic effect"[99]. These pressure forces were believed to be caused by the sudden volume change caused by vaporization of fluid surrounding the heated carbon particles

and the reaction of this vapor with carbon to initiate the endothermic carbon-steam reaction. Chemical reactions were also reported when the suspensions were made in non-aqueous solvents like toluene and benzene[103]. Formation of gas bubbles due to fluid vaporization around the heated particles as well as the product gases of chemical reaction are also believed to cause cavitation bubble dynamics which may lead to the strong pressure forces[105, 106].

This act of activating suspended carbon "nano-bombs" in a liquid with the use of a laser may be seen as analogous to ultrasound-mediated cavitation wherein ultrasonic energy is used to cause implosion of suspended gas bubbles[107]. Cavitation is the formation of pockets of vapor in a liquid. This process is caused by low pressures in the liquid. When the local ambient pressure at a point in the liquid falls below the liquid's vapor pressure, the liquid undergoes a phase change to a gas, creating "bubbles" or, more accurately, cavities, in the liquid. An important feature of cavitation which has potential in drug/gene delivery is inertial cavitation. Inertial cavitation is characterized by oscillating bubbles that collapse violently after a few cycles. This can raise the local pressure to hundreds of atmosphere. It is an energy-releasing process that creates high fluid velocities, shock waves, microjetting, and sonoluminescence. These properties of cavitation have been used in ultrasound-mediated drug delivery to create reversible breaks in the cell membrane[43, 108]. In this technique, called acoustic cavitation, an acoustic field is used to generate the cavitation bubbles. Sonoluminescence too has been observed in ultrasound-mediated delivery during acoustic cavitation[109]. The fundamental similarity between acoustic cavitation and laser-carbon mediated photoacoustic effects suggests the possibility of exploiting the latter as a potential drug delivery strategy.

2.5. Photoacoustics and its application in bioengineering

The photoacoustic effect refers to the generation of acoustic waves by the absorption of electromagnetic energy, such as optical or radio-frequency waves. Alexander Graham Bell first reported the observation of sound generated by light in 1880. Bell used this phenomena in making the photophone, a device that used light to transmit sound[110]. In modern medicine, the photoacoustic effect is used for a noninvasive diagnostic technique called photoacoustic imaging[111]. When used for more complicated structures it is called photoacoustic tomography (PAT). In photoacoustic imaging, non-ionizing laser pulses are delivered into biological tissues. Some of the delivered energy will be absorbed and converted into heat, leading to transient thermoelastic expansion and thus wideband (e.g. MHz) ultrasonic emission. The generated ultrasonic waves are then detected by ultrasonic transducers to form images. Since optical absorption is closely associated with physiological properties, such as hemoglobin concentration and oxygen saturation and since the magnitude of the ultrasonic emission (i.e. photoacoustic signal) is proportional to the local energy deposition, the US waves reveal physiology specific optical absorption contrast. 2 dimensional or 3 dimensional images of the targeted areas can then be formed. The same principle is also used in material science for photoacoustic spectroscopy, a non destructive material analysis technique[112]. Photoacoustic effects are also being investigated for the development of novel bioengineering research tools like photoacoustic flow cytometry[113].

2.6. Intracellular delivery in plant systems

Intracellular delivery in plant cells, which is chiefly gene delivery, suffers from essentially the same challenges as mammalian cells. The challenges are only compounded by the additional barrier called the cell wall[114] present outside the cell membrane. The cell wall is a network of polymers surrounding the plant cell membrane and it gives the cell structural support[115]. Most intracellular delivery strategies are effective in plant cells only after removal of the cell wall through use of enzymes. The resulting cell without the cell wall is called a protoplast. Protoplast generation is a destructive process and results in very low efficiency of gene transfer due to low cell viability[116, 117]. Hence most research in plant gene delivery are oriented towards finding a method that can deliver genes to intact cells without the need for protoplast formation[118, 119].

Improved gene delivery methods are important for the pulp and paper industry for genetic engineering of timber producing trees[120]. The global consumption of industrial timber is growing and approximately 90% of this requirement is being supplied by natural forests causing adverse effect on the environment, biodiversity and global climate. Clonal forests are one way to continue supplying sufficient wood products sustainably for a growing world population, while at the same time conserving these natural ecosystems. In such tree farms, trees genetically engineered for the desired traits will be routinely grown and harvested like food crops without endangering the natural forests. Genetic engineering is a relatively new technology for forest trees. Owing to long lifetimes of trees, only limited data are as yet available that characterizes the expression of novel genes in mature trees. Loblolly pine transformation is of particular interest

because of its dominant position in the forest products industry throughout the southeastern United States. Current methods of plant transformation have had limited success with pines, and patent claims restrict their use. Hence there is a need to develop alternative techniques[121-123].

2.7. Assessment of current delivery strategies in plant systems

Common methods of gene transfection in plants can be broadly classified as (a) biological or indirect, and (b) direct methods.

2.7.1. Biological or Indirect methods

Biological methods are based on the introduction of gene constructs into the target cells/tissue by means of Agrobacterium tumefaciens[124]. A. tumefaciens is a soil bacterium whose virulent strain causes the crown gall disease in dicotyledonous plants. This tumor-inducing capability is due to the presence of a large Ti (tumor-inducing) plasmid. During the infection process, a Ti plasmid is transferred from the bacterium to the plant where it stably integrates into the nuclear DNA. Agrobacterium-mediated transformation is the only known natural occurence of DNA transfer between kingdoms, making it the preferred system for genetically transforming plants[125, 126]. However, large-scale use of this organism in conifer transformation has been limited due to difficulty of propagation of explant material, selection inefficiencies and low transformation frequency[127, 128].

2.7.2. Direct methods

Direct transfer methods rely entirely on physical or chemical principles to deliver

DNA into the plant cells. Some of the methods described include particle bombardment[129], liposome-mediated protoplast transformation[130], electroporation[131] and whisker-mediated transformation[132]. Among these methods, particle bombardment or the gene gun approach has proved to be the most versatile and effective transformation technique, not limited by cell type. However the high expense of gene gun accessories as well as intellectual property right issues limit its use, and necessitates development of alternative methods to achieve efficient plant transformation[133]. Most of the other direct delivery techniques require the use of protoplasts, which is destructive and inefficient[134].

2.8. Ultrasound for direct gene delivery

Early studies have shown ultrasound to be disruptive to the root meristem and to reduce the growth rate of roots of Vicia faba and Pisum sativum[135, 136]. Miller et al. found an immediate reduction in DNA, RNA and protein synthesis in sonicated Pisum sativum roots exposed to therapeutic ultrasound followed by an apparent recovery several hours later. Similarly, reversible inhibition of protein, purine and pyrimidine biosynthesis has been reported in sonicated cells of Saccharomyces cerevisiae. Joersboe et al. found that protein synthesis was significantly enhanced in sugar beet suspension cells and protoplasts by a brief exposure to 20 kHz ultrasound at relatively low intensities, while at higher intensities overall protein synthesis declined[137]. One explanation was that higher uptake of nutrients from the medium due to sonication-induced cell permeability led to enhanced protein synthesis.

Ultrasound has been reported to facilitate gene uptake into plant protoplast and suspension cells[138, 139]. Stable transformation of tobacco has been reported by sonicating leaf segments at the same intensity as that for protoplasts but for a 2000-fold longer

exposure time[140]. The same conditions were used for the stable transformation of potato tuber discs[141]. Viability studies of petunia cell suspensions exposed to 2 MHz ultrasound showed the age of the cell culture to be another factor in ultrasound-induced cellular bioeffects. At 4 days after subculture the cells are in a period of maximum mitotic division with relatively thinner walls. This reduced mechanical stability might make them more susceptible to ultrasound induced damage[142]. Ultrasound is also used in sonication-assisted Agrobacterium-mediated transformation (SAAT)[143]. This involves subjecting the explant to brief periods of ultrasound in the presence of Agrobacterium. SAAT treatment produces a large number of small uniform wounds throughout the explant tissue which allows easy access by the Agrobacterium and improves transfection

These studies show that ultrasound has the potential to permeabilize the plant cell membrane and facilitate uptake of molecules including proteins and DNA. As with mammalian cells, it is important to optimize parameters such as energy intensity and exposure time so that the beneficial aspects viz. uptake is not accompanied by unwanted cell death. However relatively fewer studies involve ultrasonic transfection of intact plant cells[115], and so it is unclear as to how effective ultrasound is in permeabilizing the cell wall. Based on the few that do exist, it could be said that the thinner the cell wall, the easier it is to permeabilize them[144]. So along with optimizing ultrasound parameters, it is important to choose plant cells at the right stage of development to achieve efficient transfection. Once these questions are answered, ultrasound may become an inexpensive and simple alternative to more sophisticated methods like gene gun.

CHAPTER 3
MATERIAL AND METHODS-1

This chapter discusses the protocols used for conducting the study involving photoacoustic drug and gene delivery using short laser pulses and carbon nanoparticles in mammalian cells.

3.1. Study with femtosecond Ti: Sapphire laser

3.1.1. Laser apparatus

A femtosecond Ti: Sapphire laser system (CPA-1000, Clark-MXr, Dexter, MI) was used to irradiate cell samples[145]. The femtosecond Ti: Sapphire oscillator was pumped by a 532 nm continuous-wave diode laser (Verdi, Coherent, Santa Clara, CA) with output power of 3.5 W. The oscillator generated 100 fs laser pulses of 4 nJ at 800 nm with 90 MHz repetition rate. The pulsed output from the oscillator was stretched from 100 fs to 100 ps and sent to the regenerative amplifier. The amplifier was pumped by a 1 kHz Q-Switched Nd:YAG laser at wavelength of 532 nm with output power of 7.5 W. After amplification, the pulse was recompressed to 100 fs in the compressor. Typically, the compressor delivered 800 nm laser pulses at 1 kHz repetition rate with pulse energy of 1 mJ. The amplified femtosecond laser pulses of 800 nm wavelength were focused onto the sample holder with spot diameters (typically 0.5 mm to 3 mm) needed to achieve a given fluence using a biconvex lens (BK7-KBX058, Newport, Irvine, CA).

3.1.2. Cell sample preparation

Human prostate cancer cells (DU145, American Type Culture Collection,

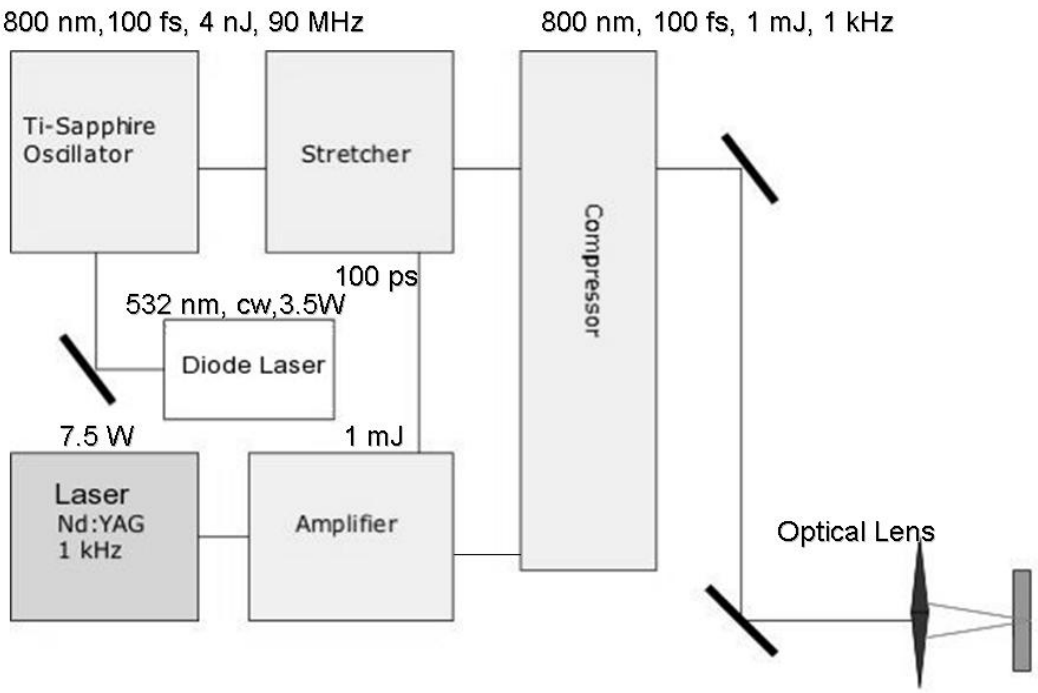

Figure 3.1: Schematic diagram of femtosecond laser apparatus

Manassas, VA) and rat gliosarcoma cells (GS 9L, courtesy of Dr. Henry Brem, Johns Hopkins University, Baltimore, MD) were cultured as monolayers in a humidified atmosphere of 95% air and 5% CO_2 at 37°C in RPMI-1640 medium (Cellgro, Herndon, VA) supplemented with 100 g/mL penicillin-streptomycin (Cellgro) and 10% (v/v) heat inactivated FBS (Atlanta Biologicals, Atlanta, GA). For each experiment, cells at 80-90% confluence were harvested by trypsin/EDTA (Cellgro) digestion, washed and resuspended in fresh growth medium with FBS at a cell concentration of 10^6 cells/ml. DU145 cells[146] were used as a model cell line in most experiments because they are well characterized; used extensively in experimental studies, including numerous ultrasound-mediated delivery experiments in our lab[42, 48, 147]; and serve as a good precursor to three-dimensional tumor models[148].

3.1.3. Cell pretreatments

CB suspensions were prepared by sonicating aqueous solutions of CB (Black Pearls® 470, courtesy of Cabot Corporation, Billerica, MA) at 0.4 mg/ml for at least 2 min in presence of 0.1% (w/v) sodium dodecyl sulfate (Sigma-Aldrich, St. Louis, MO) to minimize particle aggregation. These were the same particles that had previously been shown to cause laser-induced photoacoustic emissions[99, 101, 103, 104]. According to the manufacturer[90], the average primary particle diameter was 25 nm, but additional analysis by Microtrac Lab Services (Montgomeryville, PA) showed that these primary particles existed as aggregates of 200 nm average diameter, which corresponds to approximately 133 particles per aggregate (Appendix A). Prior to laser irradiation, CB were added at a final concentration of 29.6 μg/ml to 500 μl cell suspension, unless otherwise noted.

In some experiments, CB were replaced with MWNT (NanoLab, Newton, MA), which had 30±15 nm outer diameter and 1-5 μm length. They were dispersed at a concentration of 0.4 mg/ml according to manufacturer's instructions in presence of Nanosperse AQ (NanoLab, Newton, MA) as the surfactant. For every 0.1 g MWNT, 4 drops of Nanosperse AQ were added. In other experiments, CB were replaced with gold nanorods that were synthesized according to the seed-mediated growth method to produce rods with aspect ratio of 3.9 and longitudinal surface plasmon absorption band around 800 nm[149].

To measure intracellular uptake, solutions of fluorescent marker compounds dissolved in phosphate-buffered saline (PBS, Cellgro) were added to cell-carbon suspensions before irradiation at a final concentration of 10 μM calcein or FITC-labeled BSA (Molecular Probes, Eugene, OR). Both calcein (623 Da, radius 0.6 nm) and FITC-

BSA (66 kDa, radius 3.6 nm) are negatively charged, biologically inert green-fluorescent molecules widely used as tracers of intracellular delivery[150, 151]. To measure intracellular DNA uptake, plasmid-DNA (6.7 kbp or 100 nm radius, gWiz™ Luciferase, Aldevron, Fargo, ND) was labeled by incubation with YOYO-1 dye (Molecular Probes) for 10 min at a ratio of one YOYO-1 molecule per 10 bp of plasmid DNA[51] and then added to cell-carbon suspensions at a final concentration of 4 nM within 1 s before irradiation. Fluorescence from marker compounds retained within cells was measured by flow cytometry, as described below.

To identify nonviable cells after irradiation, and eliminate them from analysis, PI (Molecular Probes), which stains nonviable cells with red fluorescence, was added to samples at a final concentration of 0.37 μM at least 15 min after irradiation and before assaying with flow cytometry[42]. DNA transfection was studied using the Luciferase Assay System (Promega, Madison, WI) 48 h after irradiation. Relative light unit (RLU) emission due to luciferase transfection was measured using a luminometer (Turner Designs TD-20/20, Promega). RLU was converted to absolute protein concentration with a standard calibration curve prepared using luciferase protein (QuantiLum® Recombinant Luciferase, Promega)[51].

To study effects of viscosity, the kinematic viscosity of the suspension medium was increased from 1.1 cSt to 5.3 cSt by adding carboxymethylcellulose (Sigma-Aldrich) to PBS at 400 mg/ml. Viscosities were measured using a Cannon-Ubbelohde viscometer (50-B680, Cannon Instrument, State College, PA). Cells were pelleted and resuspended in the more viscous media before irradiation.

To deplete cells of K^+, cells were centrifuged and pelleted in K^+-free buffer (140 mM NaCl, 1 mM $CaCl_2$, 1 mM $MgCl_2$, 1 mg/mL D-glucose in DI H_2O, pH 7.4) followed by hypotonic shock for 5 min in K^+-free buffer diluted 1:1 with DI water[48]. After 5 min, cells were spun down and resuspended in full strength K^+-free buffer where they remained for the remainder of the experiment.

3.1.4. Experimental protocol

Exposure chambers were constructed from glass cylindrical cells (37-PX-2, Starna Cells, Atascadero, CA). The stem of the cell was cut to approximately 5 mm, and fitted with a glass stopper. Samples were prepared by mixing known volumes of carbon suspension and uptake marker with 500 µl of cell suspension and then aliquoting this solution into the exposure chamber, whose volume was approximately 560 µl. The resulting small headspace filled with air facilitated mixing of the chamber contents during irradiation.

The chamber was then mounted on a custom-made stand that could three-dimensionally microposition the sample to obtain desired spot diameters of the incident laser beam. The contents of the chamber were mixed during irradiation in part by rotating the chamber at 5 rpm manually. After irradiation, samples were transferred into 1.5 ml microcentrifuge tubes and kept at room temperature for 5 min. The tubes were then placed on ice until all samples had been irradiated (2 to 3 h). Control samples or "sham exposures" were not irradiated, but subjected to all other procedures.

3.1.5. Data acquisition and analysis

Flow cytometry was used to determine molecular uptake, i.e., fraction of cells containing intracellular fluorescent molecules, and loss of cell viability by detecting the fluorescence intensity from uptake molecules and PI, respectively, on a cell-by-cell basis. A benchtop flow cytometer (BD LSR, BD Biosciences, San Jose, CA) was used to measure the green fluorescence of cells with intracellular uptake (FITC fluorescence, 530/28 nm bandpass filter) and to distinguish viable from non-viable cells by the red fluorescence of PI (PerCP fluorescence, 670 nm longpass filter). Typically each aquisition included approximately 10,000 cells per sample. Intracellular uptake levels were quantified by converting fluorescence measurements to average numbers of molecules per cell using calibration beads (Quantum™ FITC MESF High Level, Bangs Laboratories, Fishers, IN)[152]. Because the flow cytometer could not count fragmented cells, the mass flow rate of viable cells through the flow cytometer was counted in each sample and then normalized to the mass flow rate of viable cells counted in a non-exposed sample. Because the flow cytometer operated at constant flow rate, this mass balance method accounted for both intact and fragmented non-viable cells.

Cells were imaged using a Zeiss LSM 510 confocal laser-scanning microscope or Zeiss LSM META/NLO 510 multiphoton microscope (Zeiss, Thornwood, NY). Images of intracellular uptake were captured by directing a 10X magnification air objective or a 40X magnification oil objective at the center of each cell.

3.1.6. Statistical analysis

A minimum of three replicates was performed for all conditions. Replicates enabled calculations of means and SEM. The equality of mean response (uptake/viability) between treated samples and sham exposures /control samples was tested using ANOVA (α=0.05). To test equality of mean response between pairs of data points, 1-way ANOVA followed by the post hoc Tukey's pairwise comparison was used, whereas 2-way ANOVA was employed to compare three or more data points using MINITAB (Minitab Inc., State College, PA). To test the interaction of three factors, a global 3-way ANOVA was used via a general linear model. The null hypothesis was that the average fraction of cells with uptake (or average fraction of viable cells) between a treated sample and a sham exposure were equal. Data on graphs are reported as mean ±SEM.

3.2. Study with nanosecond Nd: YAG laser

3.2.1. Laser apparatus

A pulsed Nd: YAG laser (Surelite I-10, Continuum, Santa Clara, CA) was used to irradiate samples. The laser operated at 10 Hz and the pulse energy was varied between 25 mJ to 100 mJ by changing the Q-switch delay. The laser typically emitted light with a wavelength of 1064 nm in the IR. For some experiments, the laser pulses were frequency doubled to generate light at 532 nm and 355 nm wavelengths.

3.2.2. In situ mass spectroscopy

During laser irradiation of the carbon suspension with 1064 nm photons, gas bubbles were formed within the liquid. To determine the constituency of the gas, we

injected the air volume above the post irradiated liquid into a custom built gas analyzer apparatus. The analyzer system consists of a low vacuum gas manifold for dosing the sample gas into a high vacuum chamber that is equipped with a turbo molecular pump, ionization gauge pressure reader, and a quadrupole mass spectrometer (QMS)[153]. The background pressure of the high vacuum chamber was 5×10^{-9} torr. Typically, the sample gas was injected through a septum into low vacuum manifold where the pressure was reduced to approximately 2 torr. The gas was then introduced into the high vacuum chamber until the background pressure reached 1×10^{-7} torr. The gas dosing rate was held constant until the complete mass spectrum of the sample gas was measured by the QMS.

3.2.3. Mouse preparation

For initial induction of anesthesia, each mouse (CD-1, Charles River Laboratories, Wilmington, MA) was anesthetized using isoflurane (5% delivered in 100% medical grade oxygen using mask). Once anesthetized, hair from the TA muscle was removed by treatment with the depilatory Nair. Carbon nanoparticle suspensions were prepared in DI water in presence of sodium dodecyl sulfate and then filter sterilized. Prior to experiment a solution of PI with the carbon nanoparticle suspension was prepared in sterile PBS (1X). 10 μl of PI was added to 1 ml of an aqueous CB suspension containing CB at 30 μg/ml. About 5 μl of this solution was then injected into each TA using a 26 gauge needle and the needle held there for approximately 5 min so that the solution did not leak out. Within 15 min after injection, the muscle was treated with the 1064 nm wavelength of a Nd: YAG laser. The anesthetized mouse was placed under the laser beam with the leg held taut such that the TA lay within the focal diameter of the beam. The TA on the right leg served as a negative control (not exposed to laser but subjected to

all other treatments) and the TA on the left leg was exposed to laser. Laser pulses were applied to the skin at the injected site for 1 min. The mice were euthanized while still under anesthesia 1 hour post exposure and the TA muscle was removed for subsequent microscopy and histological analysis. Results for each exposure are based on three replicates.

3.2.4. Histology and microscopy of mouse tissue

Propidium iodide (Invitrogen, Carlsbad, CA), a DNA-binding dye that is impermeable to intact cells, was used as a maker for uptake. Uptake was studied for 75 mJ/pulse, and for an exposure time of 1 min. The excised muscles were immediately immersed in Tissue Tek OCT compound (VWR, Bridgeport, NJ) and frozen using dry ice. The frozen sections were then cut along their longitudinal axis into 10 μm thick sections using a cryostat (CM3050S, Leica Microsystems, Bannockburn, IL). The slides were first examined using fluorescent microscopy and then they were stained with H&E for light microscopy. The extent of PI uptake was then visualized for the control and treated samples using a stereomicroscope (Eclipse E400, Nikon, Melville, NY).

Nitorblue tetrazolium chloride assay (NBT) was used to identify enzymatically active cells[154]. In these experiments, the biopsied TA was cut into 3 slices about 5 mm thick along the transverse axis. The sections were blotted dry and then incubated in a phosphate-buffered solution of NBT (Sigma-Aldrich) for 25 min at room temperature. NBT serves as a viability marker by labeling viable cells blue. Each section was immersed in OCT compound and frozen using dry ice. Each frozen section was then cut along the transverse axis into 10 μm thick sections using a cryostat. For each section to

be studied for uptake and viability, a corresponding section was also taken for H&E staining. The sections were then observed under the microscope.

Uptake for the transverse sections was quantified using the imaging software ImagePro-Plus (Media Cybernetics, Bethesda, MD). For each muscle section, consecutive views were captured in both light and fluorescent fields such that the entire section was captured as a montage of smaller images at 10X magnification. The area of the muscle from the bright field image was first measured using the software. The corresponding fluorescent image gave the area with PI uptake. This was then expressed as a fraction of the total area to give the percent area with uptake.

CHAPTER 4
MATERIAL AND METHODS-2

4.1. Study with ultrasound

This chapter discusses the protocols used for conducting the study involving US-mediated gene delivery in plant cells. The study was conducted with tissue cultured loblolly pine cells and reporter plasmids.

4.1.1. Ultrasound apparatus

The US chamber was made from a cylindrical piezoelectric transducer sealed between two PVC pipes. US was generated at 24 kHz by a function generator and amplifier that controlled the transducer via a matching transformer. Parameters, including the frequency, duty cycle, incident pressure, pulse length and exposure time, were set using this system. Acoustic parameters were monitored using the oscilloscope. The wave amplitude set in the function generator was sent as a voltage signal to the transducer and read in the oscilloscope as the applied voltage. This voltage was converted to incident pressure by using the equation: P= 0.0084V, where P is the pressure (atm) and V is the oscilloscope voltage. Within the apparatus, standing waves were formed with maximum amplitude along the central axis at 11 cm height above the base. Acoustic pressure had less than 5% variation within the region ± 7.5 mm in height and ±3 mm in radius around the site of maximum amplitude[46]. Cell suspension samples were placed within this region. The exposure chamber was filled with DI water, and degassed for 3 hours. The sample containers were sterilized transfer pipettes (Fisher Scientific, Pittsburgh, PA).

US was produced in a burst mode where short bursts of US were transmitted followed by a time where no US was transmitted before the next burst was produced. The sum of all of the bursts of US equaled the total exposure time for the sample, and the actual exposure time was 10% of the total exposure time. US was accurately transmitted at a defined frequency, peak pressure, burst length, number of bursts, and duty cycle. For the 24 kHz exposure, cell samples were exposed to acoustic energies between 0- 400 J/cm^2. Acoustic energy was calculated from pressure, using the relation; $E=(P/\sqrt{2})^2 t/\rho v$, where P is the pressure, t is the actual exposure time, ρ is the density of water and v is the velocity of sound in water.

4.1.2. Loblolly pine tissue culture

Loblolly pine (Pinus taeda L.) cultures were initiated as described by Pullman and Johnson[155]. Cultures were maintained with weekly transfers in liquid suspension culture medium with a ratio of 1 part settled cells in 9 parts medium. Loblolly pine was chosen as the target tissue for transformation because: (i) it is an economically important species, (ii) it had a well established tissue culture and regeneration system, (iii) the resources to maintain target tissue/cells for transformation and screening were readily available. Throughout the course of this study a deliberate effort was made to test more than one genotype.

4.1.3. Plasmid preparation

Plasmids encoding for GUS and GFP were donated by Professor Zheng-Hua Ye (Dept. of Plant Biology, University of Georgia). Plasmids were expanded in E.coli by transforming bacterial cells ((Invitrogen, Carlsbad, CA) with the plasmids using heat

shock and growing the bacterial in media supplied with kanamycin (30 μg/ml, Sigma, St. Louis, MO). Plasmids were then extracted from bacterial cells by alkaline lysis and purified with an Endonuclear Giga kit (Qiagen, Valencia, CA). The quality of purified plasmids was analyzed by electrophoresis on 1% agar gel to verify that the lengths of obtained fragments were in full agreement with the provider DNA map. The final DNA concentration was determined by measuring absorption at 260 nm.

4.1.4. Sonication protocol

Loblolly pine cultures either in their 2nd or 3rd day of weekly subculture were used for sonication experiments. This was to ensure that cells were in a phase of active cell division to facilitate DNA entry and integration. Unless otherwise mentioned, 1 ml of settled cells was mixed with 20 μL of plasmid DNA (1 μg/ml) and the mixture was incubated for at least 30 min at room temperature. Prior to sonication, the cell-DNA mixture was transferred to a sterile sample chamber (Fisher Scientific, Pittsburgh, PA) made by cutting the stem of a transfer pipette so that it resembled a U-shaped vessel with a small neck. The remaining volume in the chamber after adding the cells was filled with liquid culture medium. The mouth of the vessel was then plugged with a long plastic stem (Fisher Scientific, Pittsburgh, PA) taking care that no air bubbles remained inside the chamber. Samples were then exposed to ultrasonic fields of intensities ranging from 50 to 400 J/cm^2 for 10-50 s and then transferred back to liquid media or semi-solid media[155]. After 48 h the sonicated cells were assayed for gene transfection. Negative controls were not sonicated, but subjected to all other procedures.

4.1.5. SCMT protocol

A sterile 5% (w/v) suspension of SiC whiskers (Alfa Aesar, Ward Hill, MA), in water was prepared immediately prior to use. For each sample, 1 ml of settled cell volume of loblolly pine suspension cells was dispensed into a 1.5 ml sterile microcentrifuge tube (VWR, Bridgeport, NJ). SiC whiskers were then added to the sample at a final concentration of 0.4 mg/ml followed by 20 μl of 1 μg/μl plasmid DNA solution. The microcentrifuge tube was then vortexed for 60 s at 10 rpm using a Vortex Genie 2 (VWR). After treatment the cells were placed in 12-well plates, supplemented with fresh growth media and incubated in room temperature for 48 h.

4.1.6. Gene transfection assay

The histochemical assay to screen for expression of glucurodinase (GUS) activity in genetically modified cells was carried out according to manufacturer's protocol using a substrate called X-Gluc (Sigma)[156]. The substrate gives a blue precipitate at the site of enzyme activity indicating expression of the transferred gene. GFP expression was assayed under a Zeiss LSM META/NLO 510 multiphoton microscope (Zeiss, Thornwood, NY) using the green florescence filter sets. Cells with GFP transfection showed green florescence when compared to non exposed controls[157, 158]. Transient expression assays were normally carried out 48 h post treatment.

4.1.7. Cell proliferation assay

To study the effect of sonication on long term viability, sonicated cells were plated in semi-solid media and their ability to form new cells studied over a period of 8

weeks. 1 mL of the sample volume on an average contained about 10-20 embryos. Each of these embryos was individually plated in a well of a 24-well plate filled with semi-solid maintenance media. The plates were then stored in the dark and observed periodically. After 8 weeks, it was observed that some of the embryos had proliferated to form colonies while others had turned brown. The number of wells which contained proliferated embryos was then expressed as a fraction of the total number of wells that were plated.

CHAPTER 5
PHOTOACOUSTIC DELIVERY INTO CELLS USING CARBON NANOPARTICLES ACTIVATED BY FEMTOSECOND LASER PULSES

A major barrier to drug and gene delivery is crossing the cell's plasma membrane. Here we show a physically-based mechanism to deliver molecules into cells with high efficiency and viability using photoacoustic effects generated by carbon nanoparticles. We demonstrated intracellular delivery using this method in multiple cell types for uptake of small molecules, proteins and DNA. At optimized conditions, calcein uptake was seen in up to 50% of cells with nearly 100% viability and in 90% of cells with ≥90% viability. Uptake was not observed when cells were irradiated in the absence of carbon nanoparticles. Our studies suggest that uptake occurs due to transient membrane permeabilization resulting from explosive photoacoustic forces generated by laser-induced carbon-water reaction, $C(s) + H_2O(l) \rightarrow CO(g) + H_2(g)$. This synergistic use of nanotechnology with advanced laser technology could provide an alternative to viral and chemical-based drug and gene delivery.

5.1. Introduction

Effective drug delivery is vital to the success of pharmacological therapy. One of the key barriers in drug delivery is transport of drugs across the cell membrane. Many pharmaceutical agents such as plasmid DNA, oligonucleotides[159], siRNA[12], mitochondria-targeting proapoptotic drugs[15] and lysosomal enzymes[160] need to be delivered intracellularly to exert their therapeutic action. Intracytoplasmic delivery could also overcome important obstacles in anticancer chemotherapy such as multidrug

resistance[161]. However, the cell membrane prevents large molecules like peptides, proteins, and DNA from spontaneously entering cells unless there is an active transport mechanism, such as endocytosis[7]. Endocytosis typically subjects molecules to lysosomal degradation, which can reduce their availability inside the cell and diminish their potency. Hence, methods for direct intracytoplasmic delivery that bypass the endocytic pathway are required.

Existing intracellular delivery strategies can be broadly classified as biological, chemical and physical[16]. Biological methods include viral vectors, which are efficient, but can cause side effects like mutagenicity and host-immune rejection[17]. Chemical formulations such as cationic lipids and polymers have drawbacks associated with endocytic delivery, targeting inefficiency and cell-type dependency[162, 163]. Physical methods, on the other hand, drive molecules across the cell membrane into the cytoplasm without the use of active cellular transport mechanisms and generally work with many cell types. In contrast to most biological and chemical approaches that can diffuse away from the site of administration, physical methods lend themselves to spatial targeting only at the site of physical intervention, which minimizes side effects to neighboring tissues. However, physical methods are often associated with inefficient delivery into cells[29].

A common feature of physical techniques is that they increase cell permeability via the creation of transient, nano-scale holes in the plasma membrane. Better macromolecular delivery is possible if pores are large and open for a long time; on the other hand, large, long-lived holes increase chances that the cell will die. The challenge for physical drug delivery strategies is to optimize the size and lifetime of these holes to

obtain maximum intracellular uptake without sacrificing viability. Moreover, a desirable strategy would be one that is not only efficient, but also inexpensive, easy to use, minimally invasive and broadly applicable. Current physical methods for intracellular drug delivery include particle bombardment[31-33], electroporation[38, 39], magnetofection[34], US[164] and laser[64, 67]. However, none of these methods satisfy all the requirements discussed[29].

Our approach to intracellular delivery uses photoacoustic forces mediated by CB nanospheres and ultrashort laser pulses to create transient openings in the plasma membrane. This approach was motivated by previous work with US-mediated cavitation showing that transient bubble collapse can cause intracellular uptake via membrane permeabilization[43, 48, 165]. Although cells located an optimal distance from a collapsing bubble are reversibly permeabilized, cells are killed if they are too close and cells located farther away are unaffected[49]. Because bubble collapse is always a highly energetic event, uptake by a significant fraction of cells is usually accompanied by extensive loss of cell viability.

Photoacoustic forces generated by laser excitation of carbon nanoparticles can provide a highly controlled shock wave that we hypothesize can be tuned to reversibly permeabilize cells located close by without loss of cell viability. The phenomenon of photoacoustic shock generation in CB suspensions irradiated with short laser pulse is well established[100]. In 1995, Chen et al. showed that this anomalous photoacoustic effect was due to high-temperature chemical reactions between surface carbon and surrounding water, or the endothermic carbon-steam reaction, $C(s) + H_2O(l) \rightarrow CO(g) + H_2(g)$[99]. We therefore designed this study to address two basic components of our hypothesis: (i) Can

the laser-carbon interaction known to generate photoacoustic shock via carbon-steam reaction facilitate efficient intracellular uptake in viable cells? (ii) Is uptake mediated by photoacoustic forces via transient membrane permeabilization?

5.2. Results

5.2.1. Visual evidence of uptake

To determine if pulsed laser irradiation of CB delivers exogenous molecules into cells, we exposed suspensions of DU145 human prostate cancer cells and CB nanospheres measuring 25 nm in diameter to femtosecond 800 nm-wavelength laser pulses in the presence of calcein, FITC-labeled BSA, or YOYO-1 labeled DNA in separate experiments (Section 3.1.2-6). The intensity of the beam was adjusted near the intensity known to initiate chemical reactions[103]. Unless otherwise specified, cell samples exposed to laser in presence of carbon nanospheres are referred to as "treated" and control cell samples not exposed to laser but subjected to all other treatments are referred to as "sham exposures."

Confocal microscopy showed intracellular uptake of all three compounds, indicating that laser irradiation of CB permeabilized cells. Calcein uptake was visualized across many cells (Figure 5.1a) and found throughout the cytosol and nucleus (Figure 5.1b). BSA was mostly in cytosol but not the nucleus since BSA is larger than nuclear pores (Figure 5.1c). DNA appeared uneven and highly localized at some points due to slow diffusion in cytosol (Figure 5.1d). This analysis is consistent with cell permeability increases that selectively breach the plasma membrane[166].

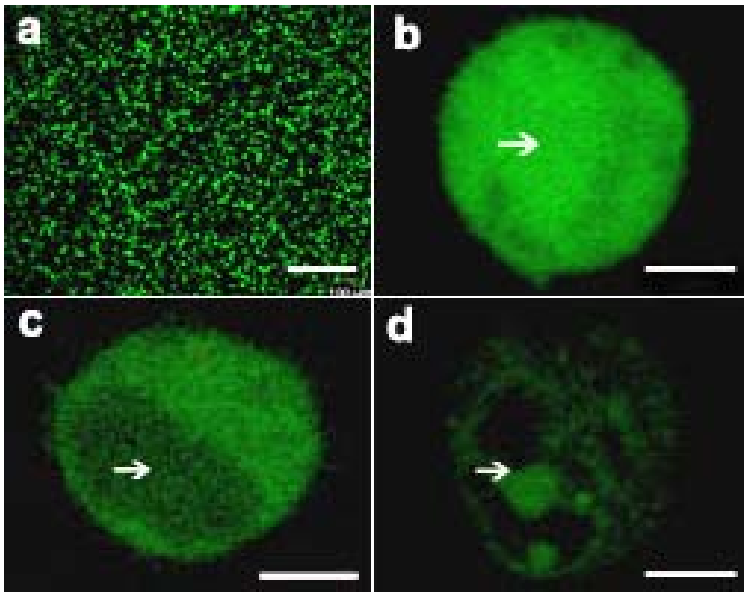

Figure 5.1: Intracellular uptake in cells exposed to femtosecond laser irradiation in presence of carbon nanoparticles. Confocal micrographs showing irradiated DU145 cells with uptake of (a,b) calcein, (c) FITC-labeled BSA and (d) YOYO1-labeled DNA. A large population of cells exhibited uptake of calcein when viewed under the 10X magnification objective. (a). Under 40X magnification, calcein is seen at high concentration throughout the cell, including the nucleus (b), however BSA and DNA were excluded from the nucleus (c,d). White arrows indicate location of the nucleus. Samples were irradiated at 5 mJ/cm^2 for 10 min in 30 mg/L carbon nanoparticles. Scale bars are, (a) 100 μm and (b-d) 5 μm.

To quantify the bioeffects for statistical treatment, treated cells were counted for uptake of calcein and BSA (Figure 5.2a) and viability (Figure 5.2b) using flow cytometry. The uptake form each run was a normal distribution with mean florescence along the x-axis and no. of cells in the y-axis. The lower and upper bounds for mean florescence was usually 100 and 1000 respectively. In a few cases, especially very high laser fluences, the upper bound was as between 1000-10,000. The peaks along the y-axis

were between 10-20 no. of cells. The increase in average intensities was about 10-times with respect to negative controls.

Additionally, intracellular florescence was quantified using calibrated beads to indicate the number of molecules delivered per cell (Figure 5.2c). Flow cytometry confirmed that, relative to sham exposures, >90% cells were calcein-positive (1-way ANOVA, $p<0.0001$) and more than 35% were BSA-positive ($p<0.0001$). Average number of molecules delivered to treated cells was on the order of 10^6 calcein molecules/cell ($p<0.0001$) and 10^5 BSA molecules/cell ($p<0.0001$). The intracellular molecule concentrations were 2.0±0.1 μM for calcein (based on the full cell volume) and 0.9±0.1 μM for BSA (based on the cystolic volume) which is about one order of magnitude less than the extracellular concentration of 10 μM. Cell viability compared to sham exposures remained close to 100% for calcein ($p=0.14$) but was lowered to 90% for BSA ($p<0.0001$).

When CB were replaced with MWNTs at the same mass concentration, intracellular uptake of calcein was reduced by 80% compared to uptake with CB (Figure 5.2a, $p=0.01$). Viability levels relative to sham exposures were unchanged ($p=0.6$, Figure 5.2b) and calcein molecules/cell when compared to that with CB decreased 10-fold ($p=0.01$, Figure 5.2c). This suggests that uptake was due to pressure generated by chemical reaction and that direct thermal effects were much less significant.

5.2.2. Uptake and transfection of plasmid DNA

DNA transfection is more challenging than uptake of smaller molecules due to the plasmid's large size and the additional barrier imposed by the nuclear membrane.

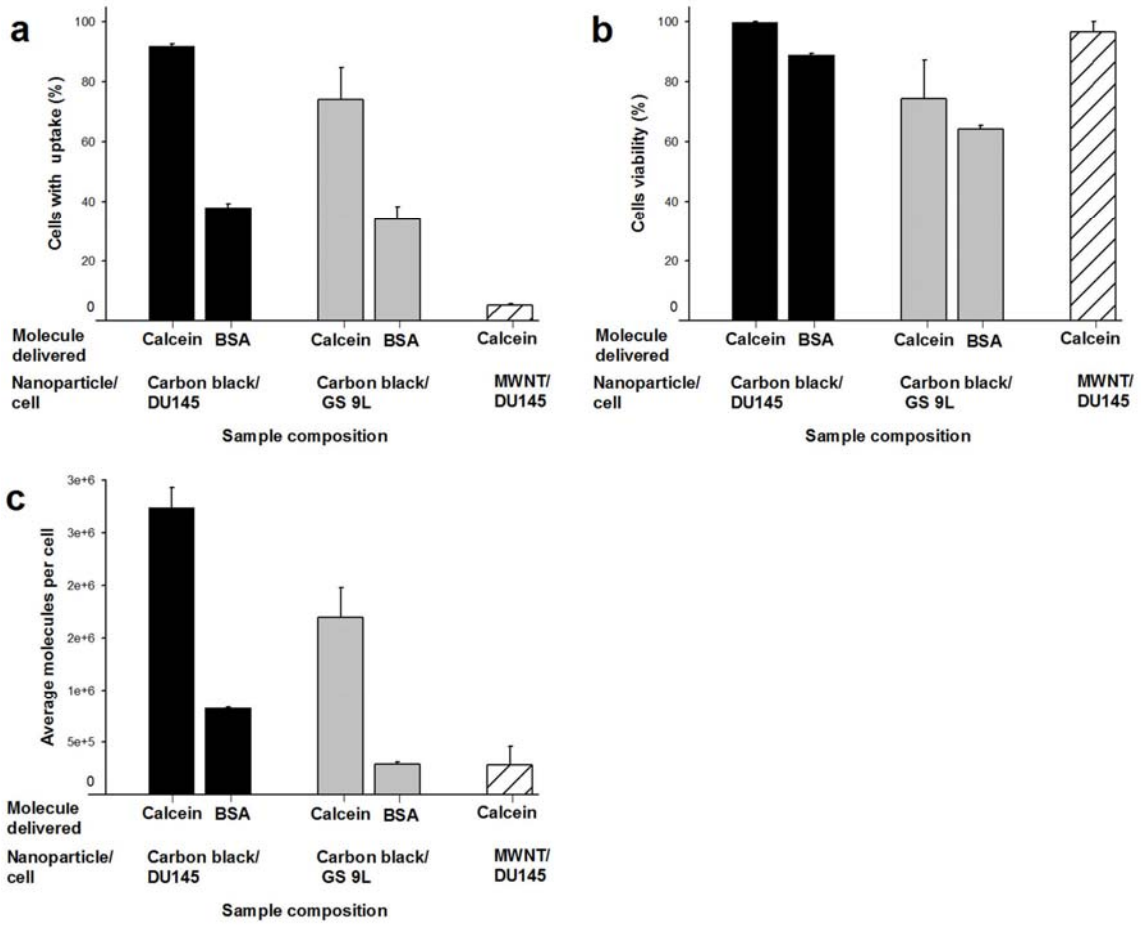

Figure 5.2: Effect of nanoparticle and cell type on intracellular uptake, cell viability and average number of molecules delivered per cell. CB nanoparticles were used with DU145 cells (black bars) and GS-9L cells (gray bars) for delivery of calcein and BSA. MWNTs were used with DU145 cells (striped bars) for delivery of calcein. (a) Percentage of cells with intracellular uptake, (b) cell viability, and (c) average number of molecules delivered per cell, are shown as functions of nanoparticle and cell type. Both CB nanoparticles and MWNTs were added at final concentrations of 30 mg/L. Samples were irradiated at 5 mJ/cm^2 for 10 min. Data represent the averages of n = 3 replicates with ±SEM shown.

Nonetheless, up to 22% of cells exhibited intracellular uptake of fluorescently labeled DNA compared to sham exposures ($p<0.0001$, Figure 5.3) and expression of luciferase was increased 17-fold in treated cells over sham exposures ($p=0.0253$, Figure 5.3).

To further validate that the irradiation procedure did not damage the plasmids, we exposed DNA to the laser-carbon system in the absence of cells and then measured the ability of this exposed DNA to transfect cells with a common cationic lipid transfection agent, Lipofectamine™. We found that transfection efficiency of irradiated DNA was similar to that of non-irradiated DNA (5.0±0.5% cells were transfected in both cases, $p=0.12$). Altogether, this showed that the laser-carbon system could drive DNA into cells without affecting its functional integrity.

5.2.3. Effect of laser fluence, exposure time and carbon concentration on cellular bioeffects

Our hypothesis is based on the idea that upon energy absorption CB act as local hot spots for producing microscopic shockwaves generated by the carbon-steam reaction. If properly optimized, nearby cells lying near possibly multiple blast centers should be reversibly permeabilized, while more distant cells remain unaffected. If excessively strong shocks are generated, then cells very close to many blast centers could be killed.

To assess the effect of input energy density, we used a laser beam having 350 mW mean power and varied the fluence by changing the focal diameter of the incident beam (i.e., the energy density was changed while keeping the total energy input constant) (Section 3.1.2-6). At the weakest fluence of 2 mJ/cm^2, exposure times of at least 20 min were

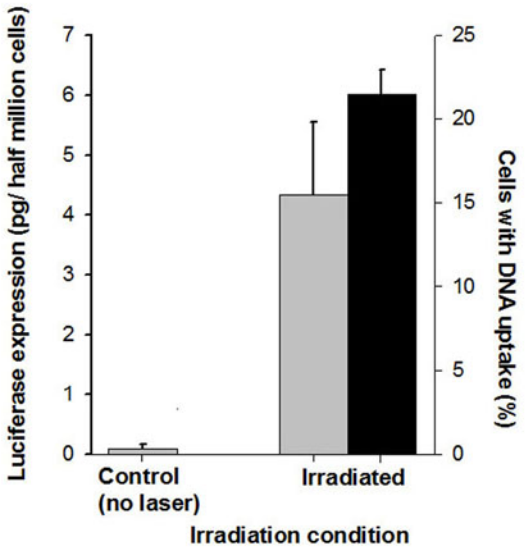

Figure 5.3: Intracellular uptake and transfection of luciferase plasmid DNA. Gray bars indicate amount of luciferase expressed per irradiated sample, each sample having 5 x 10^5 cells. Black bars show the percentage of cells with intracellular uptake of the YOYO1-labeled plasmid DNA per sample assayed < 2 h after irradiation. DNA expression was studied 48 h after irradiation. Samples were irradiated at 5 mJ/cm^2 for 10 min in 30 mg/L carbon nanoparticles. Data represent the averages of n = 3 replicates with ±SEM shown.

required to produce statistically significant uptake relative to sham exposures (ANOVA, p=0.04, Figure 5.4a). Uptake was seen in less than 10% of total cells.

When fluence was increased to 5 mJ/cm^2, an exposure of even 1 min was sufficient to cause uptake in 10% of cells compared to sham exposures (p=0.01) and beyond 10 min, uptake increased by 40% compared to uptake at shorter exposures (p=0.007). Cell viability under both these fluences remained at levels statistically indistinguishable from sham exposures (p=0.11, Figure 5.4b).

At the strongest fluence of 10 mJ/cm^2, uptake increased, went through a maximum of 80% at 3 min (p=0.01, relative to uptake at 1 min), and then decreased to

1% after 20 min ($p<0.05$, relative to uptake at 3 min and 10 min). Viability was indistinguishable from sham exposures at 1 and 3 min exposures ($p=0.08$), and decreased to approximately 30% after 10 and 20 min ($p<0.001$). Overall, fluence and exposure time synergistically impacted uptake (2-way ANOVA, $p<0.0001$). Viability was significantly affected only for fluence ≥ 5 mJ/cm^2 and exposure time ≥ 10 min ($p<0.0001$), but otherwise remained unchanged from sham exposures ($p>0.1$, for other conditions).

These observations are consistent with the blast center conceptual framework, in which short, low-fluence conditions had weaker or fewer blast centers that led to uptake among a small fraction of cells; longer and/or higher fluence generated stronger or more blast centers that led to uptake among a larger fraction of cells; and the longest, highest fluence conditions led to blast centers sufficiently powerful that extensive uptake among cells was accompanied by significant cell death too.

Again considering the blast center framework, we expected that increasing particle concentration should lead to more blast centers and thereby increase uptake. We treated cells for 3 min in presence of a range of particle concentrations ranging from 0 mg/L to 30 mg/L. We found that compared to sham exposures, uptake increased steadily with nanoparticle concentration ($p=0.001$, Figure 5.5a) while viability remained unchanged ($p=0.6$, Figure 5.5b).

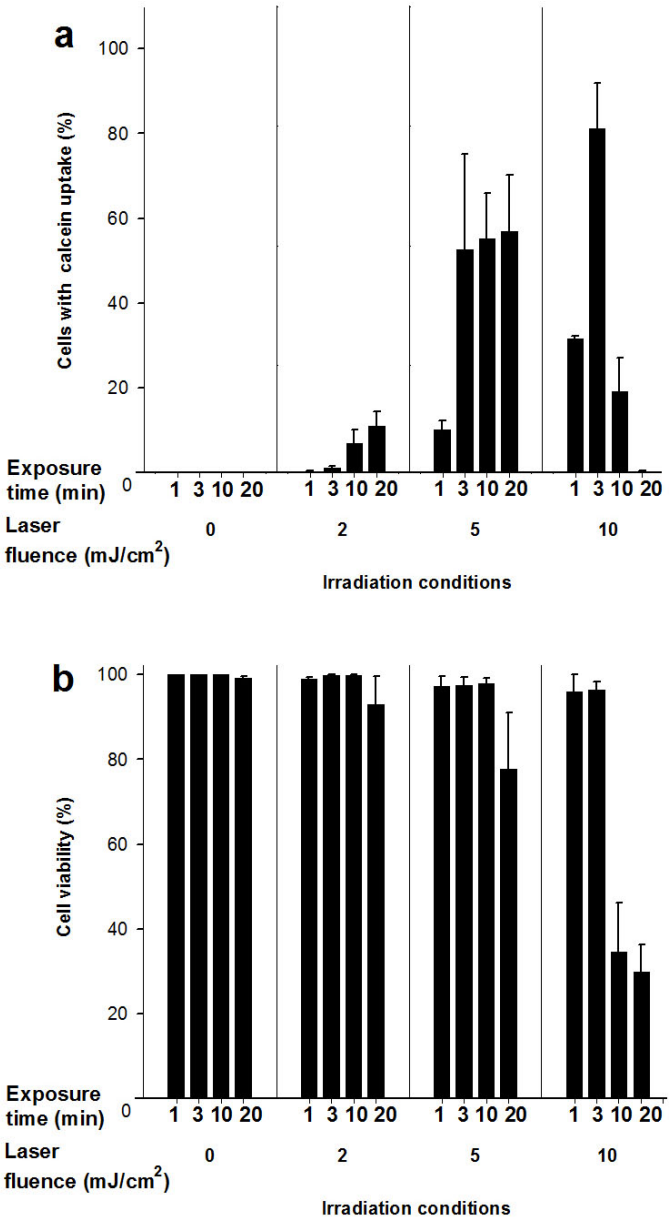

Figure 5.4: Intracellular uptake and cell viability following irradiation over a range of laser fluences and exposure times. Laser fluence and exposure time had a synergistic impact on uptake at all irradiation conditions. Viability was significantly affected only for fluence $\geq$ 5 mJ/cm^2 and exposure time $\geq$ 10 min. Samples were irradiated in 30 mg/L carbon nanoparticles. Data represent the averages of n = 3 replicates with SEM shown.

5.2.4. Mechanistic analysis

We demonstrated molecular uptake by cells under conditions involving laser-carbon interactions that have been documented in literature to cause explosive photoacoustic effects[100, 104, 105]. We hypothesized that the mechanism of uptake is transient membrane permeabilization caused by highly localized explosive forces generated due to laser-carbon interaction. To further evaluate this mechanism, we carried out additional experiments using conditions that do not generate laser-carbon induced explosive effects, but which could cause uptake if other mechanisms were involved.

Laser energy alone (i.e., without CB) has previously been shown to cause intracellular uptake either by directly puncturing the plasma membrane[67, 71] or by producing shock waves that permeabilize the membrane[76]. In this study, laser irradiation at a standard set of experimental conditions in the presence of CB yielded 65% cells with uptake (Figure 5.6, condition A). The same experimental conditions, but in the absence of CB, yielded <2% cells with uptake, which was much lower than uptake in presence of CB (Figure 5.6, condition C, $p=0.003$). Thus, laser alone did not cause high uptake in our system. Similarly, nanoparticles have been used as direct intracellular drug delivery vehicles[86]. However, using our standard experimental conditions, mixing cells with CB in the absence of laser exposure resulted in no uptake (Figure 5.6, condition B). Altogether, this shows that only the synergistic combination of laser energy and CB leads to the high uptake observed in our system.

Literature also shows that an aqueous gold solution having strong absorption at the irradiated wavelength can generate acoustic waves in the solution by thermal expansion[167]. To test whether such a thermal expansion might be involved in uptake, we

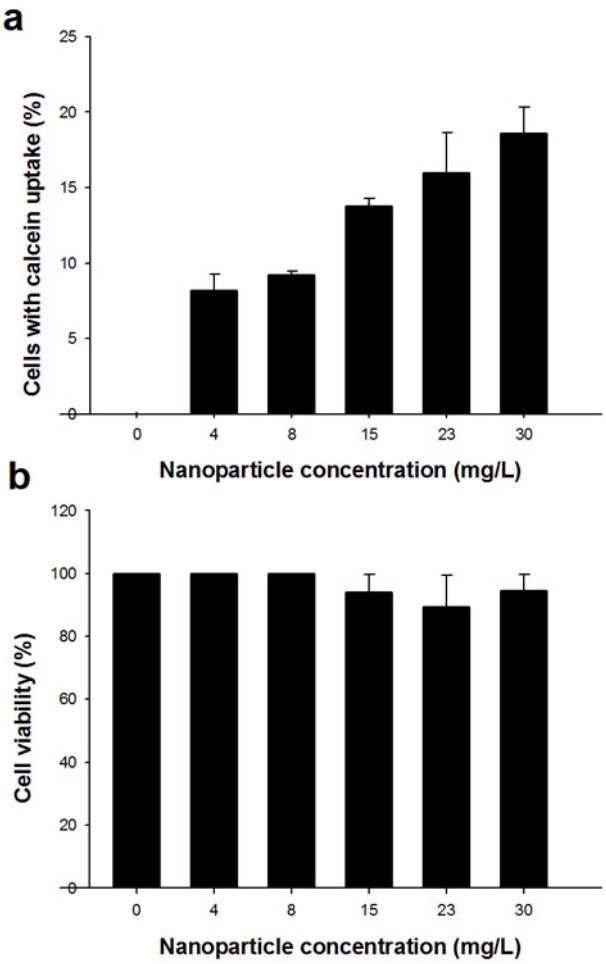

Figure 5.5: Intracellular uptake and cell viability following irradiation over a range of carbon nanoparticle concentration. Uptake increased with increasing particle concentration. Viability remained unchanged. Samples were irradiated at 5 mJ/cm^2 for 3 min. Data represent averages of n = 2 replicates with ±SEM shown.

irradiated cells under the standard conditions in the presence of gold nanorods having an absorption maximum at 800 nm. The concentration of gold nanorods was adjusted such that energy absorbed by the sample was the same as that with standard CB treatment. Relative to sham exposures (Figure 5.6, condition B), uptake was unchanged after irradiation in the presence of gold nanorods (p=0.18, Figure 5.6, condition D). This

shows that acoustic waves produced by thermal vibrations of gold nanorods[167] did not cause uptake. It also suggests that uptake is not caused by thermal damage to cell membranes, because these gold nanorods reach very high surface temperatures upon laser irradiation[145].

Another alternative is that chemical products of the reaction directly affect cells without involvement of photoacoustic effects. To test this idea, we irradiated cell-free suspensions containing carbon and calcein and then added cells within 1 s after irradiation. Relative to sham exposures (Figure 5.6, condition B), uptake was unchanged (Figure 5.6, condition E, $p=0.9$), indicating that long-lived end products of chemical reaction were not responsible for uptake.

As a further test for the role of shockwaves, we assessed the effect of fluid viscosity (Section 3.1.3). Increased fluid viscosity has a damping effect on the propagation of acoustic transients, although it can affect other processes too, such as molecular diffusion. We found that a five-fold increase in viscosity lowered uptake to levels indistinguishable from sham exposures (Figure 5.6, condition F, $p=0.8$). Although this five-fold increase in viscosity could also reduce calcein diffusion by five fold, this reduced diffusion does not explain the complete suppression of uptake. A more likely explanation is that shockwave propagation was dampened below the threshold for cell permeabilization.

Our hypothesis is based on uptake via mechanical breach of the cell membrane and not, for example, endocytosis. To assess this, we depleted intracellular K^+ which is required for clathrin-coated pits and caveoli-mediated endocytosis[48], before treating cells

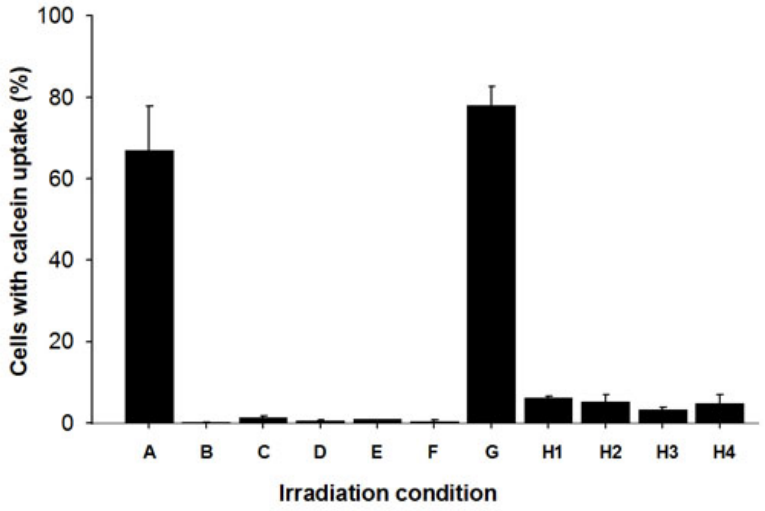

Figure 5.6: Intracellular uptake of calcein as a function of different irradiation conditions. (A) Positive control (irradiation with laser and carbon particles). (B) Negative control (no irradiation). (C) Irradiation without carbon particles. (D) Irradiation with gold nanorods. (E) Cells added within 1 s after irradiation. (F) Irradiation in five-fold higher viscosity. (G) Irradiation of cells pre-treated to block endocytic processes. (H) Calcein added (H1) < 1s, (H2) 30 s, (H3) 60 s, and (H4) 120 s after irradiation. All samples were irradiated at 5 mJ/cm^2 for 10 min, except conditions H1-H4, which were irradiated for 3 min. Data are expressed as the percentage of cells with calcein uptake among all irradiated cells, except for (G), in which data are expressed as the percentage of viable cells with calcein. This correction was made in (G) because the K^+-depletion pre-treatment to suppress endocytosis killed a large fraction of cells (i.e., ~20%). Data represent averages of mostly n = 3 replicates with SEM shown.

with the laser-carbon system (Section 3.1.3). Cell viability compared to non-K^+-depleted controls was decreased ($p<0.0001$). However, uptake was not affected by K^+ depletion relative to cells irradiated without K^+ depletion (Figure 5.6, condition G, $p=0.39$), indicating that clathirin-mediated endocytosis was not involved in uptake. Decreased viability of the K^+-depleted cells could result from a reduced ability of these cells to recover from membrane permeabilization, since the K^+ depletion procedure is physiologically stressful to cells.

Finally, we wanted to test whether membrane openings through which molecules are delivered repair over a short timescale. To study this, we added calcein to irradiated cells at different times after irradiation. When calcein was added <1 s after irradiation, uptake efficiency decreased 12-fold compared to treated standards (Figure 5.6, condition H1, p=0.0002) and continued to remain low at increasing time points for up to 2 min (Figure 5.6, conditions H2–H4). This suggested that most cells repair within 1 s after laser treatment. It should be noted that the total laser exposure time was 3 min, which means that cell membrane recovery may not have occurred as quickly as <1 s, but did generally occur over a timescale less than 3 min.

5.3. Discussion

In this study, we proposed that the explosive forces known to be generated during laser-initiated carbon-steam reaction in CB suspensions could be harnessed for reversible permeabilization of cells for intracellular delivery. Our experiments demonstrated intracellular delivery of molecules including a protein and plasmid DNA to multiple cell types. We further showed a direct dependence of physical parameters such as laser fluence, exposure time and CB concentration on cellular bioeffects, which enabled optimization of the system for high uptake and high viability.

A series of mechanistic experiments demonstrated need for simultaneous exposure to both laser irradiation and CB. Consistent with the reaction-driven photoacoustic basis for cellular effects, we showed through experiments with MWNT and gold nanorods that nanoparticles not only need to be strong energy absorbers, but also must be capable of reacting explosively during laser irradiation. These experiments, along with those involving Lipofectamine transfection of laser-treated DNA, further

indicate that heat generated in the system did not directly cause membrane or DNA damage. Cellular effects were initiated and completed during (or within 1 s after) treatment and were eliminated by an increase in fluid viscosity, both of which are consistent with transient membrane permeabilization caused by short-lived pressure forces. Finally, clathrin-mediated endocytosis and other slow, cellular transport processes were ruled out. Altogether, these data suggest that photoacoustic effects generated in CB suspensions by ultrashort laser excitation cause efficient intracellular delivery via membrane permeabilization.

Although additional study is needed to determine detailed mechanisms by which laser irradiation of carbon nanoparticles permeabilizes cells, we offer the following hypothesis. First, laser energy is absorbed by carbon nanoparticles over the course of each 100 fs-long pulse. Heat in the amount of 6.6×10^{-13} J/pulse then distributes uniformly within each 200 nm carbon-particle aggregate over a timescale of 7 ps to a temperature of 775 K (see Supplementary Information for supporting calculations in the following two paragraphs). Heat is then transferred from the particle to (i) vaporize surrounding water, (ii) heat surrounding water and steam and (iii) drive the carbon-steam reaction on a timescale of up to nanoseconds. The volume expansion caused by increased temperature and generation of gas and vapor creates a cavity that expands and subsequently collapses, thereby emitting a shockwave. This shockwave can shear holes in the plasma membrane of neighboring cells by a mechanism previously examined in the context of acoustic cavitation[48].

If all energy absorbed by carbon particles is used to drive the carbon-steam reaction adiabatically, then 1.0×10^{-17} mol of gas would be produced per aggregate,

which serves as an upper estimate. This upper estimate corresponds to a bubble forming a shell with an equilibrium thickness of 203 nm around each 200 nm carbon aggregate at a Laplace pressure of 5.8 atm and 25 ^{o}C. The maximum bubble size is expected, however, to be much larger, due to inertial forces during bubble growth, elevated temperature and other effects. Because this process is orders of magnitude faster than the delay between laser pulses (1 ms), each pulse can be treated as an independent event. In reality, not all energy would be absorbed by carbon particles, due to light scattering. Likewise, not all energy would be used to drive the carbon-steam reaction, due to heat transfer to surrounding water. Thus, bubble size would be smaller. Detailed calculations are explained in Section 5.4 and Appendix A.

While this mechanism leads to intracellular uptake of molecules, we do not believe that significant amounts of CB enter cells. CB used in this study was in the form of 12.5 nm radius particles present as 100 nm radius aggregates, which should have great difficulty crossing intact plasma membrane before laser treatment and is expected to have trouble even after membrane disruption, given the expected sieving effect of the cellular cytoskeleton[168].

Our laser-particle system is conceptually closest to cell permeabilization using ultrasonically generated cavitation[42, 43, 48]. In both systems, shockwaves are emitted from point sources, either CB in the present case or collapsing cavitation bubbles in the case of US. Our approach also appears related to other mechanical "wounding" methods that shear membranes by direct solid or fluid mechanical forces[169, 170]. These methods share a common mechanistic basis involving formation of a nanometer-scale hole in the plasma

membrane that permits entry of extracellular molecules and is subsequently resealed by active cellular processes[46].

Guided by this knowledge of the literature, we propose that the photoacoustic effects in this study create plasma membrane holes too. That argument is further supported by data, which show that endocytosis does not appear to be responsible for uptake in this study and diffusion or facilitated diffusion across an intact plasma membrane is extremely unlikely for the large, hydrophilic molecules used here[16]. The most reasonable explanation that is consistent with all of our data and with the broader literature is the formation of holes in the cell membrane. Additional studies are needed to fully validate this hypothesis.

Further comparison with the literature shows that this is the first time that CB have been used synergistically with laser excitation to manipulate cell membrane permeability and facilitate non-endocytic delivery into cells. Previous studies have separately utilized direct laser-cell interactions[64, 67, 71] or nanoparticle-cell interactions[86] to promote uptake by different mechanisms.

The results of this study suggest utility for in vitro intracellular delivery in the laboratory and possible development of in vivo drug and gene delivery for medical applications. In contrast, intracellular delivery using biological methods, such as viruses, have generated significant safety concerns and are generally limited to delivery of genetic material[17]. Chemical methods involving, for example, lipids and polymers, have similarly been designed largely for nucleic acid delivery, but are often cell-type specific and have found limited applicability in vivo[162]. Other physical methods, such as electroporation,

US, and microinjection, have been limited by inefficient delivery, cell death, the need for invasive administration and low throughput[29].

The laser-particle system studied here may address these limitations. The approach appears to be broadly applicable, based on uptake in two different cell types; demonstrated delivery of a small molecule, protein and DNA; and a physical mechanistic basis that does not appear to have biological or chemical specificity. The effects on cells appear to be gentle and efficient, as shown by minimal loss of cell viability and delivery into up to 90% of cells at high intracellular concentration. For possible application in vivo, the method lends itself to non-invasive or minimally-invasive administration through the use of 800 nm wavelength irradiation, which has high penetration efficiency through tissue[63], and targeted delivery only at sites containing both CB and laser light.

In the future, this approach could be extended for noninvasive treatment of in vivo targets for possible medical therapies. The nanoparticle-drug formulations could be injected locally, for example, to promote DNA transfection in a specific tissue. They might alternatively be injected systemically, so that they preferentially locate to tumors through leaky blood vessels to facilitate targeted cancer therapy[84]. A tissue-penetrating NIR beam could then be focused non-invasively at the targeted sites to drive localized drug or gene delivery through laser-nanoparticle interaction. Additional targeting could be achieved by functionalizing the nanoparticles so that they cause cell-specific delivery[86]. This approach could alternatively be used for selective cell killing by suitable adjustment of laser irradiation parameters, e.g., to higher fluence.

With respect to concerns over the biocompatibility of CB, their main constituent, CB, is a biologically inert material that has been used widely for imaging and medical

tattoos[98]. Although we have chosen CB as the model nanoparticle, the conclusions from this work should be applicable to other nanoparticles that react in a similar manner upon pulsed laser irradiation. This study could thus provide impetus for design of novel nanomaterials mimicking the photochemical properties of CB for drug delivery applications.

5.4. Supplementary Information

In this section, we estimate the volume change associated with conversion of C(s) and $H_2O(l)$ into CO(g) and $H_2(g)$ by the carbon-steam reaction during laser irradiation. This volume change is of interest, because it provides information relevant to the magnitude of shock wave that could be produced during laser irradiation to impact cells. We also calculate the temperature increase on the surface of the aggregates as well as the time required for the aggregate to heat up and cool down due to conduction and radiation.

Individual particle volume is 8.2×10^{-24} m^3 assuming spherical geometry for a nanoparticle 25 nm in diameter. Based on a carbon specific gravity[90] of 1.8 each nanoparticle has a mass of 1.5×10^{-17} g. Based on the observation that nanoparticles form aggregates with an average characteristic dimension of 200 nm and bulk density[90] 0.46 g/cc this means that an average of 133 nanoparticles are present in each aggregate, which corresponds to 1.95×10^{-15} g or 1.6×10^{-16} mol of carbon per aggregate.

The cylindrical sample volume irradiated during each pulse is 6.3 μl, based on the laser beam diameter of 2 mm and sample chamber width of 2 mm. Given an initial carbon concentration of 29.6 μg/ml, this means that 186 ng of carbon, which corresponds to 1.0×10^8 aggregates, is irradiated during each pulse.

Based on the difference between incident and transmitted light, the power absorbed during irradiation by carbon nanoparticles at a concentration of 29.6 μg/ml for a 350 mW beam was measured as 66.03 mW. This corresponds to energy absorption of 6.6 x 10^{-13} J/aggregate/pulse. This estimate assumes there is no light scattering or other loss of light and is therefore an upper bound; the actual energy absorbed was probably less. If specific heat of the aggregate[171] is 8.5 J/mol/K then the maximum temperature rise of each aggregate during one pulse is 477 K resulting in a final temperature of 775 K. If the thermal conductivity[172] of the carbon particle is 155 W/m/K, then the time required for the aggregate to be uniformly heated using Fourier's law of heat conduction is 7.0 x 10^{-12} s. This is longer than the pulse duration, which is 1.0 x 10^{-13} s.

Assuming that all of this energy goes into driving the carbon-steam reaction, with a specific ΔH=131 kJ/mol [173], we find that carbon is consumed at a rate of 5.04 x 10^{-18} mol/pulse. This value is an upper bound on the amount of carbon consumed. Because energy is probably dissipated in other ways, such as thermal conduction and vaporization of water, the amount of carbon consumed is probably less. This upper estimate corresponds to generating 1.0 x 10^{-17} mol of product gases. Assuming that these gases form a shell around the aggregate at 298 K and a Laplace pressure of 5.8 atm, the thickness of the shell is 203 nm.

The energy absorbed by each aggregate can increase surface temperatures to about 775 K. To determine a characteristic time over which the particle could cool down due to thermal conduction to the surrounding media, we assume that no reaction takes place and the aggregate cools down due to conductive loss of heat to surrounding water which has a thermal conductivity[174] equal to 0.6 W/m/K. Then using Fourier's law, the

time required for the aggregate to cool down completely based on a temperature difference of 477 K (775 K-298 K) at the surface is 2.0×10^{-9} s. If on the other hand the aggregate cools down due to radiation heat loss alone, then based on the Stefan-Boltzman law of black body radiation, the time required for total cool down is 2.6×10^{-4} s. This indicates that the particle cools down within at least 2 ns and probably faster due to additional heat loss to drive the carbon-steam reaction. This can also serve as a characteristic time over which bubble growth occurs. It is noteworthy that this time is much faster than the delay between laser pulses (1 ms), which suggests that each pulse can be treated as an independent event.

CHAPTER 6
PHOTOACOUSTIC DRUG DELIVERY INTO CELLS AND IN VIVO TISSUE MEDIATED BY CARBON NANOPARTICLES AND NANOSECOND LASER PULSES

This goal of this study was to study if nanosecond laser pulses could react photoacoustically with CB nanoparticles to induce intracellular delivery. In this study, pulsed laser irradiation of carbon nanoparticles was shown to deliver non-permeable molecules in the size range of proteins into cells with high efficiency and high cell viability. Uptake was shown to be a result of laser-carbon interaction and increased as conditions for generating the carbon-steam reaction became more favorable. This suggested that uptake was caused by explosive volume change resulting from laser-initiated carbon-steam reaction that produced photoacoustic forces which impacted cell membrane and transiently permeabilized it. Intracellular delivery was further demonstrated in vivo in murine skeletal muscles using this technique. Altogether, these data suggest that laser irradiation of carbon nanoparticles can efficiently drive molecules into cells with essentially no loss of cell viability both in vitro and in vivo. Additional studies may lead to nanoparticle-drug formulations injected into tissues for localized delivery of drugs, proteins and genetic material into cells.

6.1. Introduction

One of the key barriers in drug delivery is transport of drugs, proteins and genetic material across the cell membrane[2]. The cell membrane prevents large molecules from spontaneously entering cells typically unless there is endocytosis. However, endocytosis is a slow process that often subjects molecules to lysosomal degradation that reduces

their availability inside the cell and diminishes their potency. Hence, methods for direct intracytoplasmic delivery that bypass the endocytic pathway are required[162].

Direct delivery that bypasses endocytic pathway is often achieved using physical methods of membrane permeabilization[29]. The working principle behind such membrane breaks is that a physical force, be it acoustic, electrical, thermal, photoacoustic or mechanical, is used to create a local perturbation that disrupts the cell membrane. These membrane breaks then facilitate entry of exogenous molecules along a concentration, or electric filed or possibly convective gradient. The success of these techniques depends on the ability of the cell to repair the membrane breaks after entry of the molecules. In general, smaller the breaks, easier it is for the cell to repair them[48]. At the same time, the breaks need to be large enough and last long enough to facilitate entry of molecules. The challenge for physical methods is therefore to optimize the physical parameters to obtain an acceptable balance between high uptake and unwanted cell death.

There is a wide volume of literature discussing the phenomena of photoacoustic shock generation due to interaction between laser and carbon nanoparticles. According to these studies, when a suspension of carbon nanoparticles was irradiated with pulsed laser light, the temperature and pressure on the particles' surface could be driven sufficiently high to initiate the carbon-steam reaction, $C(s) + H_2O(l) \rightarrow CO(g) + H_2(g)$[99]. The rapid conversion of solid and liquid reactants to gaseous products produces strong photoacoustic effects including microscopic shock waves[100], sonoluminescence[104] and cavitation[175]. In our preceding study documented in Chapter 5, we demonstrated, for the first time, that these photoacoustic effects could be harnessed for permeabilizing cell membrane and delivering drugs. In that study, we used NIR pulses from a femtosecond

laser to irradiate suspensions of carbon nanoparticles and in vitro cells. We showed efficient delivery of extracellular molecules including small drugs, proteins and DNA with high cell viability. We hypothesized that this delivery was caused by transient nanoscale holes formed in the cell membrane as a result of the photoacoustic forces. To support this we compared several key features of US-mediated uptake which also takes place through transient membrane breaks with our method and found them to be in close agreement.

Following the germinal study with the femtosecond laser which is very expensive and requires sophisticated user skills, we wanted to see if the same results could be obtained using a less expensive and less complex laser system that could more easily be advanced to medical use. Motivated by this need for a user friendly and economical laser, we decided to replace the femtosecond laser with a nanosecond Nd: YAG laser. Nd: YAG lasers are one of the most common types of laser, and are used for many different applications. They are used in ophthalmology for corrective eye surgery[75], in cosmetic medicine for laser hair removal or tattoo removal[176], in dentistry for soft tissue surgery[177], etc. So they emerged as the natural choice for a cheap and simple laser system that could more easily facilitate the advancement of the laser-carbon drug delivery system towards clinical use. Hence it was necessary to determine the efficacy of the nanosecond laser in causing intracellular delivery via laser-carbon interaction.

This study was divided into two parts— in vitro and in vivo. The main goal of the in vitro study was to determine whether the Nd:YAG laser could interact with carbon nanoparticles and cause intracellular delivery through transient membrane breaks in a manner similar to the way the femtosecond laser did, i.e. via photoacoustic effects. Since

literature contained several studies on the parameters influencing CB-Nd: YAG laser interaction and their effect on chemical reaction and photoacoustic effects, we also wanted to find out through this study if the same parameters correlated with cellular bioeffects. For instance, one study showed that the size of the CB particle governs the thermal inertia and hence the efficacy of chemical reaction[103]. So correlating size with cellular uptake could tell us whether chemical reaction plays a role in uptake In addition we wanted to determine if comparison between the nanosecond and the femtosecond system would allow testing of other mechanistic features like effect of pulse length and timescale of action, and thereby augment the mechanistic analysis. Finally, for this study we had in situ gas analyzing equipment which could help us determine if the laser-carbon interaction led to the endothermic carbon-water reaction by providing spectroscopic analysis of the product gases formed during irradiation. So we designed this study to (i) evaluate the ability of this system to deliver small molecules as well as macromolecules in the size range of proteins to cells in vitro, (ii) evaluate whether the parameters that influence laser-carbon interaction in terms of initiating chemical reaction and generating photoacoustic effects, correlated with cellular bioeffects, (iii) compare the two laser systems to strengthen the mechanistic hypotheses, and (iv) obtain qualitative proof of the laser-initiated carbon water reaction: $C(s) + H_2O(l) \rightarrow CO(g) + H_2(g)$.

The main goal of the in vivo study was to test the effectiveness of using this technique beyond in vitro cell suspensions and in dense cellular environments in vivo. Our question was whether the photoacoustic effects believed to be the underlying force in causing uptake could propagate effectively in this dense environment. Since cell had to be in close proximity to the carbon particles, we also wanted to know how feasible it was

to perfuse a dense environment with the particles to enable the cells to suffer the impact of the photoacoustic forces. Lastly, we wanted to find out if the laser fluence used in vitro was appropriate to not only penetrate the skin and enter the deeper layers of muscle fibers underneath, but was also capable of retaining enough energy to interact photoacoustically with the carbon nanoparticles present there. Driven by the hypothesis that the laser-carbon strategy could achieve all of the above and cause intracellular delivery, our goals in the in vivo study were to (i) image the localization of intracellular uptake of a model drug by in vivo muscle fibers, (ii) assess viability of the treated muscles, and (iii) quantify intracellular uptake in the targeted region. The broad goal of this study was to demonstrate the feasibility of the laser-carbon technique, rather than the best parameters to use for in vivo applications. The objective was to assess the potential of the laser-carbon strategy for applications beyond in vitro cell suspensions to set the ground work for future optimization studies in vivo.

6.2. Results: In-vitro study

6.2.1. Evidence of uptake

We first tested the hypothesis that interacting nanosecond laser pulses with carbon nanoparticles could deliver molecules into cells (Section 3.1.4, 3.2.1). As shown in Figure 6.1, non-irradiated cells showed no intracellular uptake, whereas cells exposed to the 1064 nm output of the nanosecond laser at 50 mJ/pulse for 1 min in presence of 30 μg/ml CB showed extensive uptake of green-fluorescent calcein. Calcein uptake was uniform across the entire cell including the nucleus. As a short-term viability assay, PI, indicated by red florescence, was mostly excluded from uptake cells when added ~30 min

after irradiation. This indicated that uptake was caused by a temporary increase in cell permeability, probably due to transient membrane breaks that repaired over time[41, 42, 48]. To clarify nomenclature, samples exposed to laser irradiation in presence of model drug and carbon nanoparticles were referred to as "treated" and samples not exposed to laser but subjected to all other treatments were referred to as "sham exposures", unless otherwise mentioned. To assess the statistical relevance of the qualitative observations, calcein uptake was quantified using flow cytometry (Section 3.1.5). Approximately 60% of the cells showed calcein uptake compared to sham exposures (Figure 6.2, 1-way ANOVA, $p<0.001$). Viability remained unchanged from sham exposures and greater than 90% ($p=0.14$). This compared favorably with other physical methods of intracellular delivery like electroporation[39] and US[42].

Having shown efficient uptake of a small (623 Da) molecule, our next step was to investigate if the same conditions could be used to deliver macromolecules in the size range of therapeutic proteins. Studying the effect of molecular weight would also clarify the nature of the membrane breaks produced since previous studies have shown that uptake of large molecules through membrane breaks was diffusion limited, and that uptake of larger molecules was further limited by the cytoskeletal network of the cell[48, 168]. Carrying out similar experiments with dextran molecules over a range of sizes showed that a 150 kDa dextran was taken up into cells with approximately the same efficiency as calcein (Figure 6.2, $p=0.48$). Because this dextran is larger than most protein therapeutic molecules, it suggests that efficient intracellular delivery of proteins may be possible. Larger dextrans (i.e., 500 and 2000 kDa) were also taken up into cells, but with reduced efficiency compared to calcein and smaller dextrans (~10% uptake,

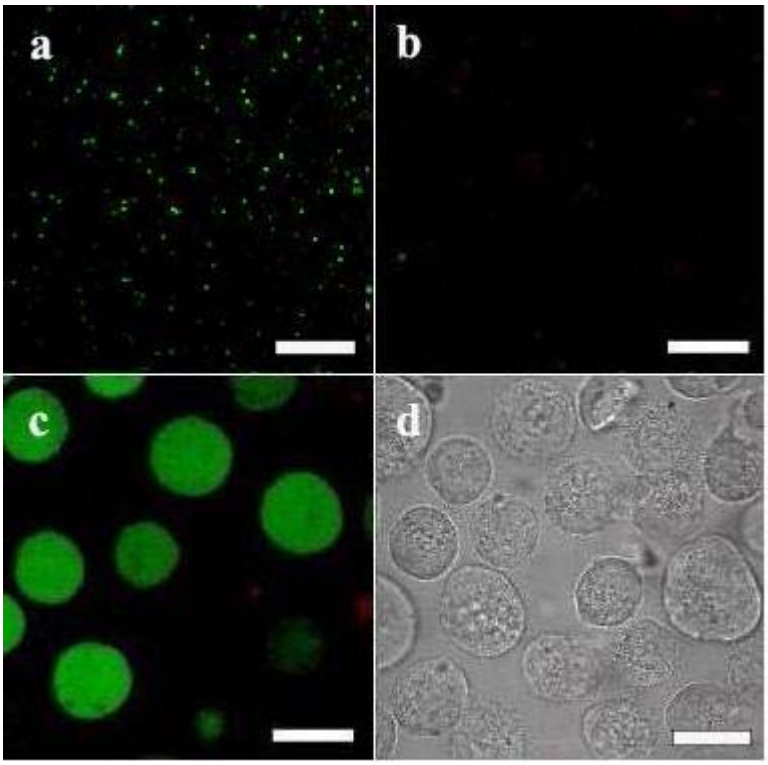

Figure 6.1: Confocal micrographs showing (a,c) cells treated with the laser-carbon system at 50 mJ/pulse for 1 min and with 30 μg/mL carbon nanoparticles, and (b,d) sham exposure. (a-c) are fluorescent views and (d) is a bright field view. Calcein uptake is shown by green fluorescence. Red fluorescence indicates nonviable cells. Scale bars are 200 μm (a.b) and 10 μm (c,d).

$p<0.001$). Cell viability remained unchanged from sham exposures under all conditions ($p=0.46$).

This dependency of uptake on molecular weight suggests a mechanism similar to that observed with US-mediated uptake[178] and electroporation where uptake decreases with molecular weight[39, 150, 152]. The nanosecond laser-carbon system was thus suitable for delivering small molecules as well as macromolecules covering the size range of

therapeutic proteins. Previous studies with US-mediated molecular uptake showed that up to 500 kDa, molecular uptake was limited only due to slower diffusion of large molecules. As molecular weight increased to 2000 kDa uptake was further limited by the cytoskeletal structure inside the cell. It was shown that US also disrupted the cytoskeleton

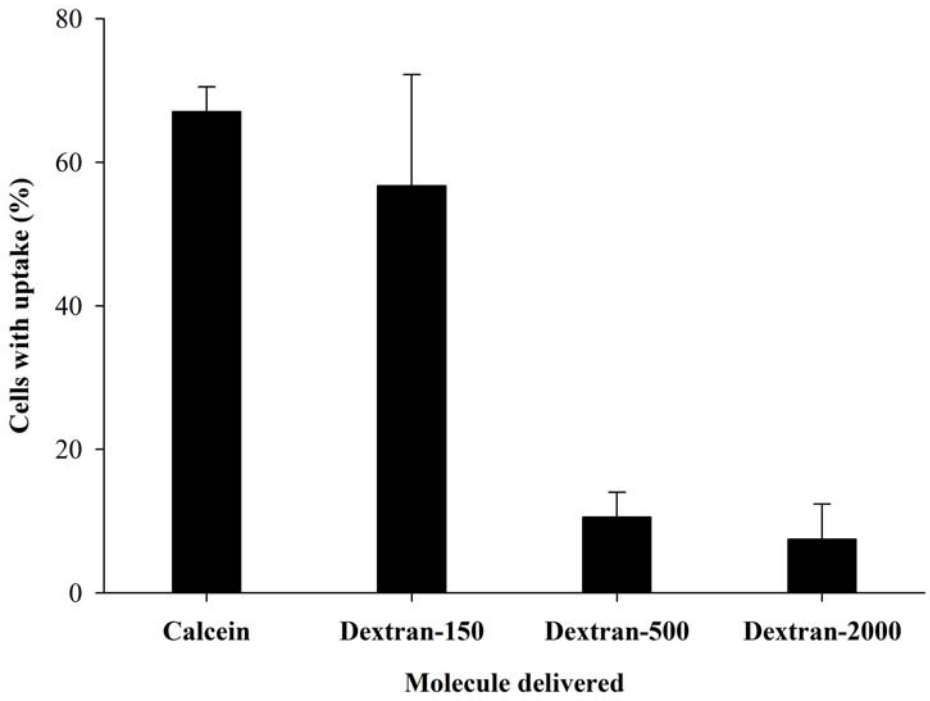

Figure 6.2: Intracellular uptake as a function size of molecule delivered. Calcein (623 Da) and FITC-labeled dextrans (150 kDa-2000 kDa) were delivered by treating samples at 50 mJ/pulse for 1 min and with 30 μg/mL CB. Data represent the averages of n=3 replicates with SEM shown.

of the cell, resulting in uptake of molecules as large as 500-2000 kDa[48]. However, in the laser-carbon system, there is a significant cut off in uptake between 150 kDa and 500 kDa sized molecules. This suggests that the membrane disruptions in the laser-carbon system

may be of a gentler nature and that the cell cytoskeleton is either not disrupted or disrupted to a lesser extent than with US.

6.2.2. Effect of carbon nanoparticle concentration, beam energy and exposure time on intracellular uptake

Having shown that our proposed system of exposing cells to nanosecond laser pulses in presence of carbon nanoparticles caused intracellular uptake, our aim was to investigate whether this uptake was due to the unique interaction between carbon and laser. If so, then uptake should increase with carbon concentration, laser power and exposure time. Intracellular uptake was studied for three different carbon concentrations (Figure 6.3). For each concentration, uptake was studied over a power range of 25-100 mJ/pulse and an exposure time range of 1-5 min.

At the lowest concentration of 15 mg/L, only power impacted uptake (2-way ANOVA, $p < 0.001$), but time had no impact on uptake ($p=0.85$). Uptake occurred in 30±10% of the total cell population. At a higher concentration of 30 mg/L, which was also the concentration typically used in experiments, power again was the only parameter that impacted uptake ($p<0.001$), not time ($p=0.32$). However, the uptake population in this case was 46±10%. At the highest concentration of 60 mg/L, power and exposure time showed a synergistic impact on uptake ($p=0.039$), and the uptake cell population was around 47±10%. The overall impact of power, concentration and exposure time was then analyzed by doing a global 3-way ANOVA using a general linear model to find the interaction between all three parameters. It was found that there was no interaction between the three parameters. Both power and concentration independently impacted

uptake such that uptake increased as power and CB concentration increased ((p<0.001). Exposure time did not impact uptake significantly for the timescales studied (p=0.31).

These results show that uptake correlated with parameters influencing laser-carbon interaction and approached a maximum for all the concentrations studied. We offer a mechanism based on laser-initiated chemical reaction[103] to explain these observations. As the laser interacted with the carbon, blasts were produced due to carbon-steam reaction and these blasts impacted nearby cells to cause transient membrane breaks. Higher the laser power, stronger was the blast and higher was the uptake. As concentration of CB increased, more blast centers were generated per pulse leading to an increase in uptake maximum. The observation of the same maximum uptake for all exposure times suggested that for each concentration, uptake stopped after a certain time, which was 1 min for conditions described by Figure 6.3a and 6.3b. This was because over time, chemical reaction would cause depletion of carbon and a reduction in the number of blast centers. When no further chemical reaction occurred, there would be no force to cause membrane breaks and hence no uptake. At higher powers, stronger blasts would lead to better uptake but this too will cease once the carbon depletes to a point where no further reaction occurs. Since the effect of exposure time was not evident for the lower concentrations it could be that that for these lower CB concentrations, 15 -30 mg/L, the limit of chemical reaction was reached at a timescale less than 1 min. However, the effect of exposure time was significant for the highest concentration of 60 mg/L and this could be due to the presence of additional blast centers that caused chemical reaction to persist even beyond 1 min. A similar effect of exposure time could also be present in case of the lower CB concentrations and might come to surface if uptake was studied at timescales

shorter than 1 min. Overall, these observations strengthen the mechanistic hypothesis that parameters governing laser-carbon interaction, particularly those that govern the generation of chemical reaction and explosive effects, are indirectly responsible for causing uptake. This in turn indicates that uptake is a consequence of chemically generated explosive effects.

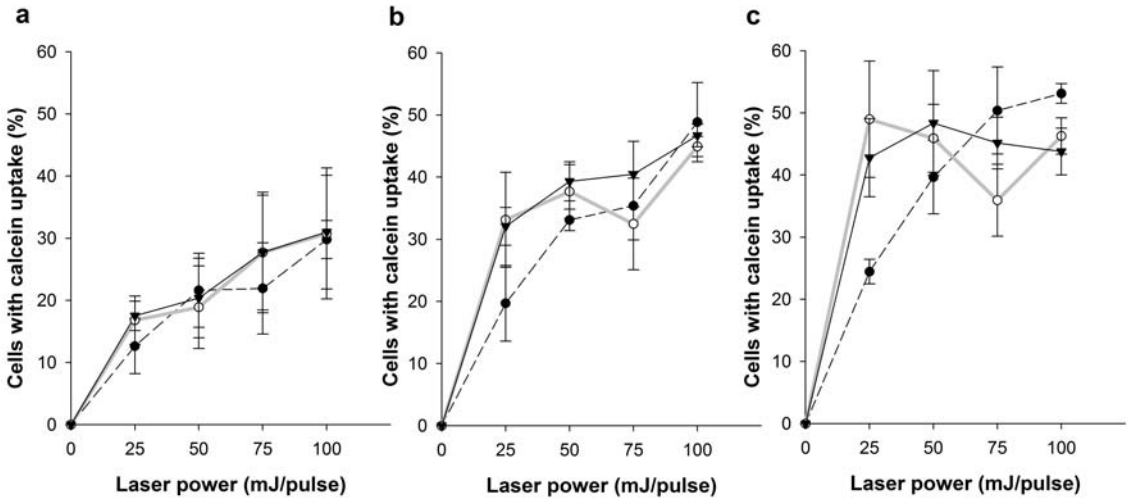

Figure 6.3: Intracellular uptake as a function of laser power for cell suspensions containing 25 nm carbon particles at (a) 15 mg/L, (b) 30 mg/L and (c) 60 mg/ for exposure times 1 min (dotted black line), 3 min (solid gray line) and 5 min (solid black line). Data represent the averages of n=3 replicates with ±SEM shown.

6.2.3. Effect of energy absorption on intracellular uptake

According to our hypothesis, uptake was caused by forces generated via laser-carbon interaction, more specifically laser-initiated chemical reaction on the surface of the CB. So if the conditions for initiating such reactions improved, more uptake would be expected due to improved generation of membrane permeabilizing forces. One of the

major parameters that impact chemical reaction is light (energy) absorbed by the CB. The light absorbed by the particles governs the rise of surface temperature and resulting increase in pressure. Stronger the absorption, greater is the temperature and pressure rise on the surface of the particles and more favorable are conditions for the CB nanoparticles to react chemically with surrounding fluid[103]. If uptake was caused by forces resulting from such chemical reactions, then the efficiency of light absorption by the particles would also be proportional to cellular uptake. To test this, we generated the absorption spectrum of the carbon particles over the spectral range of 300 nm to 1100 nm (Figure 6.4a). The absorption spectrum showed that at 355 nm and 532 nm, light absorption by water was much lower than that at 1064 nm. This meant more light was available for absorption by the CB nanoparticles at 355 nm and 532 nm than at 1065 nm. As shown in Figure 6.4a, light absorption by CB alone was highest at 355 nm, followed by 532 nm and lowest for 1064 nm. So by our logic, uptake should also be highest for 355 nm, followed by 532 nm and lowest for 1064 nm. We therefore expected uptake to decrease with increase in wavelength.

To correlate the absorption spectrum with uptake, we measured cellular uptake at laser powers ranging from 1 mJ/pulse to 50 mJ/pulse for 1 min exposure time at 1064 nm (NIR), 532 nm (VIS) and 355 nm (UV). Due to safety regulations the maximum power used for UV light was 7 mJ/pulse. As shown in Figure 6.4b, low powers of NIR laser light had little effect on uptake and power had to be increased to almost 25 mJ/pulse to induce significant uptake compared to sham exposure (20% uptake, 1-way ANOVA followed by Tukey's pairwise comparison). However, nearly the same uptake of 20%

could be induced with just 8 mJ/pulse of 532 nm and 2 mJ/pulse of 355 nm radiation. Overall, it was seen that uptake decreased as wavelength of radiation increased.

These results indicate that as efficiency of light absorption by CB increased, the intracellular uptake efficiency also increased. In other words, the uptake efficiency increased as conditions for generating the chemical reaction of CB with surrounding fluid became more favorable. These observations are consistent with the hypothesis that cellular effects are mediated by physical forces arising from laser-initiated chemical reaction on the surface of the CB particles.

6.2.4. The need for carbon particles for intracellular uptake

An important component of our mechanistic hypothesis is that the energy absorbers (CB in this case) reacted explosively upon laser irradiation to generate membrane permeabilizing forces. So it was not enough to have a strong light absorber, but the absorber had to be capable of chemically reacting with surrounding fluid to generate explosive forces for membrane permeabilization. To test this, we compared the efficiency of uptake in presence of the chemically reactive CB nanoparticles, with uptake in presence of a macroscopic absorber like water (laser alone, no CB) or in presence of non-reactive light absorbers like gold nanoparticles. Both water and gold nanoparticles can generate photoacoustic effects upon laser irradiation, but these effects are milder in comparison and generated by a purely thermal mechanism that does not involve explosive volume change resulting from chemical reaction[58, 179]. If our hypothesis was true, uptake in presence of gold or laser alone would be negligible compared to uptake in presence of CB.

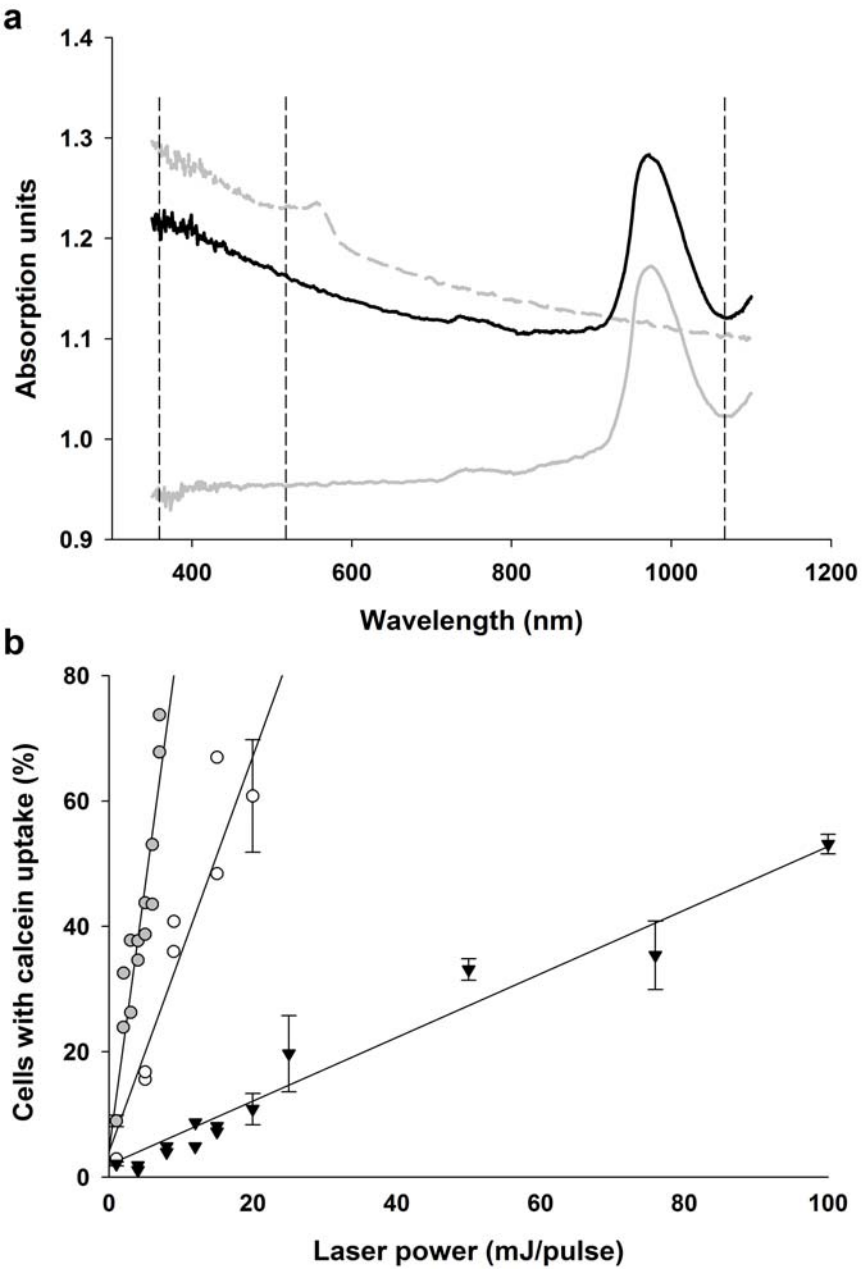

Figure 6.4: Cellular uptake at different wavelengths. (a) Absorption spectra of water (solid gray line), water with CB (solid black line), and CB alone (dashed gray line). Dotted lines are drawn perpendicular to the x-axis to indicate the wavelengths of interest viz. 355 nm, 532 nm and 1064 nm. (a) Uptake is quantified for 355 nm (UV, gray circles), 532 nm (VIS, white circles) and 1064 nm (NIR, black triangles) wavelength over a range of laser power, 1 min exposure time and with 30 μg/ml CB. Solid lines represent linear regression lines to indicate trend of uptake. Data in (b) represent the averages of n=3 replicates with ±SEM shown.

To study this, we replaced CB nanoparticles with gold nanoparticles of 50 nm diameter having their absorption maxima at 532 nm radiation. Gold nanoparticles were supplied at a concentration sufficient to absorb the same amount of light as CB. We then studied uptake after exposing samples to 532 nm pulses for 1 min over 50-100 mJ/pulse. For the same conditions, we also studied uptake in presence of laser alone. Uptake was highest when samples were irradiated in presence of CB (>70% uptake, Figure 6.5). Although the samples irradiated in presence of gold showed presence of several bubbles, the uptake at all laser powers was significantly lower than uptake caused in presence of CB particles (<20% uptake, $p<0.001$) and equal to the uptake when laser alone was used to irradiate the particles ($p>0.05$).

These results indicate that the predominant forces causing uptake in the laser-carbon system are the forces produced due to explosive chemical reaction of CB upon laser irradiation. Although the photoacoustic forces produced due to non-reactive light absorbers like gold and water may cause membrane permeabilization to some extent, these effects are around 50% less effective than the chemically generated explosive effects. This also shows that direct thermal effects are not the driving force for uptake. This strengthens our hypothesis that uptake is caused due to chemically-generated photoacoustic effects and requires a light absorber that reacts explosively upon laser irradiation.

6.2.5. Effect of carbon reactivity on intracellular uptake

As discussed earlier, size of the particle governs the thermal inertia and hence the efficacy of chemical reaction. According to literature[102-104], experiments that measured chemical reaction components in laser-irradiated carbon suspensions using similar

conditions showed that for a fixed irradiation time, amount of carbon consumed during laser irradiation was largest for the largest particles. In those experiments carbon particles

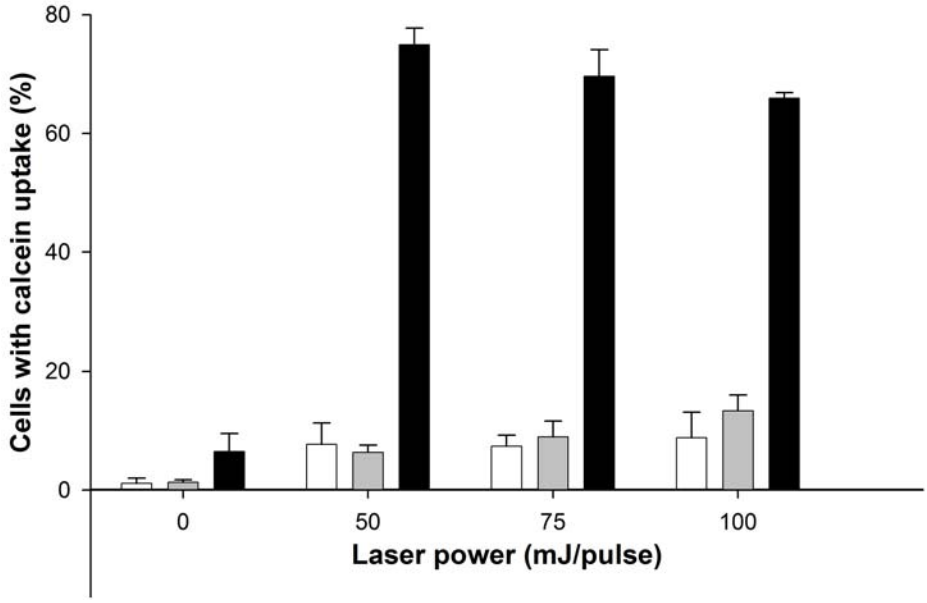

Figure 6.5: Intracellular uptake using laser with no particles (white bars), gold nanoparticles (gray bars) and CB nanoparticles (black bars). Samples were treated at 50 mJ/pulse and 1 min exposure time. CB and gold measured 25 nm and 50 nm in diameter respectively. CB particles were added at a final concentration of 30 μg/mL and gold nanoparticles were supplied at a concentration sufficient to absorb the same amount of light as CB, which was $4x10^9$ particles/mL. Data represent average of n=3 replicates with ±SEM shown.

with diameter 13 nm, 25 nm and 75 nm were irradiated with the 1064 nm output of a Nd:YAG laser for 4 hours and it was found that the absolute amount of each product gas increased with increase in size of the particle diameter[103]. The effect of size on temperature and the extent of chemical reaction can be understood from a rudimentary examination of thermal diffusion of heat from the particles. The thermal diffusion time

characterizing the cooling of a spherical particle is given by $\tau = r^2/2D$, where D is the thermal diffusivity of the liquid, assumed to be identical to that of the particle. In the present case, for a 25 nm diameter particle, the thermal diffusion time is 13 ps, whereas that for a 13 nm particle is 3.52 ps. Thus, during the 10 ns irradiation period, heat is continuously conducted away from the particle through thermal diffusion resulting in a low efficiency for heating the particle. Since the 13 nm particle cools down faster than the 25 nm particle, the latter is more efficiently heated resulting in more favorable conditions for chemical reaction. Using the conclusions from these previous studies as the basis, we hypothesized that if cellular uptake was a direct consequence of chemically generated photoacoustic effects then larger particle size would improve chemical reaction and lead to increased uptake. Further, literature also shows that MWNTs are less inclined to undergo reaction when heated to the same temperature and pressure compared to CB[180-182]. So we further hypothesized that another test of the importance of chemical reaction in causing cellular uptake would be to study uptake using MWNTs instead of CB. A decrease in uptake with MWNT would underscore the role of chemical reaction in causing intracellular uptake.

We used the same carbon particles (13-75 nm diameters) in our system and, in separate experiments, quantified the uptake for each size after an exposure of 1 min at 50 mJ/pulse radiation. We found that as particle diameter increased from 13 nm to 75 nm, the corresponding cellular uptake increased from 10±3% to 54±18% (Figure 6.6, $p<0.001$). This indicated that the particle size that favored more efficient carbon consumption due to chemical reaction, also led to higher uptake. In other words, uptake was favored by parameters favoring chemical reaction and was thus caused by forces

resulting from chemical reaction. However further increasing size of particles to 75 did not significantly change uptake relative to 25 nm particles ($p=0.9$). Since the particles exist as aggregates, it is possible that the size of aggregates formed in case of 25 nm suspensions were equal to those formed with 75 nm suspensions. Assuming this was the case, both 25 nm and 75 nm CB suspensions underwent chemical reaction in a similar manner and as a result, there was no visible difference in the resulting uptake. We then replaced the spherical CB particles with MWNTs. MWNTs were supplied at a concentration sufficient to absorb the same amount of light as CB. Cellular uptake with MWNTs was 15±10%, which was about 40% lower than uptake with 25 nm and 75 nm particles (Figure 6.6, $p=0.003$), and equal to uptake with the less reactive 13 nm particles ($p=0.45$).

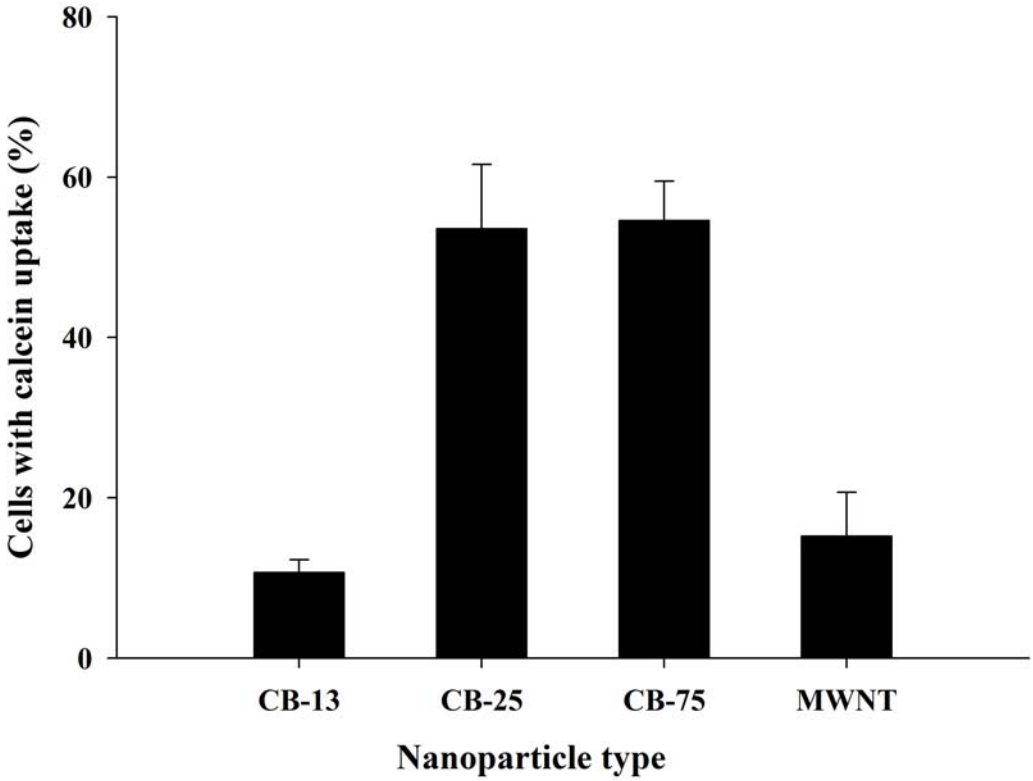

Figure 6.6: Intracellular uptake for carbon nanoparticles of different diameters and MWNTs. Samples were treated at 50 mJ/pulse and 1 min exposure time. All three CB particles were added at a final concentration of 30 μg/mL. MWNTs were added at a final concentration of 4 μg/ml. All particles were supplied at concentrations sufficient to absorb the same amount of light as 25 nm CB. CB-13, CB-25 and CB-75 represent CB particles with mean diameters of 13 nm, 25 nm and 75 nm respectively. Data represent the averages of n=3 replicates with ±SEM shown.

The fact that the size and nature of the carbon particles impact uptake in a manner similar to the way they impact chemical reaction indicates that uptake is strongly related to the extent of chemical reaction. This supports the hypothesis that forces responsible for uptake are generated predominantly due to laser-initiated reaction on the CB particles.

6.2.6. Effect of pulse width on intracellular uptake

Literature shows that the length of the laser pulse that interacts with the carbon particle determines the extent of chemical reaction on the surface of the particle [103].The

shorter the laser pulse, the higher the efficiency of heat retention and chemical reaction. These studies have shown that the time required for a 25 nm diameter particle to cool down after being hit by a laser pulse is 13 ps [103]. So if a laser pulse is shorter than 13 ps, then all heat remains within the particle during the pulse, heating is more efficient and the high temperatures attained by the particles favors chemical reaction. Since in our previous study we had used a femtosecond laser where the pulse length was 100 fs, and in this study we used a nanosecond laser where the pulse length was 10 ns, it enabled us to compare the two pulse lengths in their ability to cause intracellular uptake. If our hypothesis that uptake is governed by forces produced due to light-induced chemical reaction was true then, for the same energy, a 100 fs pulse, by virtue of being shorter and more effective in heating the particles, should also be more efficient in causing uptake than a 10 ns pulse.

We compared the uptake induced by a 1064 nm-10 ns Nd:YAG laser with the uptake induced by a 800 nm-100 fs Ti:Sapphire laser after irradiating a suspension of 25 nm diameter particles for 1 min. First we compared the uptake induced by the fs laser at an intermediate fluence of 0.01 J/cm^2, with the uptake induced by the ns laser for the same energy. As seen from Table 6-1, no uptake occurs in case of the ns laser, and fluence has to be increased to 0.17 J/cm^2 to induce the same uptake as the fs laser.

Table 6-1: Effect of pulse length on intracellular uptake

Laser	Pulse energy (J/pulse)	Fluence (J/cm^2)	% cells with uptake
100 fs Ti:Sapphire laser	0.0003	0.01	32
10 ns Nd:YAG laser	0.05	0.17	35
	0.003	0.01	0

Thus, to produce the same uptake, the fluence required by a 1064 nm-10 ns Nd: YAG laser was about 17-fold higher than the fluence required by a 800 nm-40 fs Ti:Sapphire laser (Table 6-1). According to literature, when the product gases produced due to laser-initiated chemical reactions were measured, it was found that a 1064 nm-10 ns Nd:YAG laser required about 19 times the fluence required by a 780 nm-40 fs Ti:Sapphire laser to produce the same amount of product gas[103]. There is thus a close agreement between previous reports that show the effect of laser pulse length on chemical reaction and our experimental results that show the effect of laser pulse length on cellular uptake. This further strengthens our hypothesis that chemical reaction is the primary driving force behind uptake.

6.2.7. Analysis of gas volume formed during laser irradiation of carbon suspension

Up to this point, we had shown through a series of experiments that uptake was chiefly caused by membrane permeabilizing forces that were generated due to chemical reaction of the CB with the surrounding fluid upon sufficient light absorption. We hypothesized the chemical reaction in this particular system to be the endothermic

carbon-water reaction: $C(s) + H_2O(l) \rightarrow CO(g) + H_2(g)$. To test the validity of our hypothesis we studied the elemental composition of the gases formed after irradiation of the CB suspension with laser using a gas analyzer that operated on the principle of mass spectroscopy (Section 3.2.2).

To determine the composition of the product gases, we injected the air volume above the post irradiated liquid into a quadrupole mass spectroscope[153] (QMS). We observed a peak at atomic mass 12 which corresponds to elemental carbon and monitored this carbon yield as a function of laser irradiation. The carbon yield was found to be 25% and 75% greater than background atmospheric levels after of 1 min and 5 min of irradiation respectively (Figure 6.7). This gas phase C can only be explained if CB reacted with water to produce a product gas that had C as a constituent element. One obvious product is CO, produced during the carbon-steam reaction. As CO transverses the ionization region of the QMS, a fraction of the CO unimolecularly dissociates producing elemental carbon and oxygen. Hence the peak observed at mass 12 could be a result of CO ionization formed during the carbon-steam reaction. This in turn strengthens our hypothesis that the chemical reaction involved in causing cellular uptake is the endothermic carbon-water reaction.

The in vitro study thus not only showed the feasibility of using a nanosecond laser in place of a femtosecond laser for delivering a wide range of molecules, but also strengthened several mechanistic features of our driving hypothesis. The mechanistic observations from the in vitro study together suggest that the efficient intracellular uptake

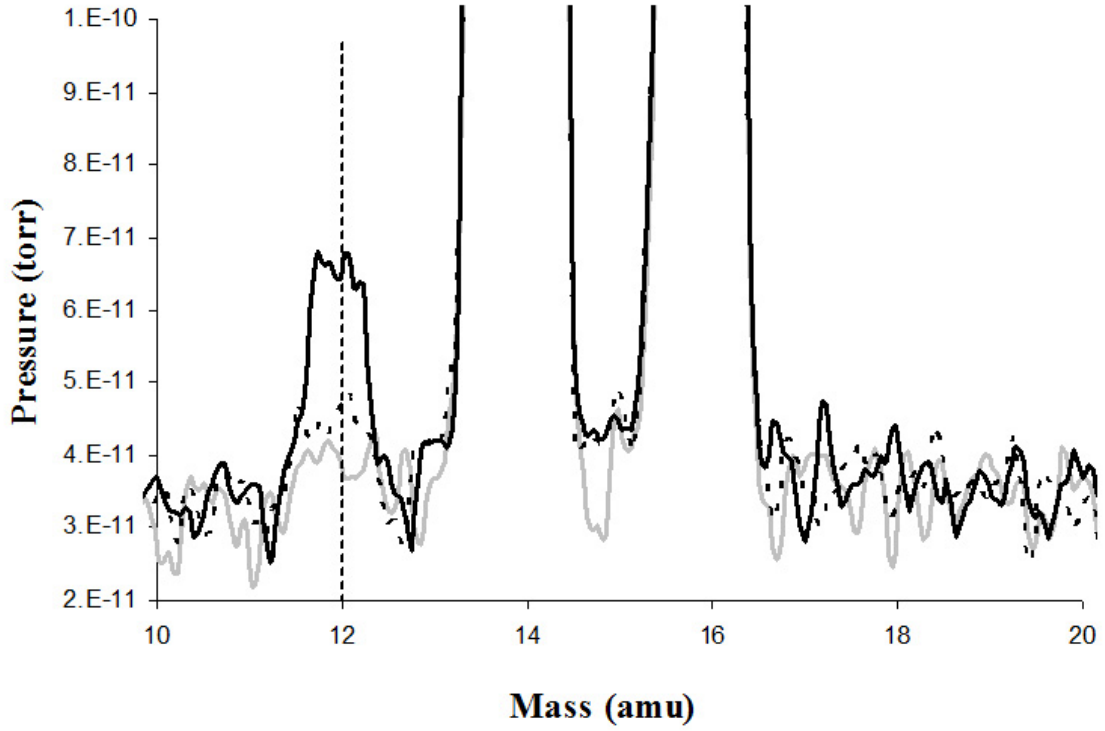

Figure 6.7: Mass spectroscopic analysis of gas volume inside sample chamber after exposure to 100 mJ/pulse laser energy for 0 min (gray line), 1 min (dotted black line) and 5 min (solid black line). The peak at 12 amu indicates increase in elemental carbon over background concentrations because of the presence of CO in the product gas volume inside sample chamber. The large peaks at 14 amu and 16 amu predominantly represent atmospheric nitrogen and oxygen respectively.

observed when CB particles are irradiated with energetic laser pulses is a result of photoacoustic forces generated due to the unique chemistry between carbon and laser energy. This unique chemistry is a strong function of laser power, exposure time, particle size and pulse length. These parameters affect uptake in a manner similar to the way they affect laser-initiated chemical reactions on the surface of the particles. The chemical reaction in this case is the endothermic carbon-water reaction. This suggests that uptake is a direct consequence of forces resulting from chemical reaction initiated by laser on the particle surface, specifically the carbon-water reaction.

Having demonstrated intracellular delivery in vitro, and having obtained stronger proof in support of the photoacoustic nature of membrane permeabilizing forces, our goal was to study if such photoacoustic forces could be equally effective in a dense cellular environment. Since the long term goal of developing this method was to find a better way for drug delivery in humans, it was important to advance the application beyond in vitro cell suspensions and investigate its feasibility in vivo. So we designed a general proof of principle study in vivo using the TA muscle in mice as the model tissue (Section 3.2.3-4). The results from this in vivo study are discussed in the following sections.

6.3. Results: In vivo study

6.3.1. Visualizing uptake in TA muscle

The goal of this study was to determine whether the optimal parameters obtained from the in vitro study could induce intracellular delivery in vivo. Cell impermeant PI was used as the model drug and florescent microscopy was used to visualize uptake.

Muscle sections injected with carbon nanoparticles and PI, but not irradiated with laser show very little uptake of PI (Figure 6.8a-8c). By comparison, the corresponding muscle exposed to nanosecond laser pulses at 75 mJ/pulse for 1 min showed extensive uptake of PI (Figure 6.8c-8e). Uptake seems to have occurred throughout the upper and middle section of the muscle. Since the laser spot was big enough to have covered the

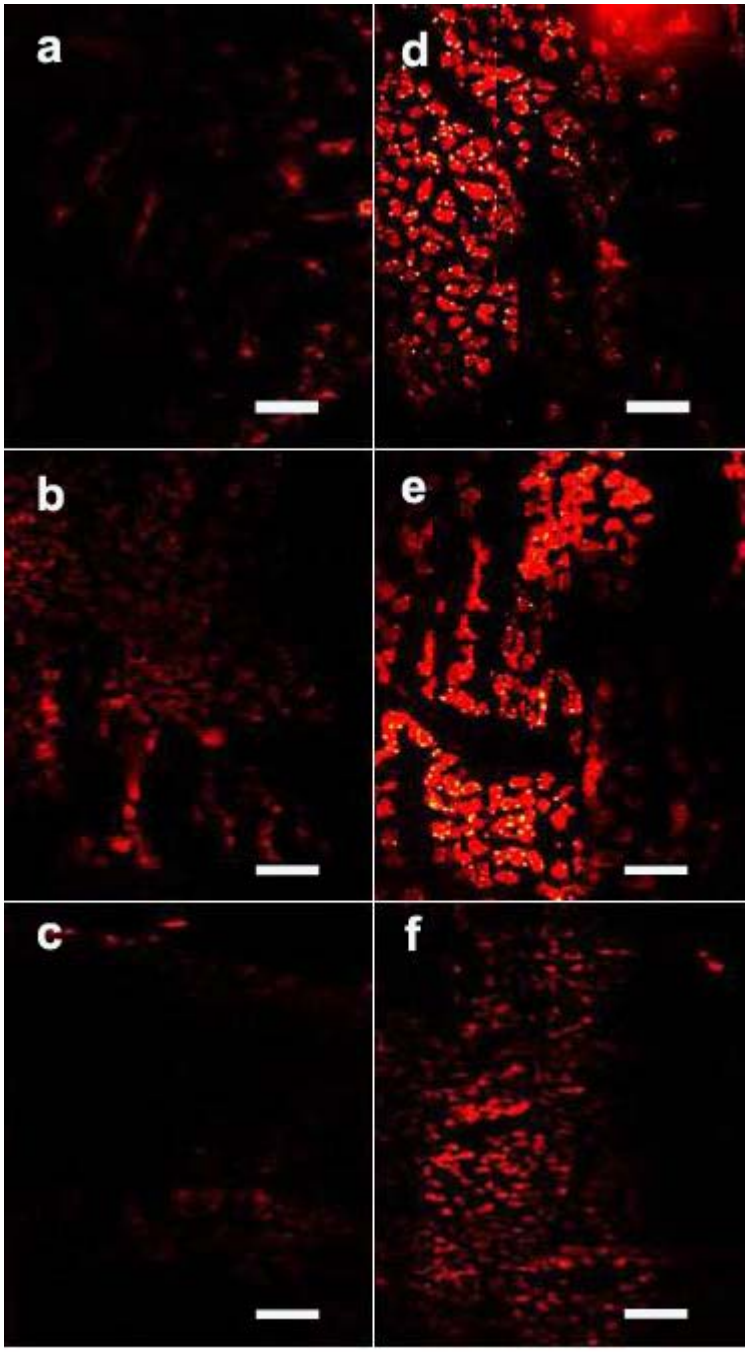

Figure 6.8: Representative transverse sections of upper (a, d), middle (b, e) and lower (c, f) sections of TA muscles as observed under a microscope. Muscle that served as a negative control was not irradiated but subjected to all other treatments (a-c). Muscle subjected to the laser-carbon treatment was exposed to laser light at 75 mJ/pulse for 1 min in presence of carbon nanoparticles at 30 μg/mL and PI. (d-f). Intracellular uptake is indicated by red fluorescence showing uptake of membrane impermeant PI. Scale bars are 500 μm. Control and treated muscles were contralateral and from the same animal.

entire muscle, the patchy nature of uptake indicates that uptake was either limited by the absence of carbon nanoparticles or by the anatomical structure of the muscle. This study thus demonstrated the feasibility of using the laser-carbon system for intracellular delivery in vivo and in dense cellular environments

6.3.2. Quantifying uptake in TA muscle

Having shown that the laser-carbon method could drive intracellular transport even in the cell-dense muscle tissue, our goal was to quantify this uptake so that optimization studies could be done in future. For each section being examined, the total pixel area of the tissue using the bright field image was measured using ImagePro Plus. For each bright field image, a corresponding fluorescent image was taken and the area with red fluorescence was measured. The area with red fluorescence was then expressed as a fraction of the total area from the bright field image. Close to 50% of the muscle fibers showed uptake of PI after the laser-carbon treatment compared to less than 10% in sham exposures (Figure 6.9, $p=0.001$). The laser-carbon system was therefore shown to be effective in causing high intracellular uptake in vivo as well. Even though parameters were not optimized for this study, the uptake was sufficiently high to warrant further studies towards preclinical advancement. With further optimization, the uptake could possibly increase.

6.3.3. Viability of TA muscle post irradiation

Having shown the laser-carbon system as a feasible tool for in vivo delivery, our goal was to study whether the muscles exposed to the system remained viable post

exposure. So we used the nitro blue tetrazolium (NBT) assay to determine the viability of TA muscles after the laser-carbon treatment. The NBT[154, 183] histochemical assay is a well-established histochemical stain for mitochondrial oxidative enzyme activity and is often used to identify viable muscle fibers. Muscle viability is indicated by reduction of colorless NBT to deep blue formazan at the site of enzymatic activity (Section 3.2.4).

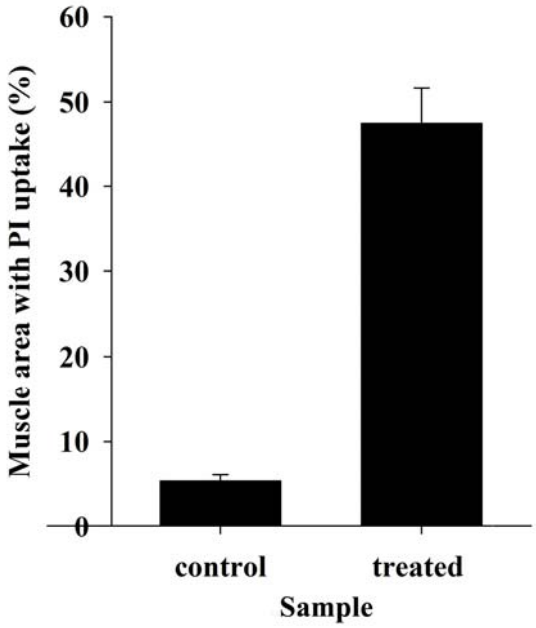

Figure 6.9: Quantifying uptake of PI in muscle. Uptake was quantified using Image-Pro Plus and expressed as a percent of total muscle area. Treated samples were irradiated at 75 mJ/pulse for 1 min in presence of 30 μg/mL CB nanoparticles. Controls were not irradiated but subjected to all other treatments Data represent the averages of n=3 replicates with ±SEM shown.

Figure 6.10a shows a negative control, not incubated in NBT. By comparison, the control incubated in NBT shows a blue staining pattern indicating viable muscle fibers (figure 6.10b). The same blue pattern was also seen in laser-carbon treated muscles

(figure 6.10c). The similarity in blue stain in both control and treated muscles indicates that the laser-carbon treatment did not reduce muscle viability.

6.4. Discussion

This study marks a significant advancement in using pulsed laser with CB nanoparticles to induce efficient intracellular delivery. In the previous study, a Ti: Sapphire femtosecond laser was used for the first time for efficient intracellular delivery via laser-carbon interaction. The main motivation for replacing the Ti:Sapphire laser with a Nd: YAG laser was to find a cheaper, less complicated alternative to the femtosecond laser, one that is already used in medicine. Since the Nd:YAG laser is already FDA approved[55] for various medical procedures, it emerged as the natural replacement. The study demonstrated that even a simple and less expensive laser like the nanosecond Nd: YAG laser can induce high intracellular uptake with high cell viability, not only in vitro but also in vivo. Efficient in vitro delivery was shown for small molecules as well as molecules representative of therapeutic proteins, while maintaining high cell viability. A significant achievement was advancing proof of delivery beyond in vitro cell suspensions and showing its feasibility in vivo in a dense cellular environment. The high uptake observed in vivo strengthens the case for further studies for advancing this system towards clinical application.

Another highlight of this study was the detailed mechanistic analysis which strengthened the mechanistic hypothesis that forces causing uptake are photoacoustic in nature and stem from laser-initiated carbon-water reaction. Since literature contains several references of using nanosecond Nd:YAG laser to induce laser-carbon interaction, this study enabled a direct correlation of those parameters that impact laser-carbon

interaction with cellular uptake. This in turn showed that uptake improved when the parameters favored laser-initiated chemical reaction on the surface of the CB particles. This study successfully integrated a simple, less expensive medically used laser with nanotechnology to achieve efficient intracellular delivery, both in vitro and in vivo. Nanosecond laser irradiation of CB nanoparticles is therefore a potentially powerful tool for efficient intracellular delivery. By providing additional proof and better understanding of the mechanism, the nanosecond laser-carbon study could provide valuable insights towards designing rational optical devices and nanoparticles that incorporate this technology for medical use.

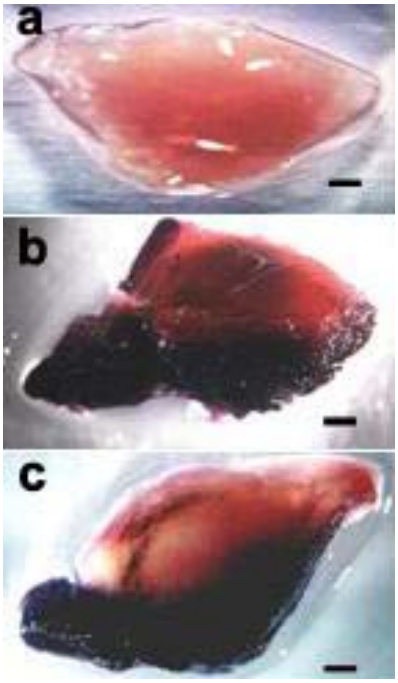

Figure 6.10: Viability of TA muscle as indicted by NBT assay. (a) shows a negative control not incubated with NBT and is representative of how the TA muscle normally looks. (b) shows a negative control incubated with NBT, and (c) shows a treated muscle incubated with NBT. Muscles treated with NBT show a blue staining pattern for both (b) and (c), indicating viable cells. Scale bars are 500 μm. Both (b) and (c) look equally blue suggesting that viability was not affected due to laser-carbon treatment

In summary, the in vitro study strengthened the hypothesis that drug uptake was caused by photoacoustic forces generated by laser-initiated carbon-water reaction, while the in vivo study validated the practicality of using it in a clinical setting. Future studies should build off on these observations and evaluate delivery of therapeutic drugs and genes in vivo. Preclinical efficacy studies, such as long-term survival post laser-carbon treatment, should be carried out in animal models. Additional studies should address optimizing parameters for in vivo application, so that maximum uptake can be obtained with minimal side effects.

6.5. Conclusion

This study demonstrated that carbon nanoparticles can be used synergistically with nanosecond pulsed laser light to facilitate intracellular uptake. The mechanism for uptake was similar to that seen with other physically-mediated intracellular delivery methods like US, viz. entry through reversible membrane breaks[48]. The forces that cause such membrane breaks were shown to be a direct consequence of energy absorption by carbon nanoparticles such that uptake increased as conditions for generating the endothermic carbon-water reaction became more favorable viz. (i) high laser power, (ii) high carbon concentration, (iii) efficient light absorption by CB, (iv) reactivity of CB, (v) short laser pulse length. Cell viability remained high even with high uptake suggesting that the membrane breaks were small enough to be repaired by the cell and large enough to facilitate uptake. In addition, we also demonstrated intracellular delivery in vivo by exposing murine TA muscles to nanosecond laser irradiation in presence of carbon nanoparticles and showing uptake of cell impermeant PI. This study successfully integrated a simple, less expensive medically used laser with nanotechnology to achieve

efficient intracellular delivery, both in vitro and in vivo. Nanosecond laser irradiation of CB nanoparticles is therefore a potentially powerful tool for efficient intracellular delivery.

CHAPTER 7
ULTRASOUND MEDIATED TRANSIENT GENE EXPRESSION IN TISSUE CULTURED LOBLOLLY PINE EMBRYOS

In this study ultrasound (US) was used to deliver reporter plasmids to tissue cultured loblolly pine embryos without generating protoplast. Transient gene expression was shown for multiple genotypes with 15-30% transfection efficiency. Expression was seen to occur over acoustic energies ranging from 70-370 J/cm^2. This study for the first time demonstrates US-mediated transfection in tissue cultured pine embryos and shows that US could be a potential tool for conifer transformation.

7.1. Introduction

Research in genetic transformation of loblolly pine is driven by the need for a sustainable source of fiber for the pulp and paper industry[120, 184]. Loblolly pine maintains a dominant position as the fiber source for the North and South American pulp and paper industry. As demand for pulp and paper products increase, the industry faces a potential shortage in timber resources due to reduction in the forest land base from which trees can be harvested[122]. In addition to environmental regulations and urban growth that reduce availability of these timber resources, yield losses also occur through natural causes like environmental stresses, pathogens and pests. Hence research efforts in forestry are chiefly directed towards creating sustainable tree plantations with trees genetically modified for improved agronomic and value-added traits. Significant advances in somatic embryogenesis of loblolly pines have produced viable methods that can regenerate and propagate plants from a small group of cells[155]. This has already helped circumvent one

of the main barriers in forest biotechnology which is recalcitrance of conifers to in vitro manipulation. As such, the goal of sustainable tree plantations seems to be largely limited by a suitable gene transfer method[185].

Agrobacterium-mediated[125] and biolistic techniques[129], the two most widely used methods of plant transformation, have been explored with varying degrees of success in loblolly pine. Agrobacterium-mediated techniques have had limited success with loblolly pine[128, 186-188]. Although biolistic or gene gun-mediated techniques have been fairly successful, their use is limited because of high maintenance cost and sophisticated operator skills involved[119]. Furthermore, most of these techniques have been patented by forests products companies, and this limits many academic laboratories from using them. Other tools of plant transformation like electroporation[131, 189, 190] and liposomes[130] require removal of the plant cell wall using enzymes to produce protoplasts. Protoplast-generation is a physiologically stressful procedure for the plant cell and consequently regeneration of plants from such cells is not very efficient[116, 117].

The limitations of existing gene delivery techniques for loblolly pine transformation led us to explore alternative techniques that were efficient, cost-effective, user friendly, and that did not require the generation of protoplasts. One such method that had been widely investigated in our laboratory in the context of mammalian cells was US[42]. US-mediated gene delivery occurs through transient breaks in the cell membrane produced as a result of acoustic cavitation[48]. To date, there have been very few studies involving ultrasound-mediated gene delivery in intact plant cells[135, 139, 142, 191]. US has been reported to facilitate gene uptake into plant protoplast and suspension cells[138]. Using almost identical ultrasonic conditions, it was shown that intact virus particles could be

encapsulated by sugar beet protoplasts leading to higher levels of infection[137]. Stable transformation of tobacco has been reported by sonicating leaf segments at the same intensity as that for protoplasts but for a 2000-fold longer exposure time[140]. The same conditions were used for the stable transformation of potato tuber discs[141]. SAAT is another area where US is using to create wounds on the explant body to facilitate entry of the Ti plasmid[143]. Using algal cells, Azencott, et. al showed that US is well suited to deliver macromolecules into intact plant cells[115].

These reports of successful US-mediated delivery in plant cells, the availability of an inexpensive US apparatus and a well developed pine tissue culture system, motivated us to investigate US as a tool for gene delivery in tissue cultured loblolly pine embryos. The long term goal was to develop an efficient in-house tool for pine genetic engineering that, when combined with the benefits of the somatic embryogenesis system, would advance forest biotechnology in general and the research efforts of the pulp and paper industry in particular.

7.2. Results

Our first question was whether US induced uptake of plasmid DNA in loblolly pine embryos. Embryogenic suspension cells of loblolly pine belonging to three different genotypes, 132, 186 and 279, were exposed to a range of US energies in presence of a GFP encoding plasmid (Section 4.1.1-4, 4.1.6). When assayed for transient GFP expression 48 h later using confocal microscopy, sonicated embryos belonging to all three genotypes showed green florescence (Figure 7.1A-C) suggesting uptake and transfection of the foreign gene. Expression was seen mostly at the tip of the embryo which consisted of actively dividing cells and the suspensor cell remained relatively

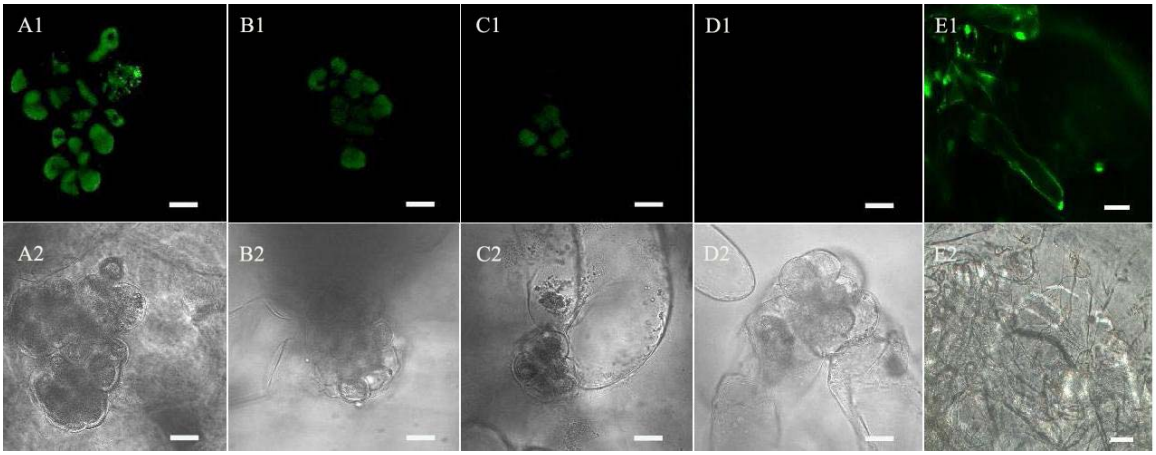

Figure 7.1: Embryonic suspension cells subjected to US (A-C) and SCMT (E) showing expression of GFP. 1 ml of settled cell suspension was mixed with 20 μL of plasmid DNA solution at a final DNA concentration of 1 μg/ml. Samples were sonicated at 5 atm for 50s which equaled 370 J/cm^2 acoustic energy (A-C), or vortexed in presence of 0.4 mg/ml SiC fibers (E). Negative controls were not sonicated or vortexed, but subjected to all other treatments (D). A1-E1 are florescent views and A2-E2 are the corresponding bright field views. Each micrograph shows a close up of a loblolly pine embryo. The clustered end at the tip is the head of the embryo and consists of actively dividing cells. This is the metabolically active part of the embryo and GFP florescence is chiefly observed in these cells. B and C belong to genotypes 186 and 279 respectively, while A, D and E belong to genotype 132. The longer tubular cell supporting the head is the suspensor and it is less metabolically active, acting more like an umbilical cord. GFP florescence is largely absent in the suspensor. Scale bars are 20 μm (A-D) and 100 μm (E).

expression-free No expression was observed in negative controls which consisted of cells not exposed to US, but subjected to all other procedures (Figure 7.1D).

Sometimes, even if the plasmid is delivered, its expression could be inhibited due to several downstream effects. To ensure that expression was not limited by defects in the promoter and thereby eliminate false negatives, we used another physical method called SiC-mediated transformation (SCMT)[132, 192] to treat cells of genotype (Section 4.1.5). GFP expression was also observed in SiC treated cells indicating that gene expression was limited by the extent of intracellular delivery, not by shortcomings of the reporter

plasmid. This was also the first time whisker-mediated gene delivery was shown in tissue cultured loblolly pine embryos.

Having obtained qualitative evidence of gene delivery, our goal was to quantify this expression so that future studies could focus on optimization of parameters. This was done by counting the number of embryos that showed GFP expression, and reporting it as a percentage of the total number of embryos sonicated. First we exposed genotype 132 to US at 5 atm and net exposure times ranging from 10-50 s. This corresponded to US energies ranging from 0-370 J/cm^2. Sonicated samples showed significant GFP expression compared to non-sonicated controls (Figure 7.2, 1-way ANOVA, p=0.004). Mean GFP expression for all US energies varied between 15-30% and there was no statistically significant difference in expression between samples based on exposure times (p=0.3). Although the effect of both pressure and time are accounted for in calculating the acoustic energy, it is worth mentioning that pressure was more important in determining the threshold energy for gene delivery and that no transfection was observed when pressures were below 5 atm even if acoustic energies were the same. In other words, longer exposure times were less important than increased US pressures.

To determine if the genotype of the embryos impacted US-mediated gene delivery, GFP expression was then quantified for all three genotypes, 132, 279 and 186, after sonication with 370 mJ/cm^2 acoustic energy. Mean GFP expression varied between 15-30% and there was no significant difference in expression between samples based on genotype (Figure 7.3, p=0.68).

The above results showed that US could deliver genes into embryos in presence of the cell wall. Cellular uptake required a threshold pressure and was relatively independent of the sonication time or the genotype of the embryos.

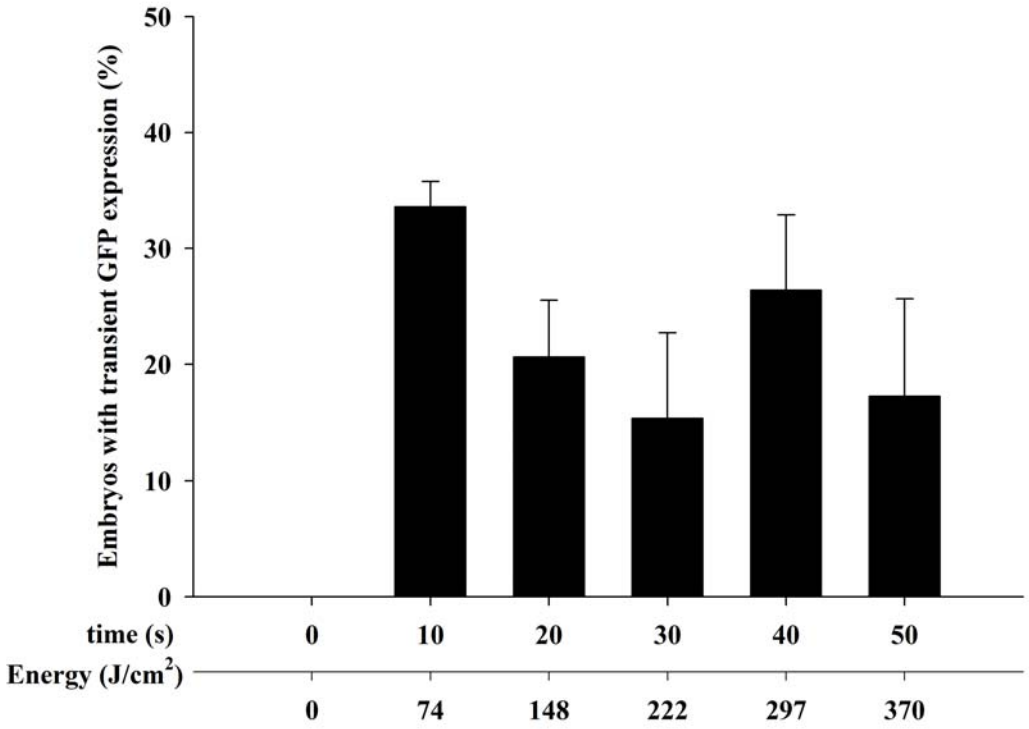

Figure 7.2: Quantifying GFP for suspension cells belonging to genotype 132. 1 ml of settled cell suspension was mixed with 20μL of plasmid DNA solution at a final DNA concentration of 1 μg/ml. Samples were sonicated at 5 atm for 10-50 s which equaled 74-370 J/cm^2 in acoustic energy. Data represent average of n=3 replicates with ± SEM shown.

One of the drawbacks associated with US as observed in mammalian systems is that it is very difficult to control the energy of cavitation and so permeabilized cells often fail to recover due to irreparable membrane wounds. So it was important to investigate whether the pine cells retained their viability or ability to proliferate post sonication.

Embryonic suspensions for the three genotypes were sonicated at 5 atm for 50 s and each embryo from a sample was plated in solid media in 24-well plates. Corresponding negative controls were also plated in separate wells for comparison. On average, each sample contained around 16 embryos. The ability of the plated embryos to proliferate was

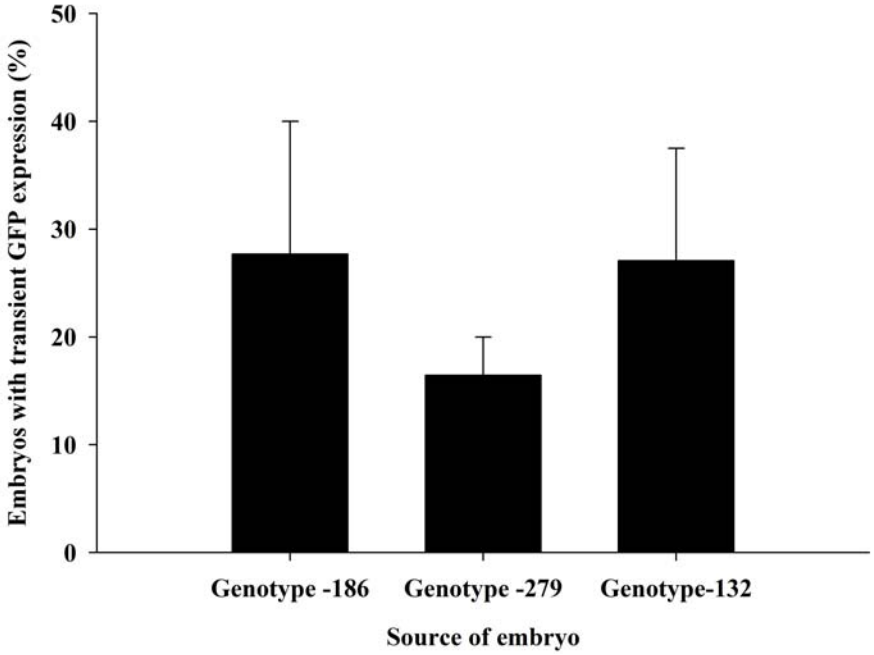

Figure 7.3: Quantifying GFP for suspension cells as a function of genotype. 1 ml of settled cell suspension was mixed with 20μL of plasmid DNA solution at a final DNA concentration of 1 μg/ml. Samples were sonicated at 5 atm for 50 s which equaled 370 J/cm2 in acoustic energy. Data represent average of n=3 replicates with ± SEM shown.

then monitored over a period of 8 weeks. After 8 weeks the number of embryos that

expressed as a percent of all the embryos that were plated (Section 4.1.7). For G-186, the viability of sonicated samples dropped by 14±9% compared to the corresponding non-sonicated controls (Figure 7.4, p=0.011). For G-279, this drop was 20±12% (p=0.03) and

for G-132 the viability dropped by 32±22% (p=0.012). Thus, viability of the sonicated cells differed between genotypes.

7.3. Discussion

Our study showed that US exposure can cause gene delivery and transient expression of the delivered gene in tissue cultured loblolly pine embryos with an intact

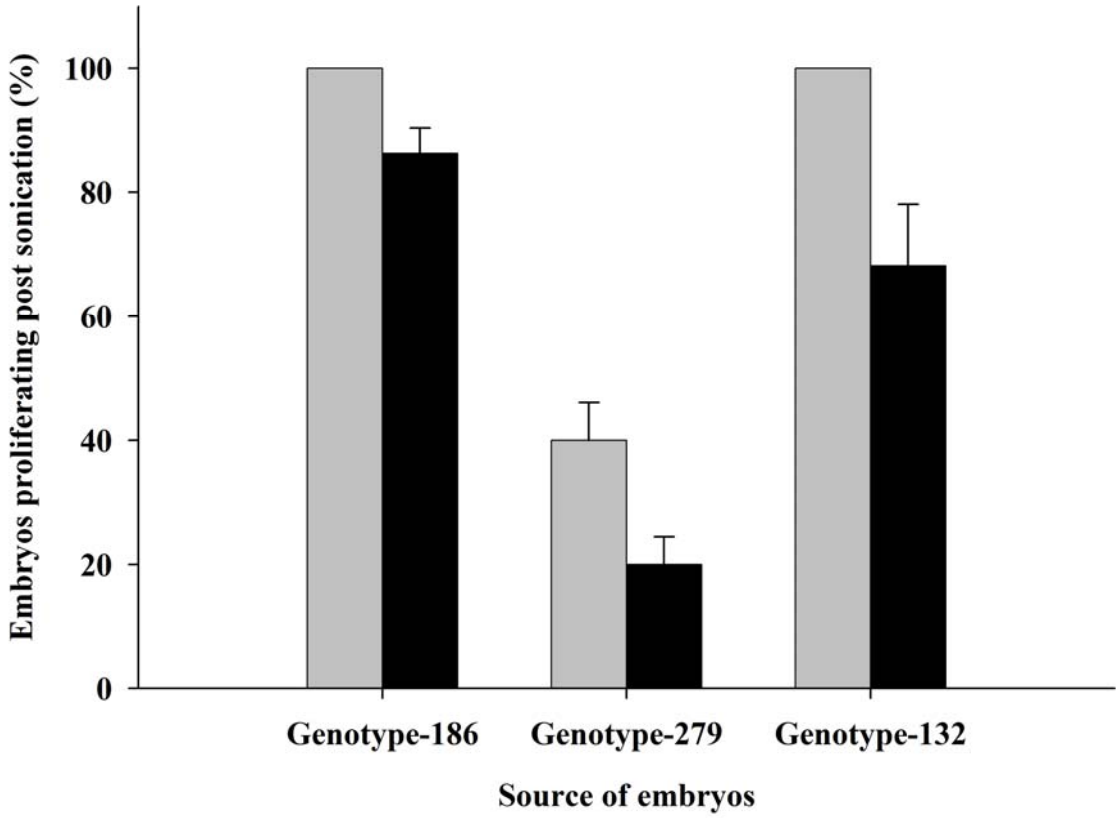

Figure 7.4: Quantifying ability of the embryos to proliferate post sonication. 1 ml of settled cell suspension was mixed with 20 μL of plasmid DNA solution at a final DNA concentration of 1 μg/ml. Samples were sonicated at 5 atm for 10-50 s which equaled 74-370 J/cm2 in acoustic energy and monitored over a period of 8 weeks. Data represent average of n ≥5 replicates with ± SEM shown.

cell wall. This is a significant advancement in the use of a physical method to deliver genes since most other methods (except gene gun and Agrobacterium) require removal of the cell wall by enzymes to create protoplasts prior to gene transfection, followed by regeneration of the cell wall. Because of the physiological stress associated with removal and regeneration of the cell wall, protoplasts generation is not a very efficient method for gene transfection and is often associated with high cell death[116, 117]. In contrast to methods like gene gun, our US apparatus is inexpensive and easy to use. It can be easily set up in small labs without infringing patent restrictions[193].

Uptake was essentially independent of nature of genotype or duration of sonication at the acoustic pressure used in the study. The energy parameters used in this study were based on the optimized parameters obtained from studies with algal cells[115]. Acoustic energy was calculated from pressure, using the relation; $E= (P/\sqrt{2})2t/\rho v$, where E is the energy in Joules/cm^2, P is the pressure, t is the total exposure time, ρ is the density of water and v is the velocity of sound in water. Since the nature of loblolly pine cell wall and membrane is different from that of algal cells, that same pressure might not be the optimal one in this case. Additional optimization studies are required to identify the best energy parameters which might lead to higher transfection efficiencies. It was also observed that as long as pressure was below a certain threshold (5 atm in this case), no expression was observed even if exposure times were increased to keep the acoustic energy constant. This agreed with the inference that since cavitation is a threshold phenomenon, and since uptake is caused by cavitation-induced membrane permeabilization, no uptake takes place below the cavitation threshold[43].

After validating GFP expression with the three genotypes, we used another plasmid encoding for GUS to study expression in genotype 132^{156}. GUS transfection was also seen with the loblolly pine cells. However, when the experiment with GUS was repeated 6 months later, no GUS expression occurred. The one obvious difference in experimental conditions was that during the first transfection study with GUS and as well all the studies with GFP, the embryonic suspensions were freshly generated in the tissue culture facility and were in a healthy metabolic state. By the end of 6 months, the suspensions had been subjected to repeated subcultures and this left them physiologically stressed. This suggests that it is important to consider the metabolic state or age of the suspension culture when evaluating the efficacy of the sonication protocol. A fresh, metabolically active culture is desirable for higher transfection. Cell viability as determined using long-term proliferation assay was dependent on the genotype of the cells, and was on an average around 85%. This further suggests that choice of genotype might be an important consideration for maintaining high cell viability post sonication.

Another highlight of this study was the use of SCMT with intact loblolly pine cells to induce transient expression. We used SCMT due to absence of a reliable positive control to test the efficacy of the reporter plasmids. However in doing so, we also achieved transfection with another easy, inexpensive physical method that did not require protoplast generation. Although we did not quantify the gene expression obtained with SCMT, its success as evidenced qualitatively should motivate further research in using SCMT as another potential gene-delivery tool. Additional studies should be carried out to optimize SCMT and validate its efficacy with the loblolly pine cells.

The efficacy of gene delivery in our study was evaluated through transient gene expression assays. Transient gene expression is helpful as a research method of assessing the short tem efficacy of a gene delivery method or in comparing the expression efficiencies of different gene constructs. However, the major impetus of exploring new methods of gene delivery is to establish a more efficient technology for stable transformation[193]. Only stably transformed embryos can grow into trees with improved traits. So it is important to assess the efficiency of the sonication method for stable integration and expression of the gene after delivery. We did conduct experiments to study stable transfection using US, but the results were inconclusive due to experimental difficulties.

7.4. Conclusion

In summary, this study demonstrated US as a fast, simple, versatile and inexpensive tool for gene delivery in tissue cultured loblolly pine embryos. As discussed earlier, much of the research efforts in the pulp and paper industry are directed towards establishing efficient gene delivery systems and in vitro tissue propagation methods for culturing these plants with improved genetic traits[120]. Research in loblolly pine tissue culture has resulted in a fairly efficient somatic embryogenesis system[155]. Combining the benefits of such a tissue regeneration system with a user friendly gene delivery tool like US could aid the research endeavors of the pulp and paper industry. At present the pulp and paper industry is carrying out fundamental research in to the molecular mechanisms that control lignin production in conifers[194]. This involves screening a large number of genes that are believed to reduce lignin content or promote lignin types that are more easily removed during pulping. Since US can be used to treat a large number of cells in

very little time, it might be preferred over other labor intensive and tedious methods like Agrobacterium and gene gun. Research is also being carried out to find a better promoter for plant gene transfer since the plant virus promoter used at present is not reliable[195]. US can be used here to deliver genes with different promoter constructs so that they can be compared and evaluated to find the promoter with the desired traits In general, this study could renew research in ultrasound-mediated gene delivery of intact plant cells.

CHAPTER 8
DISCUSSION AND CONCLUSIONS

As new drugs and therapeutics surface in the rapidly evolving world of medicine, there is a growing need to find effective and efficient methods of delivering them. Better delivery methods can also improve efficiency of existing drugs, which is often more cost effective than developing a new drug[6]. Most drawbacks associated with conventional drug delivery can be overcome by improving drug localization, targeting and entry into the cell or tissue of interest, so that side effects and high doses are minimized. In this regard, physical methods are creating a new paradigm in drug delivery by integrating mechano-physical principles in achieving desired biological effects. What makes physical methods particularly attractive is their relative non-dependency on the nature of the cell or the drug, making them broadly applicable for a wide variety of cell-drug combinations. Essentially physical methods improve drug action by facilitating entry of drugs into the cell via creation of transient holes/wounds in the cell membrane. Since only cells subjected to the physical perturbation are permeabilized, the effects are localized and lead to non-endocytic drug delivery. Depending on the intensity of the perturbation, the wounds can be large and irreparable or small/moderate and repairable. The biggest challenge with these methods however is controlling the size of the membrane holes such that they are big enough to enable entry of drugs but small enough to repair over time so that cell viability is not compromised[29].

This need for methods that ensure better control over bioeffects led us to investigate other physical phenomena that had potential for creating localized perturbations in biological systems. We found a study published in the early nineties

which showed that when aqueous suspensions of carbon nanoparticles are irradiated with pulsed laser light of appropriate intensity, the particles get heated up on a very short timescale to undergo the carbon-steam reaction with surrounding water, viz. C(s) + $H_2O(l) \rightarrow CO(g) + H_2(g)$[99]. This drove the pressure field almost explosively leading to strong photoacoustic effects like shock waves and sonoluminescence. We saw the close resemblance of these phenomena with acoustic cavitation which was already being studied for intracellular drug delivery[41]. The main problem with acoustic cavitation was that it was not easy to control the energy of imploding cavitation bubbles responsible for membrane holes and as such it was not easy to prevent cell death[49]. The carbon-laser phenomena offered the possibility of tuning the properties of the laser and the nanoparticles to achieve more controlled photoacoustic forces and hence more controlled cellular bioeffects. Thus began the study of this novel drug delivery technology which for the first time sought to exploit a unique physiochemical interaction between laser and carbon to achieve the biological goal of transient membrane permeabilization.

Initially, we reproduced conditions which had been already reported in literature to cause laser-carbon initiated photoacoustic effects. Intracellular uptake was then studied under these conditions to see if uptake could be caused by such physical forces. It was found that efficiency of uptake was strongly related to efficiency of generating photoacoustic forces via chemical-reaction and the mechanism of uptake was very similar to uptake via transient membrane openings. We then eliminated conditions which were known to cause photoacoustic forces and studied uptake under those conditions. This was to determine if uptake was being caused by alternate mechanisms. In this case uptake was

either negligible or much lower compared to uptake under conditions favorable for laser-carbon-initiated photoacoustic effects.

Our very first goal was to test whether in vitro cell suspensions could take up a small molecule when irradiated with femtosecond laser pulses in presence of carbon nanoparticles. We used laser intensities similar to the ones reported in literature to cause carbon-steam reaction, as well as similar carbon particles. The driving hypothesis was that if the cells took up the molecule, it had to be because of the photoacoustic forces described in literature[100, 101, 103, 104]. Not only were we able to induce uptake of small molecules, but also proteins and plasmid DNA using this technique. Furthermore, by varying the laser fluence and exposure time, we found that laser fluence and exposure time had a combinatorial effect on uptake such that uptake increased with increasing fluence and time, and reached a maximum. At optimized conditions calcein uptake was seen in up to 50% of cells with nearly 100% viability and in 90% of cells with ≥90% viability. Similarly, protein uptake and DNA uptake were seen in 39% and 22% of cells, respectively. As evidence of the specificity of the photoacoustic mechanism, uptake was not observed when cells were irradiated in absence of carbon nanoparticles or in the absence of laser. Consistent with an acoustic mechanism, increased media viscosity reduced uptake. Consistent with uptake via membrane poration, uptake was unaffected by suppression of clathrin receptor-mediated endocytosis by K^+-depletion of cells. Consistent with a short-lived effect on cells, uptake was seen in <10% of cells when calcein was added seconds after irradiation. Additionally, when CB particles were replaced by non reactive gold nanorods or less reactive MWNTs, uptake was significantly reduced suggesting that particles had to be capable of reacting explosively

upon irradiation to cause uptake. Since both gold and MWNTs can be heated to very high temperatures, this also suggested that direct thermal effects were not responsible for uptake. In summary, this study supported our hypothesis that laser-carbon interaction produced mild explosive forces that could transiently permeabilize cell membranes to facilitate intracellular uptake.

In the follow up study, we replaced the femtosecond laser with a nanosecond laser and observed similar effects. Physical parameters such as properties of the laser beam and the carbon nanoparticles impacted uptake in the same way as they impacted laser-initiated carbon-steam reaction suggesting that uptake was mediated by the forces resulting from such a reaction. In this study we were also able to show quantitative evidence of carbon-steam reaction by measuring the carbon content in the gas volume formed post irradiation of the suspension. This further strengthened our hypothesis that the photoacoustic effects were produced due to laser-initiated carbon-steam reaction. It also extended the versatility of the system since it showed that as long as conditions were favorable for generating carbon-steam reaction, it may not matter what kind of laser was used. However a femtosecond laser by virtue of being more efficient in heating the particles could produce desired effects at a much lower power compared to a nanosecond laser. Since a wide variety of medical lasers are already approved by FDA[37, 147], depending on the need and application, it might be possible to adapt this technology with the laser that is most suited for the application.

Having demonstrated this new technology in vitro, we then investigated its feasibility in vivo. We used the TA muscle in live mouse as the model tissue because of its convenient location for needle injections and histological analysis in its entirety[196]. We

showed uptake of a cell impermeable molecule in tissues injected with carbon nanoparticles and exposed to nanosecond laser pulses under intensities corresponding to those used in vitro. Uptake appeared as scattered patches suggesting that effects were localized, and was seen in up to 40% of the total muscle area compared to non-irradiated controls. These results illustrated that photoacoustic effects can also operate in the dense cellular environment of the tissue. The insight from this study could guide further research for use of this technology for drug and gene delivery applications in vivo.

Overall, this study demonstrated that the factors that impacted uptake were carbon concentration, carbon reactivity, carbon particle size, laser pulse intensity, exposure time, laser wavelength and laser pulse length, all of which impacted uptake in a manner similar to the way they impact generation of photoacoustic forces. Both laser and carbon had to be present along with cells for uptake to occur indicating a transient photoacoustically induced event. Uptake occurred even when clathirin-mediated endocytosis was suppressed indicating a non-endocytic delivery mechanism, and did not occur when drugs were added post irradiation suggesting the transience of membrane openings. Uptake was predominantly caused by photoacoustic forces as opposed by direct thermal forces or direct chemical forces. Understanding the impact of these forces on cellular bioeffects, viz. uptake and death, helped optimize the system for high intracellular uptake with high cell viability.

In summary, the laser-carbon study has advanced the filed of targeted drug delivery by (i) developing a novel method of intracellular drug delivery by synergistic combination of laser technology with the rapidly evolving field of nanotechnology, (ii) evaluating parameters responsible for causing uptake in the new system and optimizing

them for efficient uptake with minimal cell death, (iii) extending the prospects of clinical application by showing delivery of a range of compounds including model proteins and DNA, as well as by achieving intracellular delivery in vivo. We believe this study will lead to a new paradigm in exploiting laser-material interaction for targeted intracellular drug delivery.

Lasers have been used to remove tattoos since the 1970s[197]. In more recent years, the Q-switched laser has become the preferred method of tattoo removal because of efficient removal with minimal side effects[176]. The mechanism underlying the removal of tattoo using short laser pulses is photoacoustic material breakdown. In case of carbon based tattoos, it is believed that heat deposition in the tattoo material on a short time scale results in material fracture, followed by carbon-steam reaction and leads to lightening of the tattoo. Although Q-switched lasers have been shown to be highly effective in tattoo removal, they are not without adverse effects. Acute events include purpura, crusting, blistering, infection, and oxidative darkening of pigment[198]. Our work with photoacoustic interaction of carbon with pulsed lasers could lead to better understanding of laser-tattoo removal as well and help design more efficient laser-tattoo removal procedures. For instance, our study with the femtosecond laser shows it to be capable of interacting with carbon at much lower energy inputs than nanosecond owing to its shorter pulse length. This could lead to design of lasers for tattoo removal which employ shorter pulses, resulting in lower energy input, better heat deposition in the particle and fewer side-effects on surrounding cells and tissue. Conversely, the laser-carbon drug delivery technology could draw from existing methods in laser-tattoo removal such that it might

be possible to receive a therapeutic treatment or vaccination in a manner similar to getting a tattoo removed.

Laser–tissue interactions are usually divided into photochemical, photothermal, and photomechanical effects[56]. Photomechanical effects, from the three subject areas, are the hardest to define. They encompass a wide and disparate number of phenomena, such as ablation, plasma, cavitation, microstreaming, jet formation, and shock-wave generation[73, 76]. These phenomena, however, are not completely independent. For example, the expansion of the plasma and cavitation can lead to the generation of shock waves, while the collapse of cavitation in the proximity of a solid boundary can form jets[73]. The study of photomechanical effects is driven by the need to improve medical procedures involving high-power lasers and to explore new applications, such as drug delivery. Doukas et al. have presented several studies dealing with photomechanical effects on cells[70, 73, 76, 199]. Their method involved generating stress waves by ablating a target medium with a high power laser. In doing so, laser radiation caused decomposition of target material to small fragments which moved away from the surface of the target at high velocity. Stress waves of high amplitude could be generated by the imparted recoil momentum, and subsequently launched into an aqueous medium which contained the cells. Cells subjected to such LSWs were found to take up extracellular fluorescent markers via transient increase in membrane permeability. However, the mechanism of membrane permeabilization was thought to be similar to electroporation and not clearly elucidated. Our method falls in the realm of LSW, but uses a very different mechanism, i.e., explosive volume change caused by chemically reactive light absorbers[99]. We also found that several features of US-mediated membrane permeabilization, which had not

been studied earlier in context of LSW, were present in our system[48]. This could help throw more light on the mechanism of LSW-mediated membrane permeabilization and help advance this technique for drug delivery.

The interaction of laser light with nanoparticles, such as carbon nanotubes[200], metal nanospheres[201], nanoshells[202], etc. is a rapidly expanding area in both nanotechnology and medicine. Such interaction has previously been used for imaging[85], surgery, PDT[203] and photothermal therapy[149, 179]. Recent advances in nanotechnology have provided a variety of nanostructured materials with highly controlled and interesting properties; including exceptionally high strength[204], the ability to carry and target drugs[18], and unique optical properties[85]. By controlling structure at the nanoscale dimensions, one can control and tailor the properties of these nanostructures in a very predictable manner to meet the needs of a specific application. The nanoparticles that we used in this study were chiefly industrial grade CB[90]. The use of CB in medicine has so far been limited to tattoos[91], vascular labeling[205, 206], phagocytic labeling agent[150-152], and in studies of pollution induced toxicity in lungs[207]. We indentified a novel application for this easily available nanomaterial with very little structural or functional modification. Our use of nanoparticles and laser is different in that the cell/tissue is not directly acted upon by either the particle or the laser. It is the ensuing affects that lead to membrane permeabilization and subsequent delivery. The nanoparticles do not need to enter the cell. Their mass is consumed by laser. All this suggests the possibility of tuning the properties of the laser and nanoparticle such that the entire mass is consumed during irradiation and there is no residual nanoparticle left in the body. This technology could be used for laboratory bench top applications such as in vitro drug/gene delivery. It could be

extended for in vivo delivery for tumor targeting, drug/gene delivery, DNA vaccination, etc. With better design and functionalizing, it is possible that the particles can be tailored to undergo photoacoustic volume changes at lower energies and with more efficient cellular outcomes. Our study could thus open up a new field in design of nanomaterials for photoacoustic volume change to facilitate intracellular drug delivery. In addition to photothermal and diagnostic applications, this study could also trigger research into other non-endocytic drug delivery related applications of nanomaterials by taking advantage of their photoacoustic or photomechanical properties.

As discussed previously, although the photoacoustic interaction of carbon with short laser pulses has been known for a very long time, there is no previous report of using these phenomena for intracellular drug delivery. Germinal studies involving laser induced cavitation around melanosomes were inspired by the interaction of lasers with biological tissue containing pigment microparticles which is of interest both for medical use of lasers and for the development of laser eye safety standards[57]. Since then subsequent studies have been focused on understanding the science behind such phenomena for applications like optical phase conjugation, optical limiting, etc[208, 209]. We for the first time proposed exploiting such interactions for intracellular drug delivery. Our hypothesis was guided by the strong similarity of this system with US mediated acoustic cavitation[48]. We expected this method to not only be more effective but also more tunable since properties of the nanoparticles and laser can be controlled more easily than those of bubbles. Just as we expected, our results showed overwhelming similarity with US-mediated uptake. However one big difference lay in the high cell viability observed even under conditions that produced high uptake. We ascribe this to the non-invasiveness of

the laser near IR wavelength[63], as well as to the photoacoustic effects being highly localized and milder compared to acoustic cavitation. Unlike US, where uptake is governed by a small number of very powerful blasts, our studies suggested uptake in the laser-carbon system to be governed by a large number of weak blasts. This enabled improving uptake by optimizing carbon concentration and laser energy without causing undue cell death. This highly localized nature of bioeffects could find other applications like targeted cell killing without damage to surrounding tissue. Such techniques are already being explored with gold nanoparticles[149]. But with gold and other metallic particles, the mechanism is a purely thermal one wherein heat deposition leads to thermal destruction of cells. The nanoparticles used in our study are non-metallic and direct thermal effects on cells are minimal. This might be more useful in treating heat-sensitive areas. Additionally, the non-invasive nature of our method could find applications in overcoming blood brain .barrier for delivery of therapeutic compounds to the brain[210].

Although many studies exist regarding the fate of carbon nanoparticles inside the body[98], the reports are conflicting. Some say that if injected into skin, the particles are localized inside macrophages which remain embedded permanently in the extracellular matrix and provide a second line of defense against foreign bodies[92]. Other studies say that particles injected into the bloodstream or found loose anywhere else in the body are collected by macrophages and finally directed to the lymphatic system where they end inside lymph nodes[94, 97]. So it is important to know what happens to the remaining particles in our system following irradiation with laser. Efficacy studies will be required to ensure that what works in vitro and in animal models can translate into effective results in human beings as well. Many organelles and body fluids are sensitive to light at

different wavelengths, so proper choice of laser wavelength and energy is necessary. Also the ultimate fate of the particles inside the body needs to be thoroughly investigated so that future complications do not arise due to their accumulation within the body.

By proving to be an effective tool for efficient intracellular delivery, the photoacoustic interaction of carbon with laser presents itself as a novel method of drug delivery that can be potentially used both in vitro and in vivo, for a wide range of cell-drug combinations. This could lay the framework for exploiting other similar physical phenomena for biological application.

Lastly, in a separate study, we evaluated US exposure as a means to facilitate gene transfection in tissue cultured plant embryos. This study was motivated by the need to find an in-house method of genetic transformation for tissue cultured loblolly pine embryos that was inexpensive, easy to use and not restricted by intellectual property rights. Since US has previously shown to be effective in delivering small molecules into algal cells[115] and because of our experience with US-mediated delivery in mammalian cells[45], it emerged as the most suitable method. Our study showed that US exposure can cause gene delivery and transient expression of the delivered gene in different genotypes. Long term viability post sonication was high for some genotype and low for others. This suggests that the choice of genotype might play an important role in the success of using this method. Although further studies are required to optimize this technique, our work demonstrated the potential of ultrasound for delivering genes through intact plant cells.

The US study is important because there have been very few studies in plants that investigate this and almost none that do so in tissue cultured pine embryos[115, 139]. This study showed that US can not only drive molecules across the cell membrane but also

across the cell wall. It can do so in plant tissues that are initiated and propagated in the laboratory. Tissue culture of forest trees is very important for the environment. Genetic modification of these tissue cultured plants can lead to improved traits in trees such as greater lignin production, faster growth rate over shorter times leading to clonal forestry[122]. Our work could renew interest in US-mediated gene delivery of intact plant cells. So far, physical methods have not had much success in transforming intact plant cells without protoplasts formation[116, 127]. Studies with gene gun are restricted due to intellectual property rights. By exploring simple, unsophisticated tools like US and even possibly laser, plant transformation research could become more accessible to small labs and industries which have not been able to advance due to the aforementioned reasons. Furthermore, it could also be a tool to introduce other biologically important molecules such as siRNA, proteins and oligonucleotides, which are used for studying various aspects of plant biology[211].

Overall, this thesis advances the field of drug delivery on several fronts: (i) it introduces and validates a novel physical method that achieves more efficient intracellular drug delivery and is minimally invasive compared to existing physical methods, (ii) it uniquely integrates advanced laser technology and nanoscience in the context of drug delivery by exploiting an aspect of laser-nanoparticle interaction (explosive volume change due to chemical interaction) that had not been previously used for drug delivery, (iii) it advances the method beyond in vitro validation towards in vivo application by evaluating its feasibility in live animal models, (iv) it lays the foundation for the design of new nanomaterials that would respond in a manner similar to carbon nanoparticles upon pulsed laser irradiation while possessing improved traits in terms of

biocompatibility, energy efficiency and targeting efficiency. This study demonstrated a scientific way of investigating a purely physical phenomenon for a biological application for which it had not been previously explored. It reflected the underlying principle of drug delivery as a discipline that helps bridge the gap between biological science and other physical sciences.

It is expected that the thesis will provide the groundwork for developing new drug delivery devices based on synergistic use of laser and nanoparticles to achieve non invasive localized targeted drug delivery with high efficiency. This study thus advocates an interdisciplinary approach to solving problems in medicine and biology, and demonstrates that physical systems are in fact quite adaptable to biological applications

CHAPTER 9
RECOMMENDATIONS

9.1. Laser-carbon study

This thesis was a germinal study that showed the development of a system from concept to laboratory application. The system showed remarkable promise of being an efficient non invasive drug delivery system. To fully realize the potential of this promising new technology, I would recommend continuing the study with focus on therapeutic drugs such as mitochondria-targeting proapoptotic drugs[15], formulations for gene and antisense therapy like oligonucleotides[204] and siRNA[9], and lysosomal enzymes[160], all of which need to be delivered intracellularly to exert their therapeutic action. Another emerging field where this technique could be potentially useful is DNA vaccination[212]. DNA vaccination is a technique for protecting an organism against disease by injecting it with genetically engineered DNA to produce an immunological response. DNA vaccines are comprised of plasmids that are genetically engineered to express disease-specific pathogenic proteins characteristic of infectious organisms. When these plasmids are delivered intracellularly, the expression of pathogenic proteins causes the person's immune system to respond in a protective manner almost the same way as would occur if the person were actually infected by the infectious organism. DNA vaccines are receiving significant interest because of their advantages over conventional vaccines, including the ability to induce a wider range of immune response types. At present delivery of DNA vaccines are being studied using various methods like injection (intramuscular and intradermal), gene gun, jet injection and liposomes. Of all these

methods, gene gun has proved more efficient in terms of direct delivery into cell and using least amount of DNA[32]. Other studies of DNA inoculation in rodents have shown that muscle is 100-1000 times more permissive than other tissues for uptake and expression of DNA[213]. We have shown through our in vivo study that the laser-carbon method can be used for localized intracellular delivery of small molecules into muscle. Further work should build on this study and evaluate how effective this technique is for delivery of DNA vaccines.

Another direction for this technique could be towards tumor therapy. We have previously discussed how the CB nanoparticles could be injected systemically, so that they preferentially locate to tumors through leaky blood vessels. The process of vascular labeling utilizes the exact principle to label leaky blood vessels and India ink (CB suspended in water) has been a popular vascular labeling agent[148, 149]. Hence I recommend designing tumor models that will apply known vascular labeling techniques using CB in conjugation with anti-cancer drugs to achieve drug and nanoparticle localization[84, 214]. A tissue-penetrating NIR beam could then be focused non-invasively at the targeted sites to drive localized drug or gene delivery through laser-nanoparticle interaction. Alternatively, fiber-optic based delivery systems used to transport or guide lasers during laser-surgery on humans should also be investigated[215, 216]. The long-term goal should be development of a device that integrates this technology with the existing knowledge and instrumentation of medical imaging so that a diagnosis of a tumor using optical imaging can be followed by a photoacoustic drug delivery treatment.

The recommendations above are reflective of the scope of this technology. However, before preclinical development, I highly recommend studying individual

components of this method in greater detail so as to better characterize it for subsequent application-oriented studies. Intracellular delivery is believed to occur through the formation of temporary breaks in the membrane. This inference stems from the remarkable similarity in cellular effects caused by acoustic cavitation which has been studied in detail. To strengthen the hypothesis, similar studies involving extensive microscopy and biochemical assays needs to be done with our system as well. We chose CB that had been shown in literature to undergo explosive reaction with laser and produce photoacoustic effects. This was done so that we could be sure that the photoacoustic effects were being generated and thereby focus our experiments on studying their effect on cells, without having to prove the existence of these effects in the first place. I recommend doing detailed TEM, AFM or similar microscopy to study the morphology of these particles, before and after irradiation, in vitro and in vivo. Likewise mass spectroscopy and related techniques can help understand chemical composition of the suspension before and after irradiation. Additional studies should investigate their surface chemistry, extent of aggregation, and their long term effect on cells in terms of possible toxicity and clearance from the body. More studies on both nanoparticles and laser are required to optimize the system within parameters safe for human exposure. Experiments need to be designed to directly measure pressure, temperature, volume and chemical changes in the system so as to better characterize the mechanism involved in cell permeabilization. A theoretical model should be designed based on these experimental observations. The interaction of high-power laser radiation with suspensions of particulate carbon in water has been known to show a range of effects including optical limiting[208], chemical synthesis of gas and liquid-phase species[103], a

‘‘giant’’ photoacoustic effect[99], microscopic shock waves[101], sonoluminescence[104], and bubble formation[106]. Based on testing key components of our hypothesis, we believe uptake to be caused by a combination of all the above forces. It would be interesting to design experiments where each effect could be individually studied for its role in causing uptake. This might require close collaboration with an ultrafast physics lab for design of experiments and interpretation of physical data. I also recommend investigating other nanoparticles, including nanoparticles functionalized for cell-specific targeting, that could cause drug delivery based on the same mechanism as laser-carbon interaction. Other lasers such as FDA approved cosmetic lasers or lasers based on fiber optics should also be evaluated for use. A wider combination of physical as well as biological parameters focusing on in vivo efficacy needs to be studied since our results have shown that each unique combination of drug and cell might require different optimization conditions in terms of laser fluence, exposure time and nanoparticle concentration. These studies will lead to a better understanding of the forces at play and provide valuable insights on design of novel nanomaterials that embrace the photoacoustic properties of CB without the drawbacks and thereby improve on the system in its present form.

9.2. Ultrasound-plant study

This study was an off-shoot of the US-mediated delivery study in mammalian cells[42]. Because of the success of US in delivering genes across mammalian cell membrane it was expected that US could provide an inexpensive tool for delivering genes across plant cells too. However the study was impeded by several factors and foremost among them were lack of a reliable positive control and inability to use certain technologies and biological agents due to intellectual property rights issues. This was

further compounded by the disparity in nature of the plant embryos with the more familiar mammalian cells and absence of previous use of the mammalian bioassay methods with the plant embryos. These shortcomings will need to be addressed before attempting to further the study in future.

Lack of a reliable positive control was a major deterrent in this study. Because gene expression and promoter efficiency is genotype specific, it was hard to say whether the lack of high transfection was because of the shortcoming of the ultrasonic method or because of the low expression efficiency of the delivered plasmid in that particular genotype. Furthermore, optimal transient expression times can vary from 24-72 h or even a week depending on the nature of the plant embryo. Future work should first establish a positive control using a known method of transfection like gene gun bombardment and validate the transfection efficiency of the plasmids being considered for delivery using the known method in the genotype of interest. Once the optimal plasmid, genotype and assay times are identified using the positive controls, it will be easier to interpret results and design new experiments to test ultrasonic method.

Assuming low transfection was result of the inefficiency of ultrasonic method, further studies are required to understand the morphology of the plant embryos, their physiological characteristics and how age and passage number effects these. It was found that the same genotype, during the early stages of subculture had better transfection efficiency than during later stages. It could be that the regenerative ability of the genotype decreases with passage and this in turn reduces transfection efficiency. The nature of the cell wall is another important factor since successful delivery requires both the cell wall and cell membrane to be permeabilized. Experiments should be designed to

study effect of different US parameters on the morphology of cell wall through microscopy so that a better understanding is obtained.

I also recommend using other varieties of plant cells such as rice, maize, tobacco, etc. since US has not been tried for naked gene transfection in intact plant cells in general, not just loblolly pine. SAAT has been shown as an effective method of transfection. I recommend using the same explant as used in SAAT for US study as well to understand if US, which facilitates Agrobacterium entry via wounds in those plants, would also facilitate naked gene entry.

Since the goal of this project was to validate a simple method of loblolly pine transfection not restricted by patent rights, I recommend evaluating another relatively simple method of delivering DNA which is microneedles. Microneedles have already proved to be a viable tool for transdermal delivery of a wide range of molecules including DNA. Owing to the nature of the plant cell, which like the skin, is a strong barrier, it is possible that what we were trying to achieve using US might be more easily achieved using microneedles. However, since microneedles are 2-dimensional, the throughput is expected to be much lower than 3-dimensional technologies like US.

APPENDIX A
NUMERICAL CALCULATIONS INVOLVING CB PROPERTIES AND ENERGY BALANCE

As described in Section 5.4, energy balance calculations were used to estimate the volume of gas generated around each carbon aggregate. They were included at the end of the chapter under supplementary information. This chapter shows details of those calculations, as well others that have not been shown explicitly elsewhere in the thesis.

A.1 Aggregate Properties

Radius of 1 aggregate (r)	=100 nm
Volume of 1 aggregate	$= 4/3\pi r^3 = 4.18 \times 10^{-21}$ m^3
Bulk density of CB[195]	= 29 lb/ft^3 = 0.46 g/cc
Porosity[90, 171, 174]	= 1- (bulk density/particle density) = 1- (0.46/1.8)=0.74=74%
Volume occupied by particles in 1 aggregate	= 26% of volume of aggregate $=1.09 \times 10^{-21}$ m^3
Volume of 1 particle (diameter 25 nm)	$= 8.18 \times 10^{-24}$ m^3
No. of particles/aggregate	$=1.09 \times 10^{-21}$ m^3/8.18×10^{-24} m^3 =133
Mass of 1 particle	$=1.8$ g/cc $\times 8.18 \times 10^{-24}$ m^3 $= 1.47 \times 10^{-17}$ g
Mass of 133 particles or 1 aggregate (m)	$=195.5 \times 10^{-17}$ g $= 1.95 \times 10^{-15}$ g

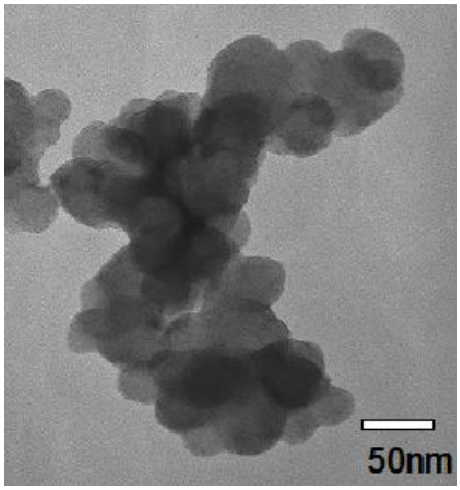

Figure A.1: TEM micrograph showing a typical CB aggregate. The average aggregate size was approximately 200 nm along at least one dimension. For ease of calculation, it was assumed that the aggregates existed as spheres of 200 nm diameter.

A.2 Temperature rise per aggregate and time constants of heat loss

For each experiment, a 2 mm wide beam at 350 mW (350 μJ/pulse) is focused on a sample of 540 μl containing 40 μl carbon suspensions with a stock concentration of 0.4 μg/μl. The power absorbed due to carbon alone is 66.03 mW (66.03 μJ/pulse).

Final concentration of carbon in each sample	=0.4 μg/μl x 40 μl / 540 μl =0.0296 μg/μl
Volume irradiated by the beam per pulse	=π (radius of beam)^2 x thickness of sample chamber which is 2 mm =6.28 x 10^{-9} m^3 =6.28 μl
Mass of carbon irradiated/pulse	=0.0296 μg/μl x 6.28 μl =186 x 10^{-9} g
No. of aggregates irradiated/beam/pulse	=186 x 10^{-9} g/ (1.95x10^{-15} g) = 9.54 x 10^7 ≈ 10^8
Energy absorbed/aggregate/pulse (E)	= 66.03 μJ/10^8 = 6.6 x 10^{-13} J

Let us assume that the energy absorbed per aggregate raises the temperature of the aggregate by ΔT, where T is the absolute temperature; C_p be the molar specific heat at constant pressure[171].

ΔT	$=E/mC_p$ $= 6.6 \times 10^{-13}$ J/ $(1.95 \times 10^{-15}$ g x 8.517/12) = 477 K
Hence T_{final}	=(298+477)K =775 K
Time required for aggregate to uniformly heat up using Fourier's law , where "k" is thermal conductivity of carbon and "A" is area of the aggregate	$=Er/kA\Delta T$ $=6.6 \times 10^{-13}$ J/ (155 W/ mK x $4\pi(100 \times 10^{-9})^2$ m^2 x 477 K/10^{-7} m) $=7 \times 10^{-12}$s
Time required for aggregate to cool down completely due to conduction heat loss alone to surrounding water, where k_w is thermal conductivity of water at 298 K	$= Er/k_wA\Delta T$ =6.6 x 10-13 J/ (0.6 W/mK x $4\pi(100 \times 10^{-9})^2$ m^2 x 477 K/10^{-7} m) $= 2 \times 10^{-9}$s
Time required for aggregate to cool down completely due to radiation heat loss alone, using Stefan–Boltzmann law	=E/(Stefan-Boltzman constant x AT_{final}^4) $=6.6 \times 10^{-13}$ J/ $(5.6703 \times 10^{-8}$ W/m^2/K^4 x 775^4 x 4π $(100 \times 10^{-9})^2$ m^2) $=2.56 \times 10^{-4}$s

A.3 Laplace pressure and thickness of gas shell around aggregate

Let us assume that the energy absorbed per aggregate per pulse goes into generating the carbon-water reaction:

$C(s) + H_2O(l) \rightarrow CO(g) + H_2$, ΔH[173]=131 kJ/mol

No. of moles of carbon consumed	$=E/\Delta H$ $=6.6 \times 10^{-13}$ J /131 kJ/mol $=5.04 \times 10^{-18}$ mol
No. of moles of product gases formed (n)	$=2 \times 5.04 \times 10^{-18}$ mol $=10^{-17}$ mol

Assuming this gas forms a shell around the aggregate, the shell has to expand against the pressure of surrounding water. So we calculated the Laplace pressure of the shell as it equilibrates to room temperature around the aggregate and from this calculated the thickness of the shell in thermal equilibrium with the surrounding water.

A.3.1 Laplace pressure using Newton's method of iteration

Let the radius of the sphere consisting of the aggregate surrounded by the gas shell be L, P be the pressure, and σ be the surface tension at the gas-water interface.

Then equation of Laplace pressure, where P_{water} = 1 atm, σ= 71.97 x 10^{-3}N/m

$=P_{gas}-P_{water},=2\sigma/L$

» $P_{gas} = 2\sigma/L + P_{water}$……(1)

We know that total volume of shell and aggregate = volume of aggregate + volume of gas formed. Using the ideal gas equation where R is the molar gas constant, and for T=298 K, R=8.314 m^3Pa/K/mol, n= 10^{-17} mol.

$4/3\pi L^3$ $=4.18 \times 10^{-21}\ m^3 + nRT/P_{gas}$

$=4.18 \times 10^{-21}\ m^3 + 2477.6 \times 10^{-17}/P_{gas}$…(2)

Combining (1) and (2) and solving for L we get,

$((2.98 \times 10^{-3}/(P_{gas}-1.01x10^5)^3)$ $=10^{-21} + 1.54 \times 10^{-14}/P_{gas}$

Let us define a function f(P) such that

f(P)= $((2.98x10^{-3}/(P-1.01x10^5)^3) - 10-^{21} - 1.54x10^{-14}/P$

Differentiating, $f'(P)= ((8.94\ x10^{-3}/(P-1.01x10^5)^4) + 1.54x10^{-14/}P^2$

We now use Newton's method of iteration to find P using the relation

$x_{n+1} = x_n - \{f(x_n)/f'(x_n)\}$, until $x_n \approx x_{n+1}$

Starting with $P_1=10 \times 10^5$ N/m^2, then

P_2 $= P_1 - \{f(P_1)/f'(P_1)\} = 577176.0927$

P_3	$=P_2 - \{f(P_2)/f'(P_2)\} = 576806.5091$
And so on, until	$P_{18} \approx P_{19}$ $=5.8 \times 10^5$ N/m^2 =5.8 atm
Substituting in P=5.8 atm in (1), L	$= 3.03 \times 10^{-7}$m = 303 nm

Therefore thickness of gas shell = 303 nm – radius of aggregate= (303-100) nm= 203 nm

APPENDIX B
EFFECT OF AVERAGE TEMPERATURE INCREASE ON CELLULAR BIOEFFECTS

B.1 Introduction

One of the questions that came up during the laser carbon study was the effect of heat on cell viability and death. We have shown through the experiments with MWNTs and gold nanorods that direct thermal effects did not cause uptake. We further showed with the DNA-Lipofectamine study that there was no thermal damage to DNA. To further validate that temperature rise did not impact uptake directly, we found it necessary to investigate the effect of uniformly heating cell suspensions on cellular bioeffects, viz. uptake and death. Since we claim that the temperature rise in our system is extremely short lived and that the particles cool down before the next pulse arrives, we wanted to see what would happen if the heat went into increasing the average temperature of the cell suspension media. So we did an experiment where we heated cell suspensions in presence of the model drug calcein for a range of times at a constant temperature of 60^{o}C.

B.2 Methods

Cells were harvested and prepared for experiment as described in Chapter 3. For each sample, 500 μl of the cell suspension containing cells at 10^6 cells/ml was mixed with 10 μl of 1 mM calcein solution. A vacuum oven (1415M, VWR) was heated to 60^{o}C. Samples were then placed inside the oven and heated for times ranging from 0-180

s. Post heating cells were treated with PI and assayed using flow cytometry as described in Chapter 3.

B.3 Results

As seen in Figure B.1, heating cell suspensions at 60^{o}C did not lead to a significant increase in uptake over a time range of 0-180 s (1-way ANOVA followed by Tukey's pairwise comparison, $p=.3$). However, at the same time, the cell viability decreased from 90 % at 120 s to 80% in 140 s, and continued to decrease to less than 10% after 180 s ($p<0.001$). This indicates that if heat or temperatures above 60^{o}C persisted in the suspension longer than 120 s (2 min), this would lead to excessive cell death. However, in our experiments, some of which lasted more than 5 min, viability remained above 80%, while uptake increased beyond 50% (Chapter 5). This suggests that there was no heat retention by the media that could contribute significantly to cellular bioeffects. This further rules out direct thermal effects, in this case uniform heating of the cells due to surrounding media, as a factor in causing cellular bioeffects.

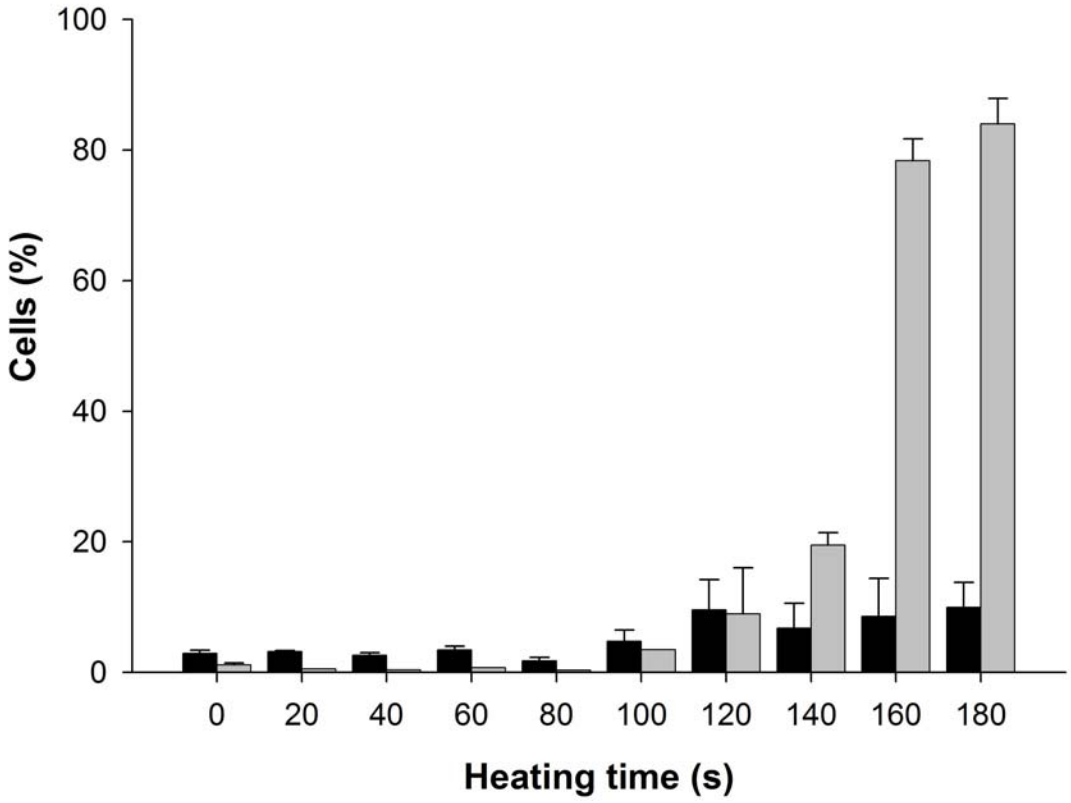

Figure B.1: Effect of uniform heat on cellular bioeffects. Cells were heated at a constant temperature of 60^{o}C in presence of model drug calcein. Black bars indicate viable cells with uptake of calcein. Gray bars indicate dead cells. Data represent average of n=3 replicates with ±SEM shown.

APPENDIX C
EFFECT OF ADDING SDS ON CELLULAR BIOEFFECTS

C.1 Introduction

The laser-carbon treatment required that cell suspensions be mixed with CB nanoparticles. Since CB suspensions were prepared in water in presence of SDS as surfactant (Chapter 3), this meant that cells were in contact with SDS in these treatments. We wanted to find out whether presence of SDS caused any detrimental effect on cells during membrane permeabilization in terms of viability and uptake. So we decided to use US-mediated delivery as a positive control, and compare the bioeffects of cells sonicated in presence of SDS with these positive controls.

C.2 Methods

Cells were harvested as described in Chapter 3. For positive controls, 1 ml cell suspensions at a final concentration of 10^6 cells/ml were mixed with 10 μl of 1 mM calcein solution. Cells were then sonicated at 15 J/cm^2 according to the protocol described in Chapter 4. The same treatments were repeated for cells containing calcein in presence of 0.1% (w/v) SDS. This concentration was equivalent to the concentrations used in laser-carbon treatments. After sonication, cells were assayed with flow cytometry after staining for viability with PI as described in Chapter 3.

C.3 Results

There was no significant difference in uptake between positive controls and cells containing SDS (Figure C.1a, p=0.2). This suggested that presence of SDS did not aid or restrict membrane permeabilization. Likewise there was no significant difference in viability between positive controls and cells containing SDS (Figure C.1b, p=0.1). This suggested that SDS did not aid or impair the ability of the cell membrane to repair itself post permeabilization.

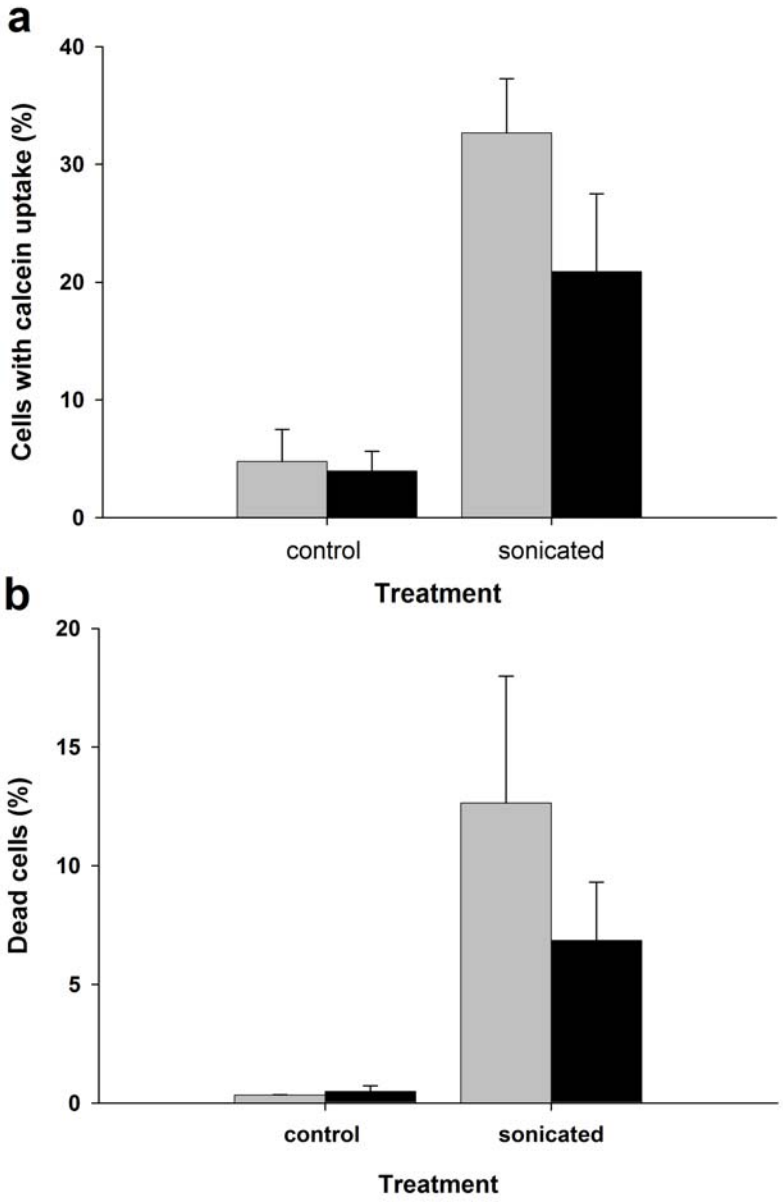

Figure C.1: Effect of SDS on cellular bioeffects. Cells were sonicated at 15 J/cm^2 acoustic energy for 20 s total exposure time in presence of calcein. Gray bars indicate positive controls and black bars indicate cells containing SDS. Data represent average of n=3 replicates with ±SEM shown.

REFERENCES

1. Langer, R. Drug Delivery: Drugs on Target. *Science* **293**, 58-59 (2001).

2. Langer, R. Drug delivery and targeting. *Nature* **392**, 5-10 (1998).

3. Langer, R. Where a Pill Won't Reach. *Scientific American* **288** (2003).

4. Langer, R. & Peppas, N.A. Advances in Biomaterials, Drug Delivery, and Bionanotechnology. *AIChE Journal* **49**, 2990-3006 (2003).

5. Breimer, D.D. Future challenges for drug delivery. *J. Control. Release* **62** (1999).

6. Langer, R. New Methods of Drug Delivery. *Science* **249**, 1527-1533 (1990).

7. Goldberg, M. & Gomez-Orellana, I. Challenges for the oral delivery of macromolecules. *Nat. Rev. Drug Discovery* **2**, 289-295 (2003).

8. Carvalho, G. et al. Cellular therapy in cardiology: analysis of research at the last 10 years. *Circulation* **118**, E481-E481 (2008).

9. Ichim, T.E. et al. RNA interference: A potent tool for gene-specific therapeutics. *Am. J. Transplant.* **4**, 1227-1236 (2004).

10. Leung, R.K.M. & Whittaker, P.A. RNA interference: from gene silencing to gene-specific therapeutics. *Pharmacol. Ther.* **107**, 222-239 (2005).

11. Lee, C.C. & Chiang, B.L. RNA interference: New therapeutics in allergic diseases. *Current Gene Therapy* **8**, 236-246 (2008).

12. Aagaard, L. & Rossi, J.J. RNAi therapeutics: Principles, prospects and challenges. *Advanced Drug Delivery Reviews* **59**, 75-86 (2007).

13. Somia, N. & Verma, I.M. Gene therapy: trials and tribulations. *Nat Rev Genet* **1**, 91-99 (2000).

14. Kaneda, Y. & Tabata, Y. Non-viral vectors for cancer therapy. *Cancer Science* **97**, 348-354 (2006).

15. Huang, X., Zhang, X., Farahvash, B. & Olumi, A.F. Novel Targeted Pro-Apoptotic Agents for the Treatment of Prostate Cancer. *The Journal of Urology* **178**, 1846-1854 (2007).

16. Stephens, D.J. & Pepperkok, R. The many ways to cross the plasma membrane. *Proc. Natl. Acad. Sci. U. S. A.* **98**, 4295-4298 (2001).

17. Tomanin, R. & Scarpa, M. Why Do We Need New Gene Therapy Viral Vectors? Characteristics, Limitations and Future Perspectives of Viral Vector Transduction. *Curr. Gene Ther.* **4**, 357-372 (2004).

18. Xua, Z.P., Zengb, Q.H., Lua, G.Q. & Yub, A.B. Inorganic nanoparticles as carriers for efficient cellular delivery. *Chemical Engineering Science* **61** (2006).

19. Xu, J.P., Ji, J., Chen, W.D., Shen, J.C. & Ji, J.C. Novel biomimetic polymersomes as polymer therapeutics for drug delivery. *J. Control. Release* **107** (2005).

20. Moghimi, S.M., Hunter, A.C. & Murray, J.C. Nanomedicine: current status and future prospects. *FASEB J* **19**, 311-330 (2005).

21. Banerjee, R. Liposomes: Applications in medicine. *Journal of Biomaterials Applications* **16** (2001).

22. Zhu, J.L. et al. Novel polycationic micelles for drug delivery and gene transfer. *J. Mater. Chem.* **18**, 4433-4441 (2008).

23. Lloyd, J.B. Lysosome membrane permeability: implications for drug delivery. *Adv. Drug Deliv. Rev.* **41**, 189-200 (2000).

24. Deshayes, S., Morris, M.C., Divita, G. & Heitz, F. Cell-penetrating peptides: tools for intracellular delivery of therapeutics. *Cellular and Molecular Life Sciences* **62**, 1839-1849 (2005).

25. Temsama, J.l. & Vidal, P. The use of cell-penetrating peptides for drug delivery. *Drug Discovery Today* **9** (2004).

26. Duncan, R. The dawning era of polymer therapeutics. *Nat. Rev. Drug Discov.* **2**, 347-360 (2003).

27. Kim, J.S., Kim, B.I., Maruyama, A., Akaike, T. & Kim, S.W. A new non-viral DNA delivery vector: the terplex system. *J. Control. Release.* **53**, 175-182 (1998).

28. Wells, D.J. Gene therapy progress and prospects: Electroporation and other physical methods. *Gene Therapy* **11**, 1363-1369 (2004).

29. Mehier-Humbert, S. & Guy, R.H. Physical methods for gene transfer: improving the kinetics of gene delivery into cells. *Adv. Drug Delivery Rev.* **57**, 733-753 (2005).

30. Griesbach, R.J. Chromosome mediated transformation via microinjection. *Plant Science* **50**, 69-77 (1987).

31. Kuriyama, S. et al. Particle-mediated gene transfer into murine livers using a newly developed gene gun. *Gene Therapy* **7**, 1132-1136 (2000).

32. Fynan, E.F. et al. DNA vaccines- protective immunizations by parenteral, mucosal, and gene-gun inoculations. *Proceedings of the National Academy of Sciences of the United States of America* **90**, 11478-11482 (1993).

33. Kitagawa, T., Iwazawa, T., Robbins, P.D., Lotze, M.T. & Tahara, H. Advantages and limitations of particle-mediated transfection (gene gun) in cancer immuno-gene therapy using IL-10, IL-12 or B7-1 in murine tumor models. *J. Gene Med.* **5**, 958-965 (2003).

34. Plank, C. et al. The magnetofection method: Using magnetic force to enhance gene delivery. *Biol. Chem.* **384**, 737-747 (2003).

35. Scherer, F. et al. Magnetofection: enhancing and targeting gene delivery by magnetic force in vitro and in vivo. *Gene Ther.* **9**, 102-109 (2002).

36. Zimmermann, U., Pilwat, G. & Rieman, F. Dielectric breakdown of cell membranes. *Biophysics Journal* **14** (1974).

37. Gehl, J. Electroporation: theory and methods, perspectives for drug delivery, gene therapy and research. *Acta Physiol. Scand.* **177**, 437-447 (2003).

38. Aihara, H. & Miyazak, J. Gene transfer into muscle by electroporation in vivo. *Nat. Biotechnol.* **16** (1998).

39. Canatella, P.J., Karr, J.F., Petros, J.A. & Prausnitz, M.R. Quantitative study of electroporation-mediated molecular uptake and cell viability. *Biophysical Journal* **80** (2001).

40. Belehradek, M. et al. Electrochemotherapy, a new antitumor treatment-1st clinical phase I-II trial. *Cancer* **72**, 3694-3700 (1993).

41. Mehier-Humbert, S., Bettinger, T., Yan, F. & Guy, R.H. Plasma membrane poration induced by ultrasound exposure: implication for drug delivery. *J. Controlled Release* **104**, 213-222 (2005).

42. Guzman, H.R., Nguyen, D.X., Khan, S. & Prausnitz, M.R. Ultrasound-mediated disruption of cell membranes. I. Quantification of molecular uptake and cell viability. *J. Acoust. Soc. Am.* **110**, 588-596 (2001).

43. Hallow, D.M., Mahajan, A.D., McCutchen, T.E. & Prausnitz, M.R. Measurement and correlation of acoustic cavitation with cellular bioeffects. *Ultrasound in Medicine & Biology* **32**, 1111-1122 (2006).

44. Wang, X.H., Liang, H.D., Dong, B.W., Lu, Q.L. & Blomley, M.J.K. Gene transfer with microbubble ultrasound and plasmid DNA into skeletal muscle of mice: Comparison between commercially available microbubble contrast agents. *Radiology* **237**, 224-229 (2005).

45. Guzman, H.R. (Georgia Institute of Technology, Atlanta; 2001).

46. Schlicher, R.K. 220 (Georgia Institute of Technology, Atlanta; 2006).

47. Wei, W., Zheng-zhong, B., Yong-jie, W., Qing-wu, Z. & Ya-lin, M. Bioeffects of Low-Frequency Ultrasonic Gene Delivery and Safety on Cell Membrane Permeability Control. *Journal of Ultrasound in Medicine* **23** (2004).

48. Schlicher, R.K. et al. Mechanism of intracellular delivery by acoustic cavitation. *Ultrasound Med. Biol.* **32**, 915-924 (2006).

49. Guzman, H.R., McNamara, A.J., Nguyen, D.X. & Prausnitz, M.R. Bioeffects caused by changes in acoustic cavitation bubble density and cell concentration: a unified explanation based on cell-to-bubble ratio and blast radius. *Ultrasound in Medicine & Biology* **29**, 1211-1222 (2003).

50. Lefesvre, P., Attema, J. & van Bekkum, D. A comparison of efficacy and toxicity between electroporation and adenoviral gene transfer. *Bmc Molecular Biology* **3** (2002).

51. Zarnitsyn, V.G. & Prausnitz, M.R. Physical parameters influencing optimization of ultrasound-mediated DNA transfection. *Ultrasound Med Biol* **30**, 527-538 (2004).

52. Herd, R.M., Dover, J.S. & Arndt, K.A. Basic laser principles. *Dermatol. Clin.* **15**, 355-& (1997).

53. Kurtz, R.M. et al. Nonlinear effects and potential surgical advantages of femtosecond lasers. *Invest. Ophthalmol. Vis. Sci.* **35**, 1786-1786 (1994).

54. Vogel, A. Mechanisms of femtosecond laser nanosurgery of cells and tissues. *Applied Physics B: Lasers and Optics* **81**, 1015-1047 (2005).

55. Weiblinger, R.P. Review of the clinical literature on the use of the Nd-YAG laser for posterior capsulotomy. *J. Cataract. Refract. Surg.* **12**, 162-170 (1986).

56. Waynant, R.W. Lasers in medicine. (oca Raton : CRC Press, c2002).

57. Sakimoto, T., Rosenblatt, M.I. & Azar, D.T. Laser eye surgery for refractive errors. *Lancet* **367**, 1432-1447 (2006).

58. Spicer, M.S. & Goldberg, D.J. Lasers in dermatology. *J. Am. Acad. Dermatol.* **34**, 1-25 (1996).

59. Cotton, P.B. et al. Endoscopic laser lithotripsy of large bile-duct stones. *Gastroenterology* **99**, 1128-1133 (1990).

60. McCaughan, J.S. Photodynamic therapy - A review. *Drugs Aging* **15**, 49-68 (1999).

61. Ochsner, M. Photodynamic therapy: The clinical perspective - Review on applications for control of diverse tumorous and non-tumorous diseases. *Arzneimittelforschung* **47**, 1185-1194 (1997).

62. Huang, Z. A review of progress in clinical photodynamic therapy. *Technol. Cancer Res. Treat.* **4**, 283-293 (2005).

63. Weissleder, R. A clearer vision for in vivo imaging. *Nat Biotechnol* **19**, 316-317 (2001).

64. Clark, I.B. et al. Optoinjection for efficient targeted delivery of a broad range of compounds and macromolecules into diverse cell types. *Journal of Biomedical Optics* **11** (2006).

65. Schneckenburger, H., Hendinger, A., Sailer, R., Strauss, W.S.L. & Schmitt, M. Laser-assisted optoporation of single cells. *Journal of Biomedical Optics* **7**, 410-416 (2002).

66. Montag, M. Laser-induced immobilization and plasma membrane permeabilization in human spermatozoa. *Human Reproduction* **15**, 846-852 (2000).

67. Tao, W., Wilkinson, J., Stanbridge, E.J. & Berns, W. Direct Gene-Transfer into human cultured-cells facilitated by laser micropuncture of the cell membrane. *Proc. Natl. Acad. Sci. U. S. A.* **84**, 4180-4184 (1987).

68. Umebayashi, Y., Miyamoto, Y., Wakita, M., Kobayashi, A. & Nishisaka, T. Elevation of Plasma Membrane Permeabilty on Laser Irradiation of extracellular Latex Particles. *The Journal of Biochemistry* **134**, 219-224 (2003).

69. Menezes, V., Takayama, K., T.Ohki & J.Gopalan Laser-ablation-assisted microparticle acceleration for drug delivery. *Applied Physics Letters* **87** (2005).

70. Lee, A.U. & Doukas, A.G. Laser-generated stress waves and their effects on the cell membrane. *IEEE J. Sel. Top. Quantum Electron.* **5**, 997 997-1003 (1999).

71. Tirlapur, U.K. & Konig, K. Targeted transfection by femtosecond laser. *Nature* **418**, 290-291 (2002).

72. Berg, K., Selbo, P.K., Prasmickaite, L. & Hogset, A. Photochemical drug and gene delivery. *Current Opinion in Molecular Therapeutics* **6**, 279-287 (2004).

73. Doukas, A.G. & Flotte, T.J. Physical Characteristics and Biological Effects of Laser-Induced Stress Waves. *Ultrasound Med. Biol.* **22**, 151-164 (1996).

74. Doukas, A.G., Daniel, J., Venugopalan, V. & Flotte, T.J. Physical factors involved in stress-wave-induced cell injury: The effect of stress gradient, Vol. 21. (1995).

75. Vogel, A., Capon, M.R.C., Asiyovogel, M.N. & Birngruber, R. Intraocular photodisruption with picosecond and nanosecond laser pulses- tissue effects in cornea, lens, and retina. *Invest. Ophthalmol. Vis. Sci.* **35**, 3032-3044 (1994).

76. Doukas, A.G. & Flotte, T.J. Biological Effects of Laser-Induced Shock-Waves - Structural And Functional Cell-Damage Invitro. *Ultrasound Med. Biol.* **19**, 137-146 (1993).

77. Chang, D.C. & Reese, T.S. Changes in membrane structure induced by electroporation as revealed by rapid freezing electron microscopy. *Biophysical Journal* **58**, 1-12 (1990).

78. Thomas, J.F., Anderson, T., Daniel J. McAuliffe, Sr., Tayyaba, H. & Apostolos, G.D., Vol. 1882. (eds. L.J. Steven & K. Abraham) 122-129 (SPIE, 1993).

79. Akerman, M.E., Chan, W.C.W., Laakkonen, P., Bhatia, S.N. & Ruoslahti, E. Nanocrystal targeting in vivo. *Proceedings of the National Academy of Sciences of the United States of America* **99**, 12617-12621 (2002).

80. Ferrari, M. Cancer nanotechnology: Opportunities and challenges. *Nat. Rev. Cancer* **5**, 161-171 (2005).

81. Pankhurst, Q.A., Connolly, J., Jones, S.K. & Dobson, J. Applications of magnetic nanoparticles in biomedicine. *J. Phys. D-Appl. Phys.* **36**, R167-R181 (2003).

82. Bai, S.H., Thomas, C., Rawat, A. & Ahsan, F. Recent progress in dendrimer-based nanocarriers. *Crit. Rev. Ther. Drug Carr. Syst.* **23**, 437-495 (2006).

83. Pitsillides, C.M., Joe, E.K., Wei, X., Anderson, R.R. & Lin, C.P. Selective Cell Targeting with Light-Absorbing Microparticles and Nanoparticles. *Biophys. J.* **84**, 4023-4032 (2003).

84. Yuan, F. et al. Vascular-Permeability in a Human Tumor Xenograft - Molecular-Size Dependence and Cutoff Size. *Cancer Res.* **55**, 3752-3756 (1995).

85. Gao, X.H., Cui, Y.Y., Levenson, R.M., Chung, L.W.K. & Nie, S.M. In vivo cancer targeting and imaging with semiconductor quantum dots. *Nat. Biotechnol.* **22**, 969-976 (2004).

86. Kam, N. Carbon nanotubes as multifunctional biological transporters and near-infrared agents for selective cancer cell destruction. *Proc. Natl. Acad. Sci. U. S. A.* **102**, 11600-11605 (2005).

87. Liu, Z. et al. Drug delivery with carbon nanotubes for in vivo cancer treatment. *Cancer Research* **68**, 6652-6660 (2008).

88. Kam, N.W.S. & Dai, H.J. Single walled carbon nanotubes for transport and delivery of biological cargos. *Physica Status Solidi B-basic Solid Stat Physics* **243**, 3561-3566 (2006).

89. Cai, D. et al. Highly efficient molecular delivery into mammalian cells using carbon nanotube spearing. *Nat. Methods* **2**, 449-454 (2005).

90. Cabot, I. *Material Safety Data Sheet* (Alpharetta, GA).

91. Nizam, R., Siddiqi, N., Landas, S.K., Kaplan, D.S. & Holtzapple, P.G. Colonic tattooing with India ink: Benefits, risks, and alternatives. *Am. J. Gastroenterol.* **91**, 1804-1808 (1996).

92. Fujita, H., Nishii, Y., Yamashita, K., Kawamata, S. & Yoshikawa, K. The uptake and long-term storage of India ink partilces and latex beads by fibroblasts in the dermis and subcutis of mice, with special regard to the non-inflammatory defense reaction by fibroblasts. *Arch. Histol. Cytol.* **51**, 285-294 (1988).

93. Koszewski, B.J., Emerick, C.W. & Dicus, D.R. Studies of phagocytic activity of lymphocytes. 3.Phagcytes of intravenous India ink in human subjects. *Blood* **12**, 559-566 (1957).

94. Haigh, P.I. et al. Carbon dye histologically confirms the identity of sentinel lymph nodes in cutaneous melanoma. *Cancer* **92**, 535-541 (2001).

95. Brandwood , A., Noble, K.R. & Schindhelm, K. Phagocytosis of carbon particles by macrophages in vitro. *Biomaterials* **13**, 646-648. (1992).

96. Donald, K.J. & Tennent, R.J. Relative roles of platelets and macrophages in clearing particles from blood- value of carbon clearance as a measure of reticuloendothelial phagocytosis. *J. Pathol.* **117**, 235-& (1975).

97. Oghiso, Y. & Matsuoka, O. Time-dependent changes of microscopic localization of intravenously administered colloidal carbon particles in mouse lymph nodes. *J Toxicol Sci.* **8**, 291-300. (1983).

98. Freitas-Jr., R.A. & Nanomedicine, Volume IIA: Biocompatibility. (Landes Bioscience, Georgetown; 2003).

99. Chen, H.X. & Diebold, G. Chemical Generation of Acoustic-Waves - A Giant Photoacoustic Effect. *Science* **270**, 963-966 (1995).

100. Beveridge, A.C., McGrath, T.E. & Diebold, G.J. Photoacoustic shock generation in carbon suspensions. *Appl. Phys. Lett.* **75**, 4204-4206 (1999).

101. Lowen, H. & Madden, P.A. A microscopic mechanism for shock-wave generation in pulseci-laser- heated colloidal suspensions. *J. Chem. Phys.* **97**.

102. Chen, H., McGrath, T. & Diebold, G. Laser Chemistry in Suspensions: new products and Unique Reaction Conditions for the Carbon-Steam Reaction. *Angew. Chem., Int. Ed. Engl.* **36**, 163-166 (1997).

103. McGrath, T.E. & Diebold, G.J. Laser-Initiated Chemical Reactions in Carbon Suspensions. *J. Phys. Chem.* **106**, 10072-10078 (2002).

104. McGrath, T.E., Beveridge, A.C. & Diebold, G.J. Sonoluminescence initiated by laser irradiation of carbon suspensions. *Applied Physics Letters* **73**, 1029-1031 (1998).

105. Lin, C.P. & Keiiy, M.W. Cavitation and acoustic emission around laser-heated microparticles. *Appl. Phys. Lett.* **72** (1998).

106. Kotaidis, V. Cavitation dynamics on the nanoscale. *Applied Physics Letters* **87**, 21 (2005).

107. Apfel, R.E. Sonic effervescence: A tutorial on acoustic cavitation. *Journal of the Acoustical Society of America* **101**, 1227-1237 (1997).

108. Miller, M.W., Miller, D.L. & Brayman, A.A. A review of in vitro bioeffects of inertial ultrasonic cavitation from a mechanistic perspective. *Ultrasound in Medicine and Biology* **22**, 1131-1154 (1996).

109. Cochran, S.A. & Prausnitz, M.R. Sonoluminescence as an indicator of cell membrane disruption by acoustic cavitation. *Ultrasound in Medicine and Biology* **27**, 841-850 (2001).

110. Bell, A.G. On the Production and Reproduction of Sound by Light. *American Journal of Sciences* **20**, 305-324 (1880).

111. Xu, M.H. & Wang, L.H.V. Photoacoustic imaging in biomedicine. *Review of Scientific Instruments* **77** (2006).

112. Rosencwa, A. Photoacoustic spectroscopy of biological materials. *Science* **181**, 657-658 (1973).

113. Zharov, V.P. et al. Photoacoustic flow cytometry: principle and application for real-time detection of circulating single nanoparticles, pathogens, and contrast dyes in vivo. *Journal of Biomedial Optics* **12** (2007).

114. Tepfer, M. & Taylor, I.E.P. The permeability of plant cell walls as measured by gel-filtration chromatography. *Science* **213**, 761-763 (1981).

115. Azencott, H.R., Peter, G.F. & Prausnitz, M.R. Influence of the cell wall on intracellular delivery to algal cells by electroporation and sonication. *Ultrasound Med Biol. 2007 Nov;33(11):1805-17. Epub 2007 Jun 28.*

116. Simmonds, D.H. Plant cell wall removal- cause for microtubule instability an division abnormalities in protoplast cultures. *Physiologia Plantarum* **85**, 387-390 (1992).

117. Larkin, P.J. Purification and viability determinations of plant protoplasts. *Planta* **128**, 213-216 (1976).

118. Wu, F.S. & Cahoon, A.B. Plasmolysis facilitates the accumulation of protein and DNA into extra-plasmalemma spaces of intact plant cells. *Plant Science* **104**, 201-214 (1995).

119. Rakoczy-Trojanowska, M. Alternative methods of plant transformation - A short review. *Cellular & Molecular Biology Letters* **7**, 849-858 (2002).

120. Pullman, G.S., Cairney, J. & Peter, G. Clonal forestry and genetic engineering: where we stand, future prospects, and potential on mill operations. *TAPPI Journal* **81**, 57-64 (1998).

121. Tang, W. & Newton, R.J. Genetic transforamtion of conifers and its application in forest biotechnoliogy. *Plant Cell Reports* **22**, 1-15 (2003).

122. Merkle, S.A. & Dean, J.F.D. Forest Tree Biotechnology. *Current Opinion in Biotechnology* **11**, 298-302 (2000).

123. Walter, C. Genetic engineering in conifer forestry: technical and social considerations. *In Vitro Cellular and Developmental Biology-Plant* **40**, 434-441 (2004).

124. Zambryski, P. Basic processes underlying Agrobacterium-mediated DNA transfer to plant cells. *Annual Review of Genetics* **22**, 1-30 (1988).

125. Klee, H., Horsch, R. & Rogers, S. Agrobacterium-mediated plant transformation and its further applications to plant biology. *Annual Review of Plant Physiology* **38**, 467-486 (1987).

126. Tzfira, T. & Citovsky, V. Partners-in-infection: host proteins involved in the transformation of plant cells by Agrobacterium. *Trends in Cell Biology* **12**, 121-129 (2002).

127. Songstad, D.D., Somers, D.A. & Griesbach, R.J. Advances in alternative DNA delivery techniques. *Plant Cell, Tissue, and Organ Culture* **40**, 1-15 (1995).

128. Tang, W., Sederoff, R. & Whetten, R. Regeneration of transgenic loblolly pine (Pinus taeda L.) from zygotic embryos transformed with Agrobacterium tumefaciens. *Planta* **213**, 981-989 (2001).

129. Taylor, N.J. & Fauquet, C.M. Microparticle Bombardment as a Tool in Plant Science and Agricultural Biotechnology. *DNA and Cell Biology* **21**, 963-977 (2002).

130. Gad, A.E., Rosenberg, N. & .Altman, A. Liposome-mediated gene delivery into plant cells. *Physiologia Plantarum* **79**, 177-183 (1990).

131. Fromm, M., Taylor, L.P. & Walbot, V. Expression of genes transferred into monocot and dicot plant cells by electroporation. *Proc Natl Acad Sci USA* **82**, 5824-5828 (1985).

132. Wang, K., Drayton, P., Frame, B., Dunwell, J. & Thompson, J.A. Whisker-mediated plant transformation: an alternative technology. *In Vitro Cellular and Developmental Biology* **31**, 101-104 (1995).

133. Birch, R.G. Plant transformation: problems and strategies for practical application. *Annual Review of Plant Physiology and Plant Molecular Biology* **48** (1997).

134. Sharma, K.K., Bhatnagar-Mathur, P. & Thorpe, T.A. Genetic transformation technology: status and problems. *In Vitro Cellular and Developmental Biology-Plant* **41**, 102-112 (2005).

135. Bleaney, B.I. & Oliver, R. The effect of irradiation of Vicia faba roots with 1.5 MHz ultrasound. *British Journal of Radiology* **45**, 358-361 (1972).

136. Child, S.Z., Carstensen, E.L. & Miller, M.W. Growth of pea roots exposed to pulsed ultrasound. *Journal of the Acoustical Society of America* **58**, 1109-1110 (1975).

137. Joersboe, M. & Brunstedt, J. Protein synthesis stimulated in sonicated sugar beet cells and protoplasts. *Ultrasound in Medicine and Biology* (1990).

138. Joersboe, M. & J.Brunstedt Direct gene transfer to plant protoplasts by mild sonication. *Plant Cell Reports* **9**, 207-210 (1990).

139. Lui, Y., Yang, H. & Sakanishi, A. Ultrasound: Mechanical gene transfer into plant cells by sonoporation. *Biotechnology Advances* **24** (2005).

140. Zhang, L.J. et al. Efficient transformation of tobacco by ultrasonication. *Biotechnology* **9**, 996-997 (1991).

141. Sawahel, W.A. Ultrasound-mediated stable transformation of potato tuber discs. *Biotechnology Techniques* **10**, 821-824 (1996).

142. Choudhary, M.L. & Chin, C.K. Ultrasound mediated delivery of compounds into petunia protoplasts and cells. *Journal of Plant Biochemistry and Biotechnology Techniques* **4**, 37-39 (1995).

143. Trick, H.N. & Finer, J.J. SAAT: sonication-assisted Agrobacterium-mediated transformation. *Transgenic Research* **6**, 329-337 (1997).

144. Bohm, H. et al. Viability of plant cell suspensions exposed to homogeneous ultrasonic fields of different energy density and wave type. *Ultrasonics* **38**, 629-632 (2000).

145. Link, S., Burda, C., Nikoobakht, B. & El-Sayed, M.A. Laser-induced shape changes of colloidal gold nanorods using femtosecond and nanosecond laser pulses. *J. Phys. Chem. B* **104**, 6152-6163 (2000).

146. Kenneth R. Stone, Mickey, D.D., Wunderli, H., Mickey, G.H. & Paulson, D.F. Isolation of a human prostate carcinoma cell line (DU 145). *International Journal of Cancer* **21**, 274-281 (1978).

147. Zarnitsyn, V.G., Prausnitz, A.R. & Chizmadzhev, Y.A. Physical methods of nucleic acid delivery into cells and tissues. *Biol. Membr.* **21**, 355-373 (2004).

148. Canatella, P.J., Black, M.M., Bonnichsen, D.M., McKenna, C. & Prausnitz, M.R. Tissue Electroporation: Quantification and Analysis of Heterogeneous Transport in Multicellular Environments. *Biophys. J.* **86**, 3260-3268 (2004).

149. Huang, X., El-Sayed, I.H., Qian, W. & El-Sayed, M.A. Cancer Cell Imaging and Photothermal Therapy in the Near-Infrared Region by Using Gold Nanorods. *J. Am. Chem. Soc.* **128**, 2115-2120 (2006).

150. Prausnitz, M.R. et al. Millisecond measurement of transport during and after an electroporation pulse. *Biophysical Journal* **68**, 1864-1870 (1995).

151. Guzman, H.R., Nguyen, D.X., McNamara, A.J. & Prausnitz, M.R. Equilibrium loading of cells with macromolecules by ultrasound: Effects of molecular size and acoustic energy. *Journal of Pharmaceutical Sciences* **91**, 1693-1701 (2002).

152. Prausnitz, M.R. et al. Quantitative study of Electroporation Showing a Plateau in Net Molecular-Transport. *Biophys. J.* **65**, 414-422 (1993).

153. Pettke, T., Heinrich, C.A., Ciocan, A.C. & Gunther, D. Quadrupole mass spectrometry and optical emission spectroscopy: detection capabilities and representative sampling of short transient signals from laser-ablation. *Journal of Analytical Atomic Spectrometry* **15**, 1149-1155 (2000).

154. Labbe, R. et al. Quantitation of postischemic skeletal-muscle necrosis-histochemical and radioisotope techniques *J. Surg. Res.* **44**, 45-53 (1988).

155. Pullman, G.S., P.Montello, J.Cairney, Xu, N. & X.Feng Loblolly pine (Pinus taeda L.) somatic embryogenesis: maturation improvements by metal analyses of zygotic and somatic embryos. *Plant Science* **164**, 955-969 (2003).

156. Jefferson, R.A., Kavanagh, T.A. & Bevan, M.W. GUS fusions: beta-glucuronidase as a sensitive and versatile gene fusion marker in higher plants. *EMBO Journal* **6**, 3901-3907 (1987).

157. Bellucci, M., De Marchis, F., Mannucci, R. & Arcioni, S. Jellyfish green fluorescent protein as a useful reporter for transient expression and stable transformation in Medicago sativa L. *Plant Cell Reports* **22**, 328-337 (2003).

158. Tian, L., Seguin, A. & Charest, P.J. Expression of the green fluorescent protein gene in conifer tissues. *Plant Cell Reports* **16**, 267-271 (1997).

159. Jansen, B. & Zangemeister-Wittke, U. Antisense therapy for cancer - the time of truth. *Lancet Oncology* **3**, 672-683 (2002).

160. Desnick, R.J. & Schuchman, E.H. Enzyme replacement and enhancement therapies: Lessons from lysosomal disorders. *Nature Reviews Genetics* **3**, 954-966 (2002).

161. Nobili, S., Landini, I., Giglioni, B. & Mini, E. Pharmacological strategies for overcoming multidrug resistance. *Current Drug Targets* **7**, 861-879 (2006).

162. Torchilin, V.P. Recent Approaches to Intracellular Delivery of Drugs and DNA and Organelle Targeting. *Annu. Rev. Biomed. Eng.* **8**, 343-375 (2006).

163. Orive, G., Gascon, A.R., Hernandez, R.M., Dominguez-Gil, A. & Pedraz, J.L. Techniques: New approaches to the delivery of biopharmaceuticals. *Trends Pharmacol. Sci.* **25**, 382-387 (2004).

164. Taniyama, Y., Tachibana, K. & Hiraoka, K. Development of safe and efficient novel non viral gene transfer using ultrasound: Enhancement of transfection efficiency of naked plasmid DNA in skeletal muscle. *Gene Therapy* **9**, 372-380 (2002).

165. Sundaram, J., Mellein, B.R. & Mitragotri, S. An Experimental and Theoretical Analysis of Ultrasound-Induced Permeabilization of Cell Membranes. *Biophysical Journal* **84**, 3087-3101 (2003).

166. Lukacs, G.L. et al. Size-dependent DNA Mobility in Cytoplasm and Nucleus. *J. Biol. Chem.* **275**, 1625-1629 (2000).

167. Fayer, M.D. Picosecond Holographic Grating Generation of Ultrasonic Waves. *IEEE Journal of Quantum Electronics* **22**, 1437-1452 (1986).

168. Zarnitsyn, V.G., Rostad, C.A. & Prausnitz, M.R. Modeling transmembrane transport through cell membrane wounds created by acoustic cavitation *Biophys. J.* (August 1, 2008).

169. Hallow, D.M. et al. Shear-induced intracellular loading of cells with molecules by controlled microfluidics. *Biotechnology and Bioengineering* **99**, 846-854 (2008).

170. McNeil, P.L. & Steinhardt, R.A. Plasma membrane disruption: Repair, prevention, adaptation. *Annu. Rev. Cell Dev. Biol.* **19**, 697-731 (2003).

171. Bauccio, M. ASM engineered materials reference book. (ASM International, Materials Park, OH; 1994).

172. Buschow, K.H. et al. Encyclopedia of Materials - Science and Technology, Volumes 1-11. (Elsevier 2001).

173. Chase, M.W., National Institute of, S. & Technology NIST-JANAF thermochemical tables. Part II, Cr-Zr. (American Chemical Society ; American Institute of Physics for the National Institute of Standards and Technology, [Washington, D.C.]; Woodbury, N.Y.; 1998).

174. Yaws, C.L. Chemical Properties Handbook. (McGraw-Hill.1999).

175. Diebold, G.J., Beveridge, A.C. & Hamilton, T.J. The photoacoustic effect generated by an incompressible sphere. *Journal of the Acoustical Society of America* **112** (2002).

176. Ferguson, J.E., Andrew, S.M., Jones, C.J.P. & August, P.J. The Q-switched neodymium: YAG laser and tattoos: a microscopic analysis of laser-tattoo interactions. *British Journal of Dermatology* **137**, 405-410 (1997).

177. Yamamoto, H. & Sato, K. Prevention of dental-caries by acousto-optically Q-switched Nd:YAG laser irradiation. *J. Dent. Res.* **59**, 137-137 (1980).

178. Guzman, H.R., Nguyen, D.X., McNamara, A.J. & Prausnitz, M.R. Equilibrium loading of cells with macromolecules by ultrasound: Effects of molecular size and acoustic energy. *J. Pharm. Sci.* **91** (2002).

179. Gobin, A.M. et al. Near-infrared resonant nanoshells for combined optical imaging and photothermal cancer therapy. *Nano Lett.* **7**, 1929-1934 (2007).

180. Brukh, R. & Mitra, S. Kinetics of carbon nanotube oxidation. *J. Mater. Chem.* **17**, 619-623 (2007).

181. Ajayan, P.M. et al. Nanotubes in a Flash--Ignition and Reconstruction. *Science* **296**, 705- (2002).

182. Zhao, N.Q., He, C.N., Jiang, Z.Y., Li, J.J. & Li, Y.D. Physical activation and characterization of multi-walled carbon nanotubes catalytically synthesized from methane. *Mater. Lett.* **61**, 681-685 (2007).

183. Knight, K.R., Zhang, B.M., Morrison, W.A. & Stewart, A.G. Ischaemia-reperfusion injury in mouse skeletal muscle is reduced by N-omega-nitro-L-arginine methyl ester and dexamethasone. *European Journal of Pharmacology* **332**, 273-278 (1997).

184. Poupin, M.J. & Arce-Johnson, P. Transgenic trees for a new era. *In Vitro Cell. Dev. Biol.--Plant* **41**, 91-101 (2005).

185. Campbell, M.M., Brunner, A.M., Jones, H.M. & Strauss, S.H. Forestry's fertile crescent: the application of biotechnology to forest trees. *Plant Biotechnol. J.* **1**, 141-154 (2003).

186. Wenck, A.R., Quinn, M., Whetten, R.W., Pullman, G.S. & Sederoff, R. High-efficiency Agrobacterium-mediated transformation of Norway spruce (Picea

abies) and loblolly pine (Pinus taeda). *Plant Molecular Biology* **39**, 407-416 (1999).

187. Tzfira, T., Yarnitzky, O., Vainstein, A. & Altman, A. Agrobacterium rhizogenes-mediated DNA transfer in Pinus halepensis Mill. *Plant Cell Reports* **16**, 26-31 (1996).

188. Huang, Y., Diner, A.M. & Karnosky, D.F. Agrobacterium rhizogenes-mediated plant transformation and regeneration of a conifer: Larix decidua. *In Vitro Cellular and Developmental Biology.* **27**, 201-207 (1991).

189. Xu, X. & Li, B. Fertile transgenic Indica rice plants obtained by electroporation of the seed embryo cells. *Plant Cell Reports* **13**, 237-242 (1994).

190. Halluin, K.D., Bonne, E., Bossut, M., DeBeukeleer, M. & Leemans., J. Transgenic maize plants by tissue electroporation. *The Plant Cell* **4**, 1495-1505 (1992).

191. Miller, M.W., Ciaravino, V., Allen, D. & Jensen, S. Effect of 2 MHz ultrasound on DNA, RNA and protein synthesis in Pisum sativum root meristem cells. *International Journal of Radiation Biology* **30**, 217-222 (1976).

192. Singh, N. & Chawla, H.S. Use of silicon carbide fibers for Agrobacterium-mediated transformation in wheat. *Curr. Sci.* **76**, 1483-1485 (1999).

193. Lindsey, K. Transgenic Plant Research. (CRC Press, 1998).

194. Baucher, M. et al. Red Xylem and Higher Lignin Extractability by Down-Regulating a Cinnamyl Alcohol Dehydrogenase in Poplar. *Plant Physiol.* **112**, 1479-1490 (1996).

195. Benfey, P.N. & Chua, N.-H. The Cauliflower Mosaic Virus 35S Promoter: Combinatorial Regulation of Transcription in Plants. *Science* **250**, 959-966 (1990).

196. Dellorusso, C., Crawford, R.W., Chamberlain, J.S. & Brooks, S.V. Tibialis anterior muscles in mdx mice are highly susceptible to contraction-induced injury. *J. Muscle Res. Cell Motil.* **22**, 467-475 (2001).

197. Ho, D.D.M., London, R., Zimmerman, G.B. & Young, D.A. Laser-tattoo removal - A study of the mechanism and the optimal treatment strategy via computer simulations. *Lasers in Surgery and Medicine* **30**, 389-397 (2002).

198. Nanni, C. Complications of laser surgery. *Dermatol. Clin.* **15**, 521-& (1997).

199. Doukas, A.G. & Kollias, N. Transdermal drug delivery with a pressure wave. *Adv. Drug Delivery Rev.* **56**, 559 EP 579 (2004).

200. Bianco, A., Kostarelos, K. & Prato, M. Applications of carbon nanotubes in drug delivery. *Curr. Opin. Chem. Biol.* **9**, 674-679 (2005).

201. Skala, M.C., Crow, M.J., Wax, A. & Izatt, J.A. Photothermal Optical Coherence Tomography of Epidermal Growth Factor Receptor in Live Cells Using Immunotargeted Gold Nanospheres. *Nano Lett.* **8**, 3461-3467 (2008).

202. Loo, C., Lowery, A., Halas, N., West, J. & Drezek, R. Immunotargeted nanoshells for integrated cancer imaging and therapy. *Nano Lett.* **5**, 709-711 (2005).

203. Gao, D., Agayan, R.R., Xu, H., Philbert, M.A. & Kopelman, R. Nanoparticles for two-photon photodynamic therapy in living cells. *Nano Lett.* **6**, 2383-2386 (2006).

204. Zobel, H.P. et al. Cationic polyhexylcyanoacrylate nanoparticles as carriers for antisense oligonucleotides. *Antisense Nucleic Acid Drug Dev.* **7**, 483-493 (1997).

205. Joris, I., Cuenoud, H.F., Doern, G.V., Underwood, J.M. & Majno, G. Capillary leakage in inflammation- a study by vascular labeling. *Am. J. Pathol.* **137**, 1353-1363 (1990).

206. Majno, G., Palade, G.E. & Schoefl, G.I. Studies on inflammation. 2.Site of action of histamine and serotonin along vascular tree- a topographic study. *Journal of Biophysical and Biochemical Cytology* **11**, 607-& (1961).

207. Xia, T. et al. Comparison of the abilities of ambient and manufactured nanoparticles to induce cellular toxicity according to an oxidative stress paradigm. *Nano Lett.* **6**, 1794-1807 (2006).

208. Mansour, K., Soileau, M.J. & Vanstryland, E.W. Nonlinear Optical-Properties of Carbon-Black Suspensions (Ink). *J. Opt. Soc. Am. B: Opt. Phys.* **9**, 1100-1109 (1992).

209. Perry, J.W. et al. Organic optical limiter with a strong nonlinear absorptive response. *Science* **273**, 1533-1536 (1996).

210. Sheikov, N., McDannold, N., Vykhodtseva, N., Jolesz, F. & Hynynen, K. Cellular mechanisms of the blood-brain barrier opening induced by ultrasound in presence of microbubbles. *Ultrasound in Medicine and Biology* **30**, 979-989 (2004).

211. Plant Molecular Biology: Molecular Genetic Analysis of Plant Development and Metabolism. (Berlin:Springer-Verlag, 1994).

212. Donnelly, J.J., Ulmer, J.B., Shiver, J.W. & Liu, M.A. DNA vaccines. *Annu. Rev. Immunol.* **15**, 617-648 (1997).

213. Wolff, J.A. et al. Direct gene transfer into mouse muscle in vivo. *Science* **247**, 1465-1468 (1990).

214. Moghimi, S.M., Hunter, A.C. & Murray, J.C. Long-circulating and target-specific nanoparticles: Theory to practice. *Pharmacol. Rev.* **53**, 283-318 (2001).

215. Choma, M.A., Hsu, K. & Izatt, J.A. Swept source optical coherence tomography using an all-fiber 1300-nm ring laser source. *Journal of Biomedical Optics* **10**, 6 (2005).

216. Dressel, M., Jahn, R., Neu, W. & Jungbluth, K.H. Studies in fiber guided excimer laser-surgery for cutting and drilling bone and meniscus. *Lasers in Surgery and Medicine* **11**, 569-579 (1991).